NTIS # PB2004-101320

SSC-429

RAPID STRESS INTENSITY FACTOR SOLUTION ESTIMATION FOR SHIP STRUCTURE APPLICATIONS

SHIP STRUCTURE COMMITTEE
2003

SHIP STRUCTURE COMMITTEE

RADM Thomas H. Gilmour
U. S. Coast Guard Assistant Commandant,
Marine Safety and Environmental Protection
Chairman, Ship Structure Committee

Mr. W. Thomas Packard
Director,
Survivability and Structural Integrity Group
Naval Sea Systems Command

Dr. Donald Liu
Senior Vice President
American Bureau of Shipping

Mr. Joseph Byrne
Director, Office of Ship Construction
Maritime Administration

Mr.Gerard A. McDonald
Director General, Marine Safety,
Safety & Security
Transport Canada

Mr. Thomas Connors
Director of Engineering
Military Sealift Command

Dr. Neil Pegg
Group Leader - Structural Mechanics
Defence Research & Development Canada - Atlantic

CONTRACTING OFFICER TECHNICAL REP.
Chao Lin / MARAD
Natale Nappi / NAVSEA
Robert Sedat / USCG

EXECUTIVE DIRECTOR
Lieutenant Eric M. Cooper
U. S. Coast Guard

SHIP STRUCTURE SUB-COMMITTEE

AMERICAN BUREAU OF SHIPPING
Mr. Glenn Ashe
Mr. Yung Shin
Mr. Phil Rynn
Mr. William Hanzalek

DEFENCE RESEARCH & DEVELOPMENT ATLANTIC
Dr David Stredulinsky
Mr. John Porter

MARITIME ADMINISTRATION
Mr. Chao Lin
Mr. Carlos Setterstrom
Mr. Richard Sonnenschein

MILITARY SEALIFT COMMAND
Mr. Joseph Bohr
Mr. Rick A. Anderson
Mr. Michael W. Touma

NAVAL SEA SYSTEMS COMMAND
Mr. Jeffery E. Beach
Mr. Edward E. Kadala
Mr. Allen H. Engle
Mr. Charles L. Null

TRANSPORT CANADA
Mr. Jacek Dubiel

UNITED STATES COAST GUARD
Mr. Rubin Sheinberg
Mr. Robert Sedat
Commander Ray Petow

CANADIAN COAST GUARD
Mr. Daniel Gauvin

Member Agencies:

American Bureau of Shipping
Defence Research Establishment Atlantic
Maritime Administration
Military Sealift Command
Naval Sea Systems Command
Society of Naval Architects & Marine Engineers
Transport Canada
United States Coast Guard

Ship
Structure
Committee

Address Correspondence to:

Executive Director
Ship Structure Committee
U.S. Coast Guard (G-MSE/SSC)
2100 Second Street, SW
Washington, D.C. 20593-0001
Ph: (202) 267-0003
Email: ecooper@comdt.uscg.mil

SSC – 429
SR – 1430

November 2003

RAPID STRESS INTENSITY FACTOR SOLUTION ESTIMATION FOR SHIP STRUCTURES APPLICATIONS

The results of the investigation have demonstrated that the Shen-Glinka weight function solutions appear to provide reasonable estimates of the Mode I crack tip stress intensity factor, K_I, for cracks in ship structural details provided that the details are subjected to load control boundary conditions. Under displacement control, the weight function solutions can provide significantly conservative estimates of K_I, (more than 1.5 times higher than the FE model K_I, estimates generated in this project).

The stress intensity factor calculation software has been supplied in electronic form with this report. The electronic files include the ANSI C source code, an executable version of the calculator software and an interface module. A description of the software and help information is provided in Appendix B.

T. H. GILMOUR
Rear Admiral, U.S. Coast Guard
Chairman, Ship Structure Committee

Technical Report Documentation Page

1. Report No. SSC-429	2. Government Accession No. PB2004-101320	3. Recipient's Catalog No. SR-1430
4. Title and Subtitle RAPID STRESS INTENSITY FACTOR SOLUTION ESTIMATION FOR SHIP STRUCTURES APPLICATIONS		5. Report Date December 2003 6. Performing Organization Code
7. Author(s) L.B. Carroll, S. Tiku, A.S. Dinovitzer		8. Performing Organization Report No. 5383C.DFR
9. Performing Organization Name and Address BMT Fleet Technology Ltd. 311 Legget Drive Kanata, Ontario Canada K2K 1Z8		10. Work Unit No. (TRAIS) 11. Contract or Grant No.
12. Sponsoring Agency Name and Address Ship Structure Committee C/O Commandant (G-MSE/SSC) United States Coast Guard 2100 Second Street, SW Washington, DC 20593-0001		13. Type of Report Final Report 14. Sponsoring Agency Code G-M
15. Supplementary Notes Sponsored by the Ship Structure Committee and its member agencies		

16. Abstract

The objective of this project was to investigate the application of Shen-Glinka weight function solutions to calculate the Mode I crack tip stress intensity factor, K_I, in complex ship structure details.

The project was divided into the following 6 tasks:

- Task 1: FE Modeling for Weight Function Calibration
- Task 2: Weight Function Generalization
- Task 3: FE Modeling for Weight Function Validation and Demonstration
- Task 4: Develop Weight Function Parametric Equations
- Task 5: Produce Stress Intensity Calculator Software
- Task 6: Project Management and Reporting

The results of the investigation have demonstrated that the Shen-Glinka weight function solutions appear to provide reasonable estimates of K_I for cracks in ship structural details provided that the details are subjected to load control boundary conditions. Under displacement control, the weight function solutions can provide significantly conservative estimates of K_I (more than 1.5 times higher than the FE model K_I estimates generated in this project).

17. Key Words	18. Distribution Statement Distribution Available From: National Technical Information Service U.S. Department of Commerce Springfield, VA 22151 Ph. (703) 605-6000		
19. Security Classif. (of this report) **Unclassified**	20. Security Classif. (of this page) **Unclassified**	21. No. of Pages **120**	22. Price PC - $38 (A07) ED - $23(A00)

CONVERSION FACTORS
(Approximate conversions to metric measures)

To convert from	to	Function	Value
LENGTH			
inches	meters	divide	39.3701
inches	millimeters	multiply by	25.4000
feet	meters	divide by	3.2808
VOLUME			
cubic feet	cubic meters	divide by	35.3149
cubic inches	cubic meters	divide by	61,024
SECTION MODULUS			
$inches^2$ $feet^2$	$centimeters^2$ $meters^2$	multiply by	1.9665
$inches^2$ $feet^2$	$centimeters^3$	multiply by	196.6448
$inches^4$	$centimeters^3$	multiply by	16.3871
MOMENT OF INERTIA			
$inches^2$ $feet^2$	$centimeters^2$ meters	divide by	1.6684
$inches^2$ $feet^2$	$centimeters^4$	multiply by	5993.73
$inches^4$	$centimeters^4$	multiply by	41.623
FORCE OR MASS			
long tons	tonne	multiply by	1.0160
long tons	kilograms	multiply by	1016.047
pounds	tonnes	divide by	2204.62
pounds	kilograms	divide by	2.2046
pounds	Newtons	multiply by	4.4482
PRESSURE OR STRESS			
$pounds/inch^2$	$Newtons/meter^2$ (Pascals)	multiply by	6894.757
kilo $pounds/inch^2$	mega $Newtons/meter^2$ (mega Pascals)	multiply by	6.8947
BENDING OR TORQUE			
foot tons	meter tons	divide by	3.2291
foot pounds	kilogram meters	divide by	7.23285
foot pounds	Newton meters	multiply by	1.35582
ENERGY			
foot pounds	Joules	multiply by	1.355826
STRESS INTENSITY			
kilo $pound/inch^2$ $inch^{1/2}$ ($ksi\sqrt{in}$)	mega Newton $MNm^{3/2}$	multiply by	1.0998
J-INTEGRAL			
kilo pound/inch	$Joules/mm^2$	multiply by	0.1753
kilo pound/inch	kilo $Joules/m^2$	multiply by	175.3

EXECUTIVE SUMMARY

The US Ship Structures Committee Project, SR-1430, "Rapid Stress Intensity Factor Solution Estimation for Ship Structures Applications," was awarded to the Columbia Research Corporation with subcontracts for the completion of the Project Tasks awarded to BMT Fleet Technology Limited (BMT FTL), BMT Designers and Planners and Stress and Fatigue-Fracture Design Inc. (SaFFD). The objective of this project was to investigate the application of Shen-Glinka weight function solutions to calculate the Mode I crack tip stress intensity factor, K_I, in complex ship structure details.

The project was divided into the following 6 tasks:

- Task 1: FE Modeling for Weight Function Calibration
- Task 2: Weight Function Generalization
- Task 3: FE Modeling for Weight Function Validation and Demonstration
- Task 4: Develop Weight Function Parametric Equations
- Task 5: Produce Stress Intensity Calculator Software
- Task 6: Project Management and Reporting

Tasks 1, 3 and 6 were conducted primarily by BMT FTL with some numerical modeling completed by BMT Designers and Planners Ltd. Tasks 2 and 4 were conducted primarily by SaFFD. To satisfy the requirements for Task 5, the stress intensity factor software code was developed by SaFFD. The code was converted to ANSI C format by BMT FTL who also developed a MS Windows™ based interface.

The results of the investigation have demonstrated that the Shen-Glinka weight function solutions appear to provide reasonable estimates of K_I for cracks in ship structural details provided that the details are subjected to load control boundary conditions. Under displacement control, the weight function solutions can provide significantly conservative estimates of K_I (more than 1.5 times higher than the FE model K_I estimates generated in this project).

Determining whether local ship structural components are subjected to primarily load or displacement control boundary conditions under service loading was not within the scope of this project. Given the complexity of the details and redundant load paths present in these structures, the potential for displacement control and load shedding may exist.

Attempts were made to apply correction factors to the weight function solutions to account for load versus displacement controlled boundary conditions, but at this time the attempts were not successful in developing universally applicable correction factors (see Appendix A). A more fundamental approach to developing correction factors or the derivation of displacement control weight function solutions may be of interest for future investigations.

The stress intensity factor calculation software has been supplied in electronic form with this report. The electronic files include the ANSI C source code, an executable version of the calculator software and an interface module. A description of the software and help information is provided in Appendix B.

TABLE OF CONTENTS

LIST OF FIGURES

LIST OF TABLES

1. INTRODUCTION

BMT Fleet Technology Limited (BMT FTL) has been subcontracted by Columbia Research Corporation to investigate the application of the weight function methodology developed by Bueckner [1] and Rice [2] to determine stress intensity factor (K_I) solutions for cracks in ship structures. In turn, BMT FTL has subcontracted the weight function solution generalization and calibration phases to Dr. G. Glinka of Stress and Fatigue-Fracture Design (SaFFD) and a portion of the finite element analysis work to BMT Designers and Planners.

The project has been broken down into 6 Tasks as follows:

- Task 1: FE Modeling for Weight Function Calibration
- Task 2: Weight Function Generalization
- Task 3: FE Modeling for Weight Function Validation and Demonstration
- Task 4: Develop Weight Function Parametric Equations
- Task 5: Produce Stress Intensity Calculator Software
- Task 6: Project Management and Reporting

Task 1: FE Modeling for Weight Function Calibration:

Three structural details were modeled in ANSYS, including six different crack sizes each, to develop stress intensity factor data for use in calibrating the weight function calculations. The six crack sizes for each detail included a range of crack depths and lengths. The finite element models were developed using twenty noded linear elastic brick elements with crack tip elements along the crack front. ANSYS crack tip elements and the displacement extrapolation techniques were used to estimate the stress intensity factor solutions.

Task 2: Weight Function Generalization:

The weight function technique for developing stress intensity factor solutions was generalized for use with ship structural details. This generalization considered both structural geometry but also further developed the elements of the calculation process. This task was concluded with the assembly of the details describing the stress intensity factor weight function calculation approach and theory. The document includes illustrative examples outlining the data requirements and use of the weight function approach.

Task 3: FE Modeling for Weight Function Validation and Demonstration

Six additional structural details were modeled in ANSYS. Each detail was modeled twice, once in the uncracked condition and once containing a crack. The uncracked models were used to generate stress estimates for the weight function calculations of the stress intensity factor solution while the cracked models were used in an attempt to validate the weight function procedures proposed in Task 2. The weight function solutions were applied to these details by staff at BMT FTL, independent of SaFFD.

Task 4: Develop Weight Function Parametric Equations

The parametric equations were in fact developed under Task 2, however, the proposed correction factors for the geometry and loading within the structural details were investigated in detail using simplified geometries that the standard weight function solutions were developed for. The complexity of the geometry and load distribution in a ship structure suggested such an investigation was warranted.

Task 5: Produce Stress Intensity Calculator Software

As a deliverable to this project, a software program has been supplied to provide quick calculation of the crack tip stress intensity factor using the weight functions presented.

Task 6: Project Management and Reporting

All of the information generated in Tasks 1 to 5 of this project has been documented in this report. The weight function calculator software is supplied in electronic form including both a run time version and the ANSI C source code. The instructions for the software have been provided in Appendix B of this report and also as a separate document for distribution with the software. The work has been completed on budget with the Final Report submitted approximately 2 months behind the original schedule after receiving approval from the Project Technical Committee for the extension.

It should be noted by the reader that improvements were made to the original finite element models discussed in the Interim Report for this project leading to significant differences in the estimates for stress intensity factors and generating new information regarding the application of the weight functions. These improvements arose from information obtained during the course of the investigation and included, primarily, increases in submodel dimensions to satisfy guidelines noted in handbooks for cracked specimen dimensions.

The specific details of the modeling changes are discussed throughout this report. It was identified that the distance between the crack plane and the free edge of the specimen where loading was applied could influence the stress intensity factor estimate. Most of the submodels, where therefore increased in size over those originally reported in the Interim Report and a sensitivity study was conducted to determine that the model sizes were sufficient to lead to convergence of the stress intensity factors for the loading scenarios.

2. TASK 1: FE MODELING FOR WEIGHT FUNCTION VALIDATION

Details of the global model generation along with the cracked and uncracked submodel solutions are discussed in this section. Changes made to the model geometry since the issue and approval of the Technical Scope document in July 2002 are presented in detail in this section.

The global model structure contains details typical of tankers. It was not based upon any one particular ship design, but instead incorporates details from a variety of designs in order to provide a variation in cracked component geometries for this study.

2.1 Global Model Generation

The global model geometry and loading were modified slightly from the Technical Scope document. The general geometry and net scantlings are provided in Figure 2.1.

The only geometry change was incorporated into Structural Detail 4 shown in Figure 2.2. Originally this side shell stiffener was shown as a rolled plate section, however, to facilitate butt welding of the web stiffener to the side shell stiffener it was decided that an upset bulb section would be more appropriate.

Several changes were made to the global model loading at the request of the PTC. The end restraints shown in Figure 3.1 of the Technical Scope document were corrected as shown in Figure 2.3 to ensure that proper rotational boundary restraints were applied to the free edges. In addition, the 1 mm longitudinal displacement was replaced with a bending load similar to a ship sagging condition with a maximum displacement of 1 mm applied to the bottom of the structure decreasing linearly with height.

The neutral axis position for the ship structure was assumed to be 8100 mm above the bottom shell shown in the global model. This number was arbitrarily chosen but is representative of some tankers containing the structural details included in the model. The bending load was linearly varied in the vertical direction along the side shell and shell stiffeners over the 3100 mm of the height of the global model. The loading is depicted schematically in Figure 2.4 and results in a load of 1 mm at the bottom of the structure reducing to 0.61 mm at the top of the structure. It should be emphasized that the structural details of the global model were chosen as typical examples and were not based upon a particular ship design. They were selected in order to demonstrate the applicability of weight function solutions to the complex geometries in a ship structure. The selection of the neutral axis height was also arbitrarily chosen so that the longitudinal loading would be representative of a sagging load and is not based upon a particular ship design.

The crack positions were located so that the crack planes were oriented perpendicular to the model Z axes. Under the loading conditions specified, stresses in the X and Y directions were often small or compressive and not conducive to crack opening. The mean through thickness X and Z directions stresses are shown in Figure 2.5.

For the models discussed in Sections 2, 3 and 4, loading was applied to the edges of the submodel using the degree of freedom interpolation feature in ANSYS based on the global model solution. Sections 5 and 6 discuss the implications of this approach in more detail.

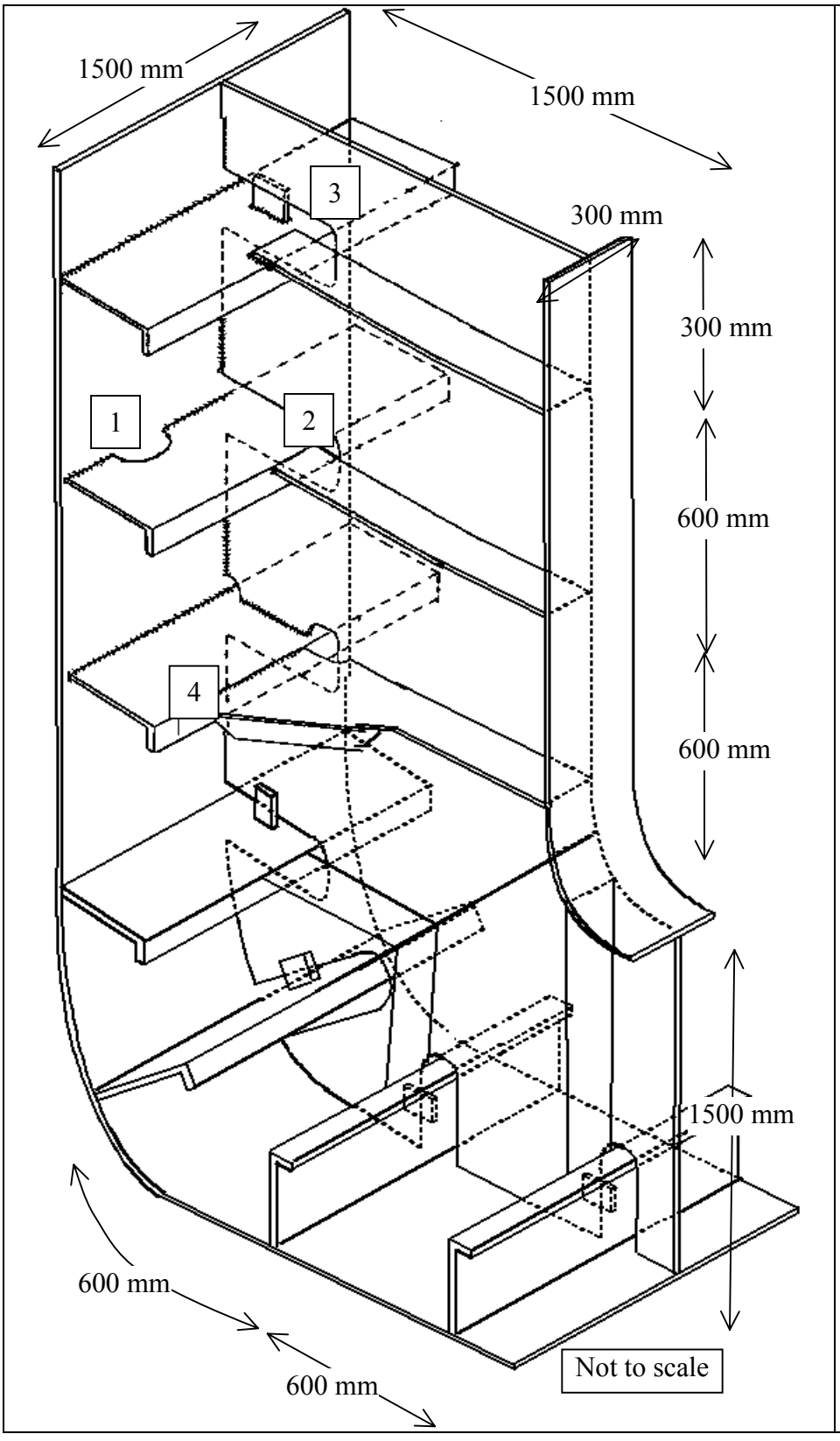

Scantlings:

Hull Plating
18 mm

Side Shell Long.
A 300x50x8

Web Frame Plate
12 mm

Web Frame Flange
12 mm

Web Stiffener
FB 150x8 mm

Bracketing
8 mm plate

Figure 2.1: Structural Geometry and Scantlings

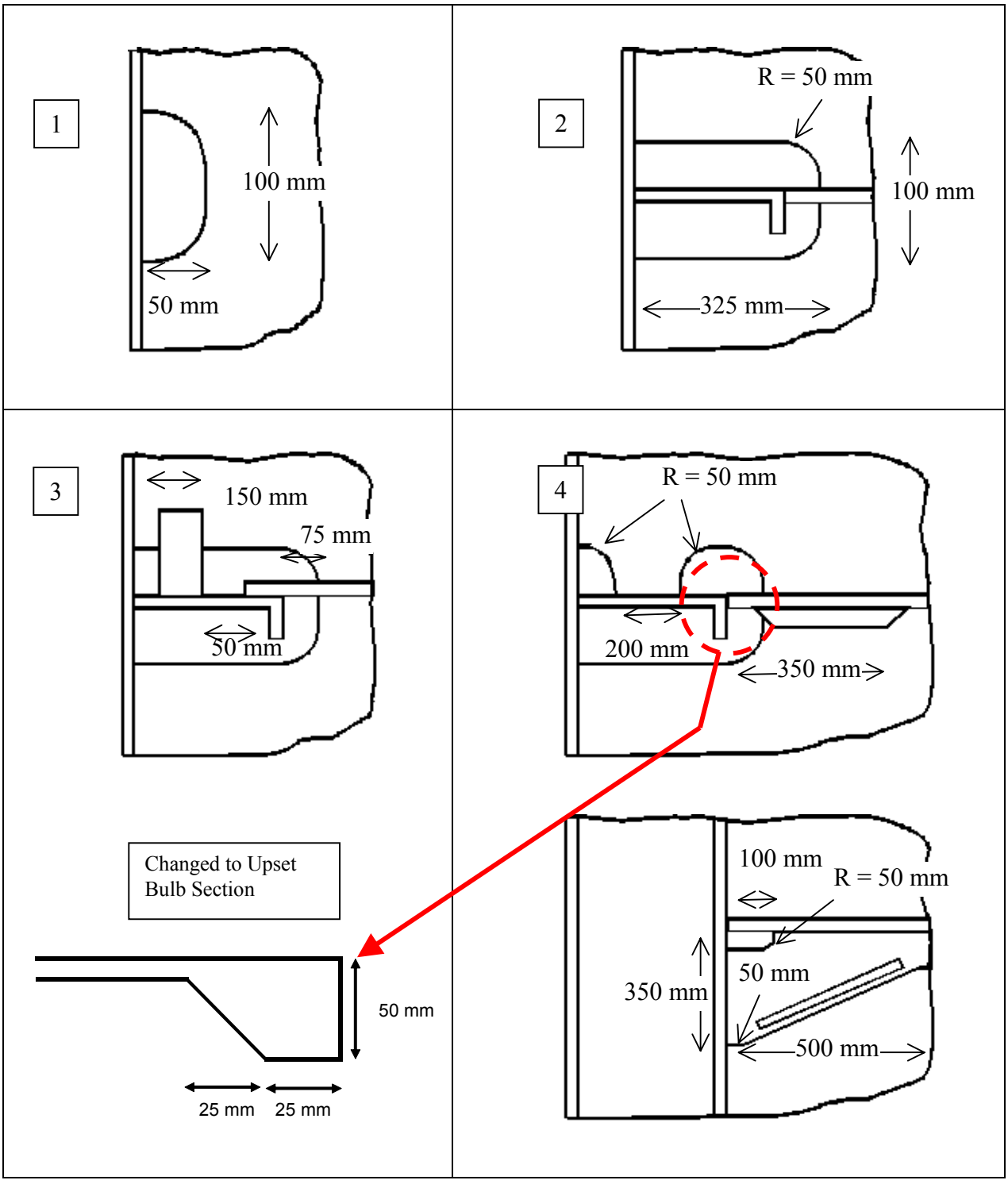

Figure 2.2: Local Detail Geometry (not to scale)

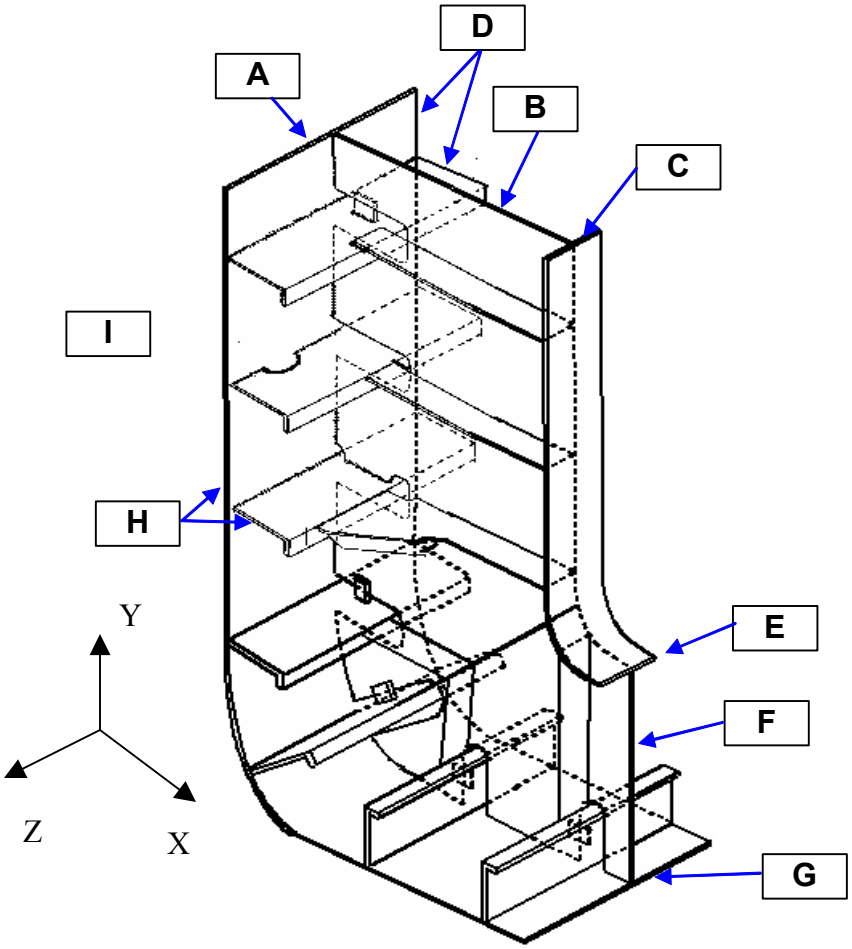

A – Boundary restraint on shell: Rot Z = 0
B – Boundary restraint on web: Rot X = 0
C – Boundary restraint on flange: Rot Z = 0
D – Boundary restraints on shell and shell stiffeners: Uz = 0, Rot X = 0, Rot Y = 0
E – Boundary restraint on flange: Ux = 0, Rot Z = 0
F – Boundary restraint on web: Ux = 0, Rot Y = 0
G – Boundary restraint on shell: Ux = 0, Rot Z = 0
H – Linear displacement load on shell and shell stiffeners (see Figure 2.4)
I – Pressure on shell = 100 kPa

Figure 2.3: Boundary Conditions and Loading on Global Model

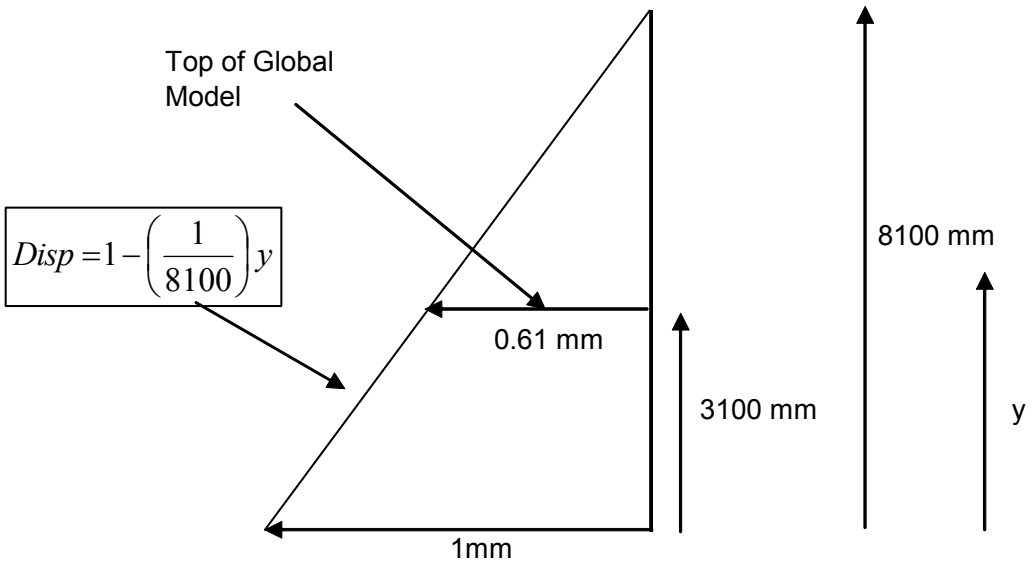

Figure 2.4: Displacement Loading Diagram for H in Figure 2.3 (y and Disp are in mm)

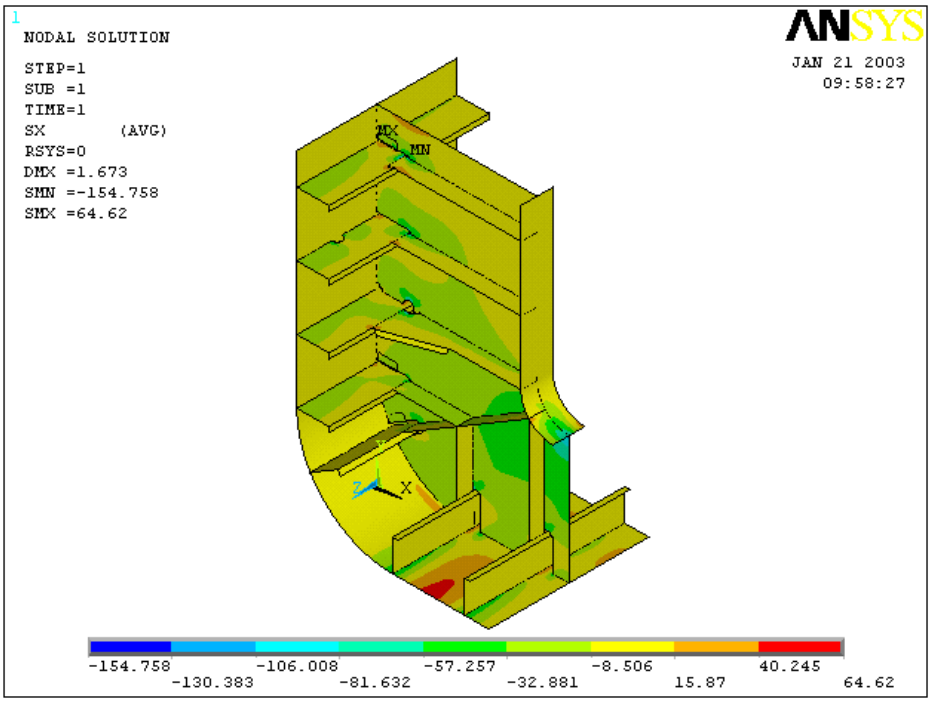

(a)

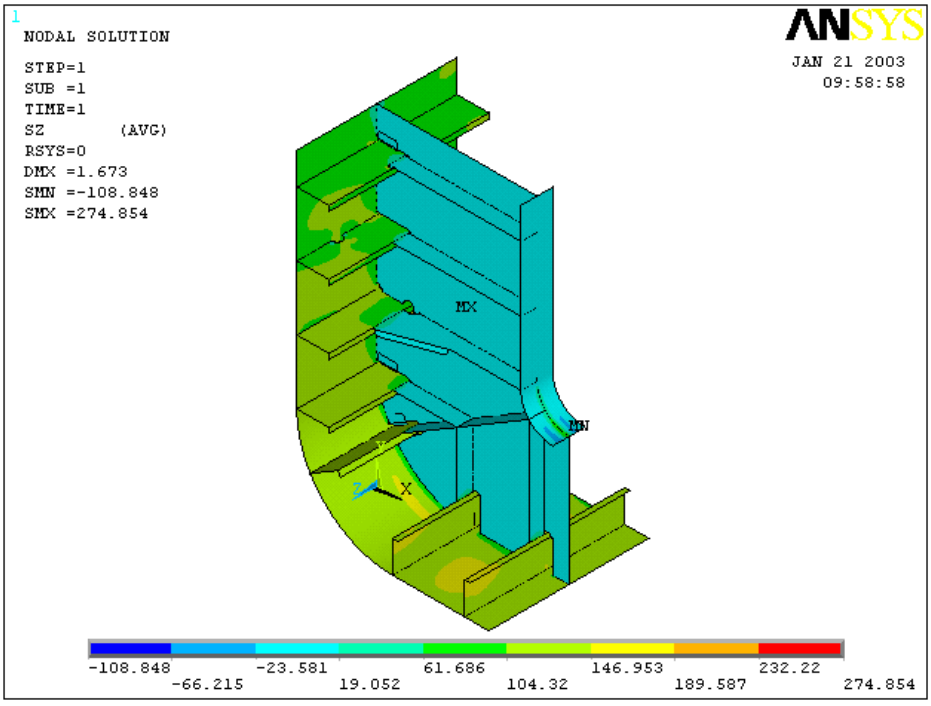

(b)

Figure 2.5: (a) Average X-Direction and (b) Average Z-Direction Stresses Resulting from the Global Model Loading

2.2 Edge Crack Location Submodels

2.2.1 Uncracked Model for Edge Crack Weight Function Calibration

In order to apply weight functions, the stress distribution perpendicular to the intended crack plane is required for the uncracked geometry. The position of the edge crack in the global model is illustrated in Figure 2.6. The crack is assumed to have originated at the bottom of the flange and is propagating upwards towards the web (Figure 2.7). The submodel geometry is shown in Figure 2.8.

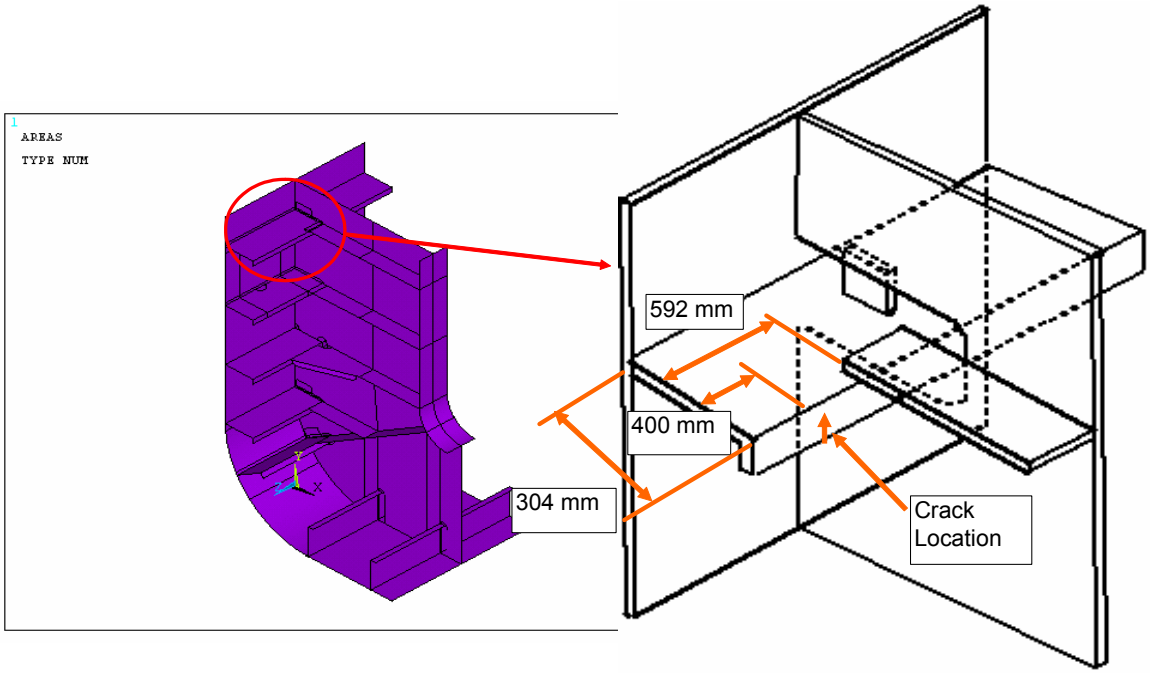

Figure 2.6: Position of Edge Crack Calibration Example in Global Model

The element mesh was refined in the region of the crack plane as illustrated in Figure 2.9. The ANSYS Solid95 brick elements were refined at the region of interest to cubes with 0.5 mm edge lengths.

The stress profile required for the weight function solution is oriented perpendicular to the crack plane along the model's Z axis at mid-thickness of the flange. The stress distribution is provided in Figure 2.10.

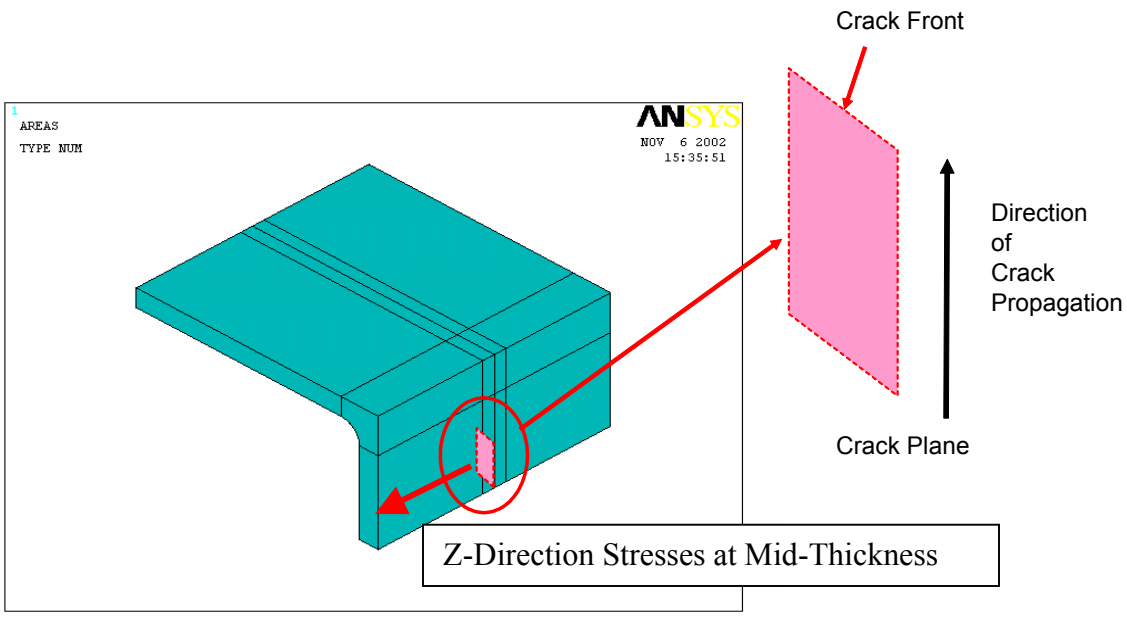

Figure 2.7: Crack Plane and Crack Front Definitions for Edge Crack Calibration Examples

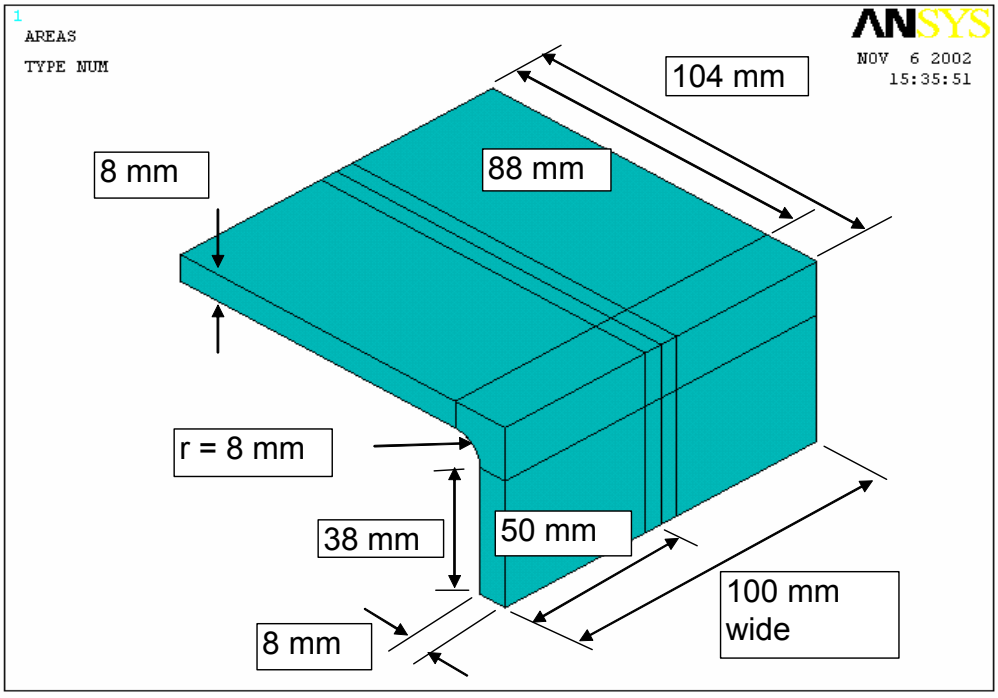

Figure 2.8: Submodel Dimensions for Edge Cracked Submodels

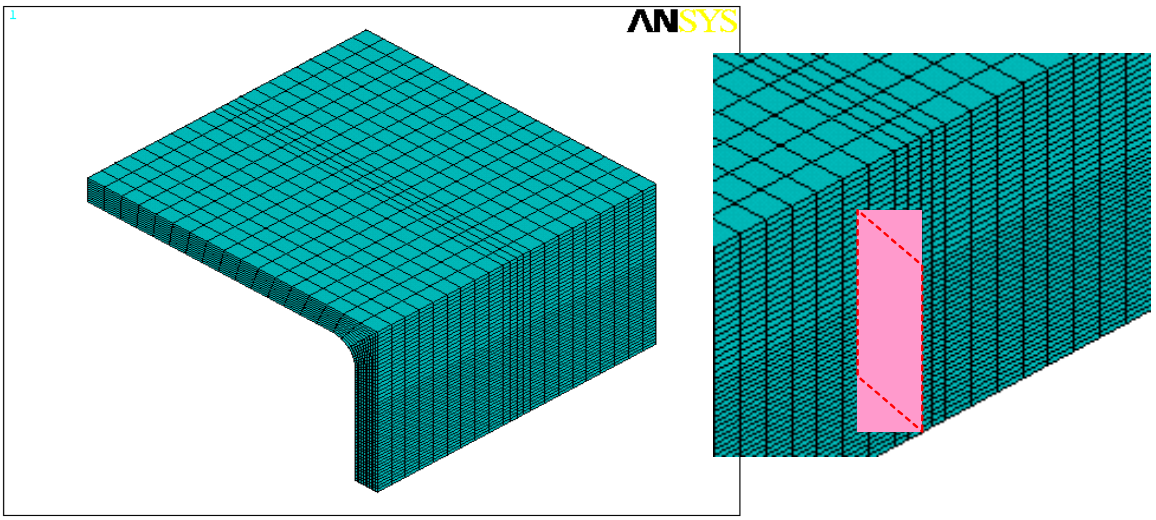

Figure 2.9: Submodel Element Mesh for the Uncracked Geometry at the Edge Crack Location

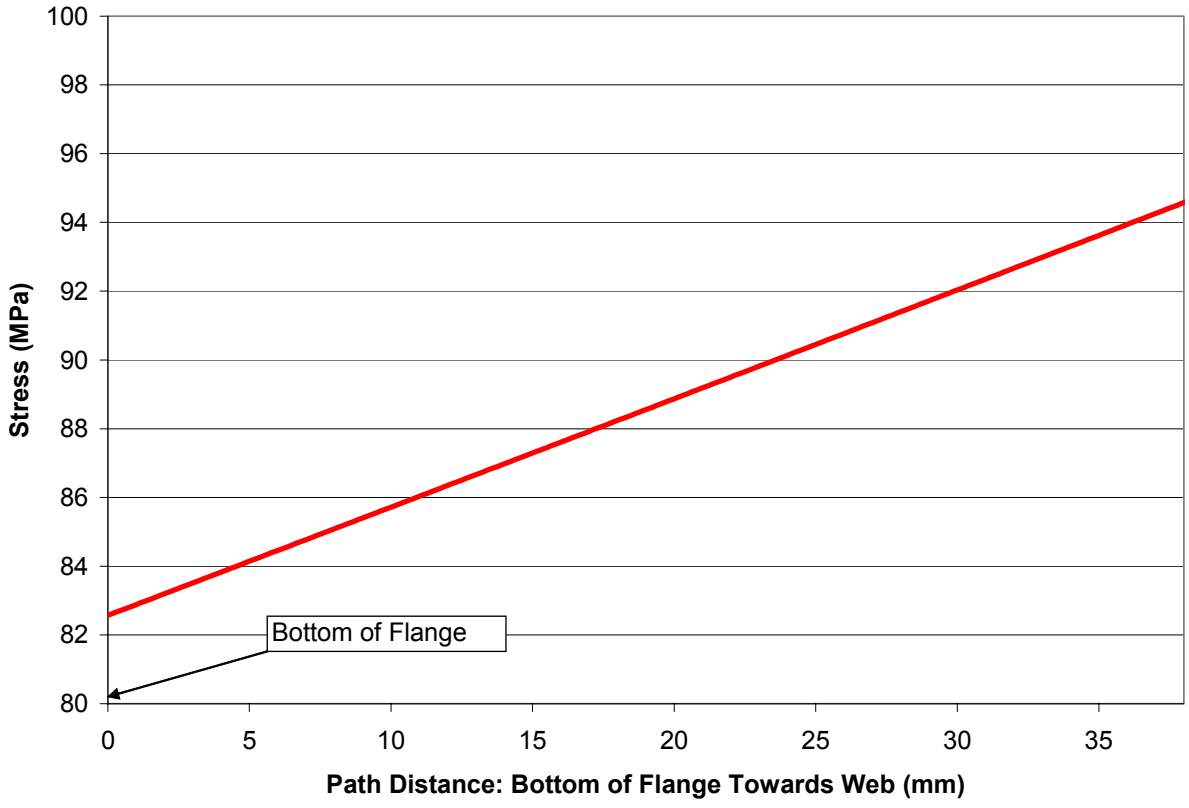

Figure 2.10: Stress Profile in Uncracked Edge Crack Calibration Example Normal to the Crack Plane at Mid-Thickness

2.2.2 Edge Cracked Calibration Submodels

Six edge-cracked submodels were created in ANSYS using the submodel geometry shown in Figure 2.11. Tada et. al. [1] reported that standard K_I solutions for edge cracks in a finite width plate are generally derived for plates with the distance from the crack plane to the loaded ends equal to or greater than the width of the plate. In this example, it is not possible to truly meet these conditions if the assumed effective stiffener width is approximately the height of the flange (~50 mm) plus the width of the web (~ 300 mm) or 350 mm. The crack plane is located at Z = 350 mm in the global model and the total distance from the web to the end of the side shell is 750 mm. Therefore, in the forward direction it is possible to extend the length far enough. In the aft direction however, there is a lap welded connection to the stiffener beginning at approximately Z = 160 mm. It is therefore not possible to extend the model far enough in the aft direction without interacting with the web stiffener.

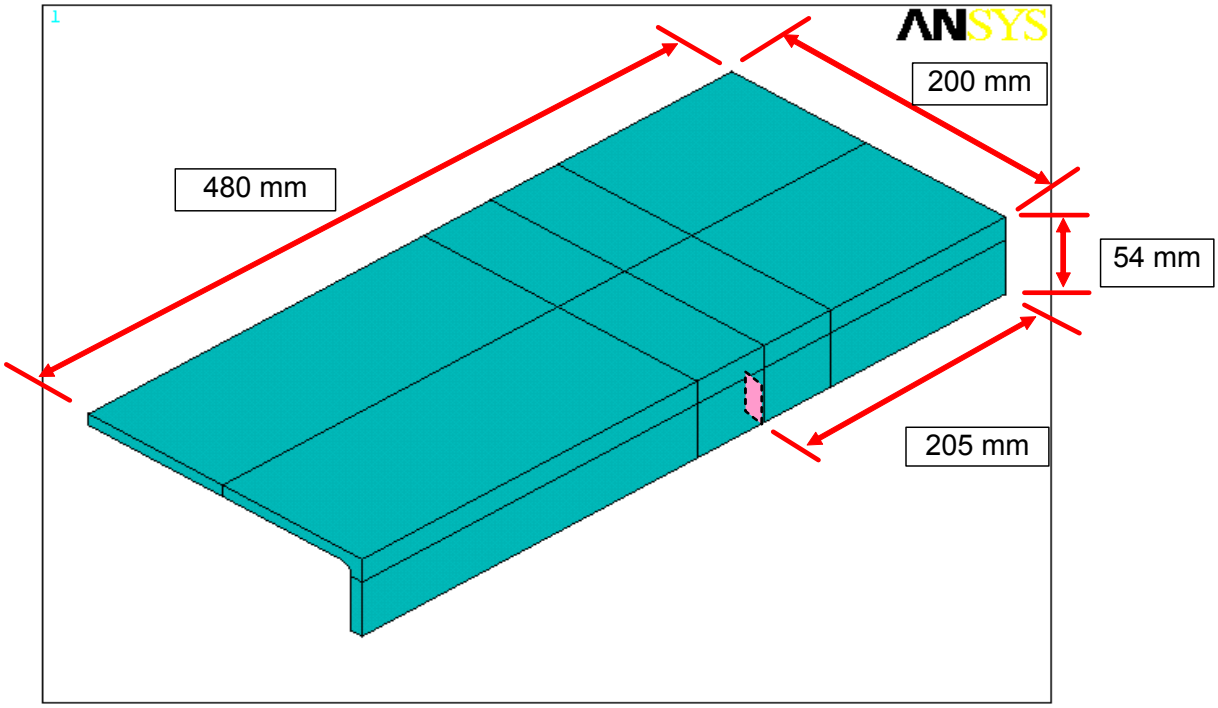

Figure 2.11: Geometry of Crack Submodels for Edge Crack Calibration Examples

Modifications were made to the mesh to introduce the cracks (Figure 2.12). ANSYS Solid95 crack tip singularity elements were used along the crack front. The six crack lengths chosen were 5 mm, 10 mm, 15 mm, 20 mm, 25 mm and 30 mm. Figure 2.13 shows an example of the crack opening under loading. The K_I estimates are presented in Table 2.1 with a plot of K_I versus crack length shown in Figure 2.14. ANSYS allows an estimation of the stress intensity factor assuming either plane strain (triaxial stress state) or plane stress (biaxial stress state). Depending upon the actual stress state, K_I should be bounded by these two values.

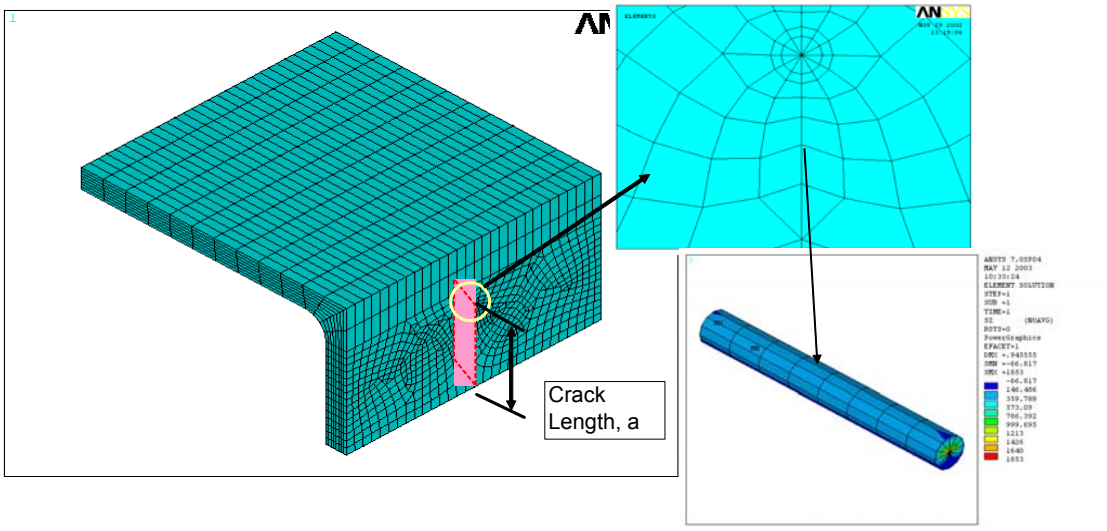

Figure 2.12: Example of Model Mesh for Edge Cracked Models (Additional Volumes Removed from Picture for Clarity)

Table 2.1: K_I Estimates from Edge Cracked Calibration Models

Crack Length, a mm	ANSYS Stress Intensity Factor Estimates MPa(mm)$^{1/2}$	
	Plane Strain	Plane Stress
5	402	366
10	612	557
15	818	744
20	1030	938
25	1241	1130
30	1424	1296

Several iterations of submodel geometries were used to generate K_I estimates. The first models had the same dimensions shown for the uncracked model in Figure 2.8. This resulted in larger K_I estimates (Plane strain = 594, Plane stress = 540) for the 5 mm long crack and smaller K_I estimates (Plane strain = 1033, Plane stress = 940) for the 30 mm long crack. The values for the 20 mm long flaw were quite close to those shown in Table 2.1. The reasons for the differences in K_I estimates can be attributed to the application of displacement controlled boundary conditions and model size effects. These influences will be discussed in later sections of this report.

To ascertain the effects of a further increase in the submodel size in the forward and width directions, a second submodel was run for the deepest crack case and compared to the original result. The new geometry is shown in Figure 2.15. The new K_I estimate was 1437 MPa(mm)$^{1/2}$ for plane strain assumptions and 1308 MPa(mm)$^{1/2}$ using plane stress assumptions.

These results agree to within 1% of the value shown in Table 2.1 and suggest that there is no further value to be gained by increasing the submodel size in these directions.

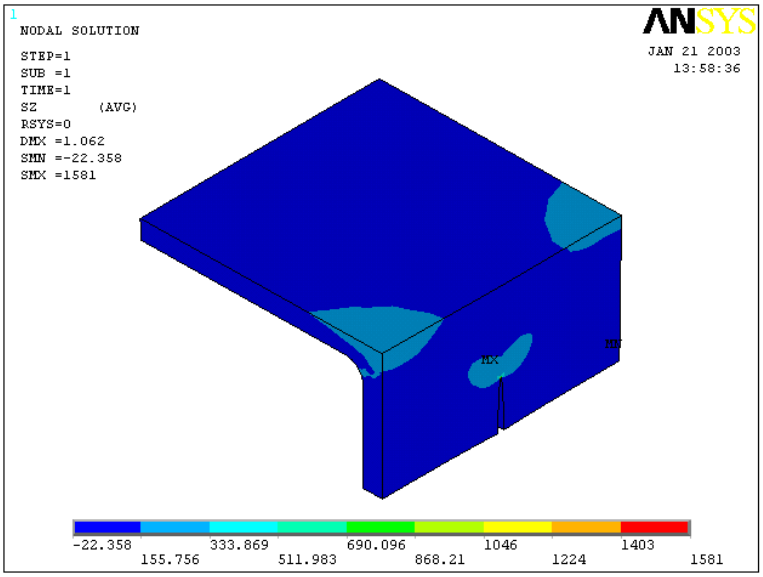

Figure 2.13: Crack Opening (at exaggerated scale) for an Edge Cracked Submodel (Additional Volumes Removed from Picture for Clarity)

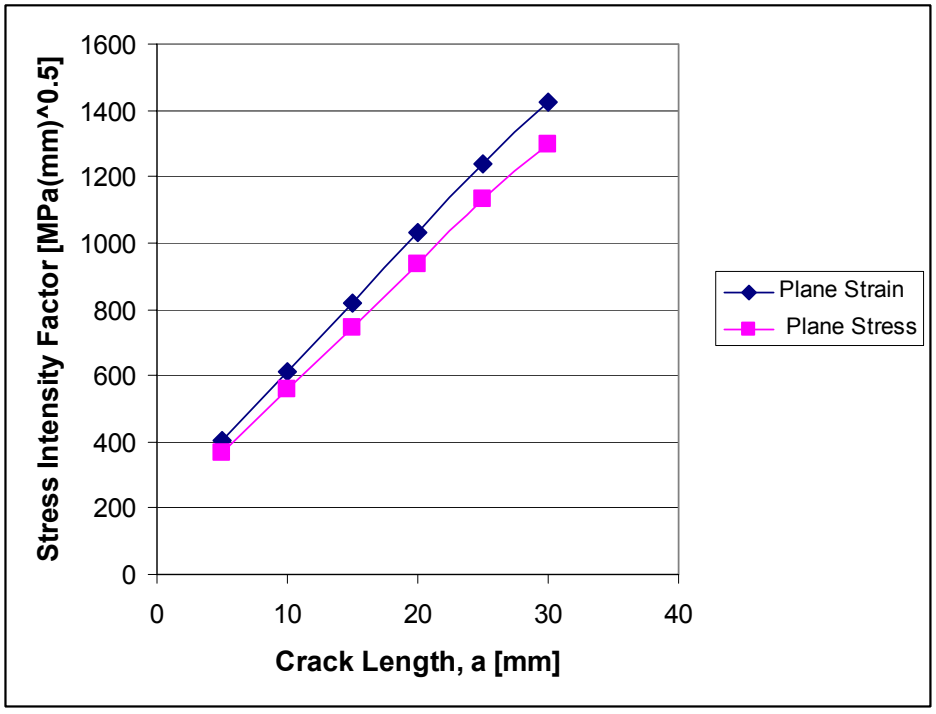

Figure 2.14: Relationship between Stress Intensity Factor and Crack Length for the Edge Crack Calibration Models Based Upon ANSYS Model Estimates

The stiffener is essentially comprised of thin plates and analysis of the uncracked submodels showed that the through thickness stress component and shear stresses are essentially zero indicating that the stress state is predominantly a state of plane stress. Both the plane strain and plane stress ANSYS results are presented in Section 2 for all models, but later comparisons between the weight function and FE model solutions for the calibration edge cracks will be made to the ANSYS plane stress solutions.

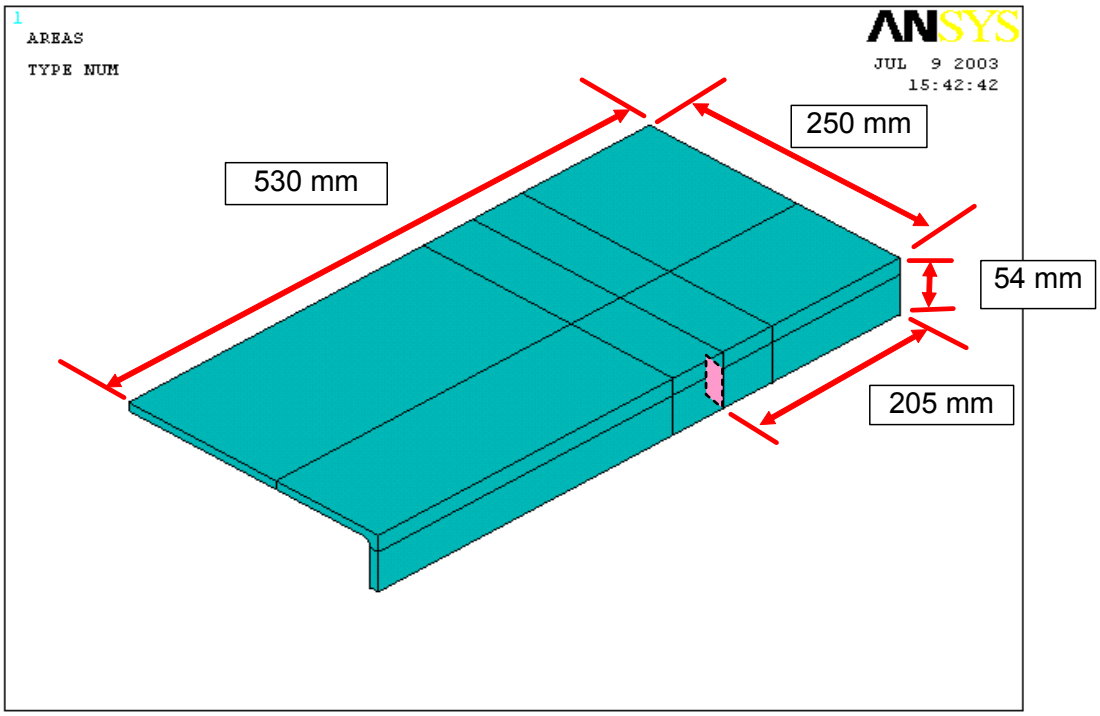

Figure 2.15: Revised Model Geometry for Edge Crack Calibration Example to Examine the Effects of Increasing Model Size in the Forward and Width Directions

2.3 Through Thickness Crack Location Submodels

2.3.1 Uncracked Model for Through Thickness Crack Weight Function Calibration

The location of the through thickness crack in relation to the global model geometry is shown in Figure 2.16. The crack is in the side shell at the toe of the web to the side shell connection with the crack face oriented in the X-Y plane. The Z-direction stresses were extracted from the mid thickness of the side shell in the submodel to use with the weight function formulas.

The weld for this model was assumed to be full penetration with a weld leg of 10 mm. The weld size is likely exaggerated compared to an actual weld of this type however, the example was selected to demonstrate the application of the weight function solution to this geometric configuration and the weld dimensions have been arbitrarily chosen.

Because of the addition of the weld penetration, it was decided to submodel this geometry first using a coarse mesh (Figure 2.17) including the entire welded connection and then with a refined mesh model including only the weld details in the crack region (Figure 2.18). As it turned out, two refined meshed submodels were required to achieve the desired mesh density. The entire length of the weld toe was split into two submodels each covering ½ of the total weld length (Figure 2.19).

The weld toe was modeled assuming a 1 mm radius and using four 20-noded brick elements along the fillet (Figure 2.19) to get a realistic stress concentration prediction.

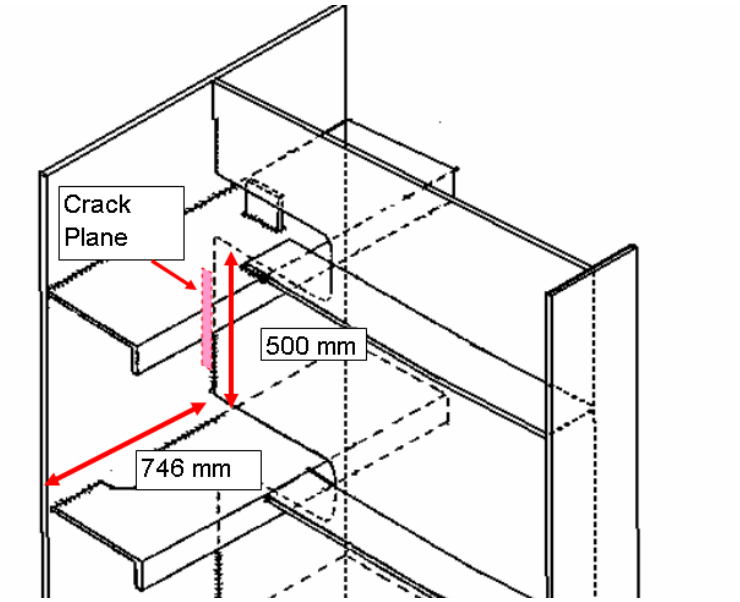

Figure 2.16: Location of Through Crack in Global Model Geometry

The through thickness stress estimates perpendicular to the crack plane are provided in Figure 2.19. The mid-thickness profile was used to estimate K_I from the weight function solution however, it can be seen that due to the welded connection and the bending of the side shell around the web, there is a variation in stress in the through thickness direction. In addition, there is a variation in stress along the length of the weld due to the bending load applied in the longitudinal orientation.

The through-thickness variation in stress at the mid-point of the cracks is illustrated in Figure 2.20. The bending of the plate around the web is evident with the increase in stress from about 4.5 mm below the weld toe towards the outer surface of the side shell. The spike near the inner surface is a result of the weld toe stress concentration.

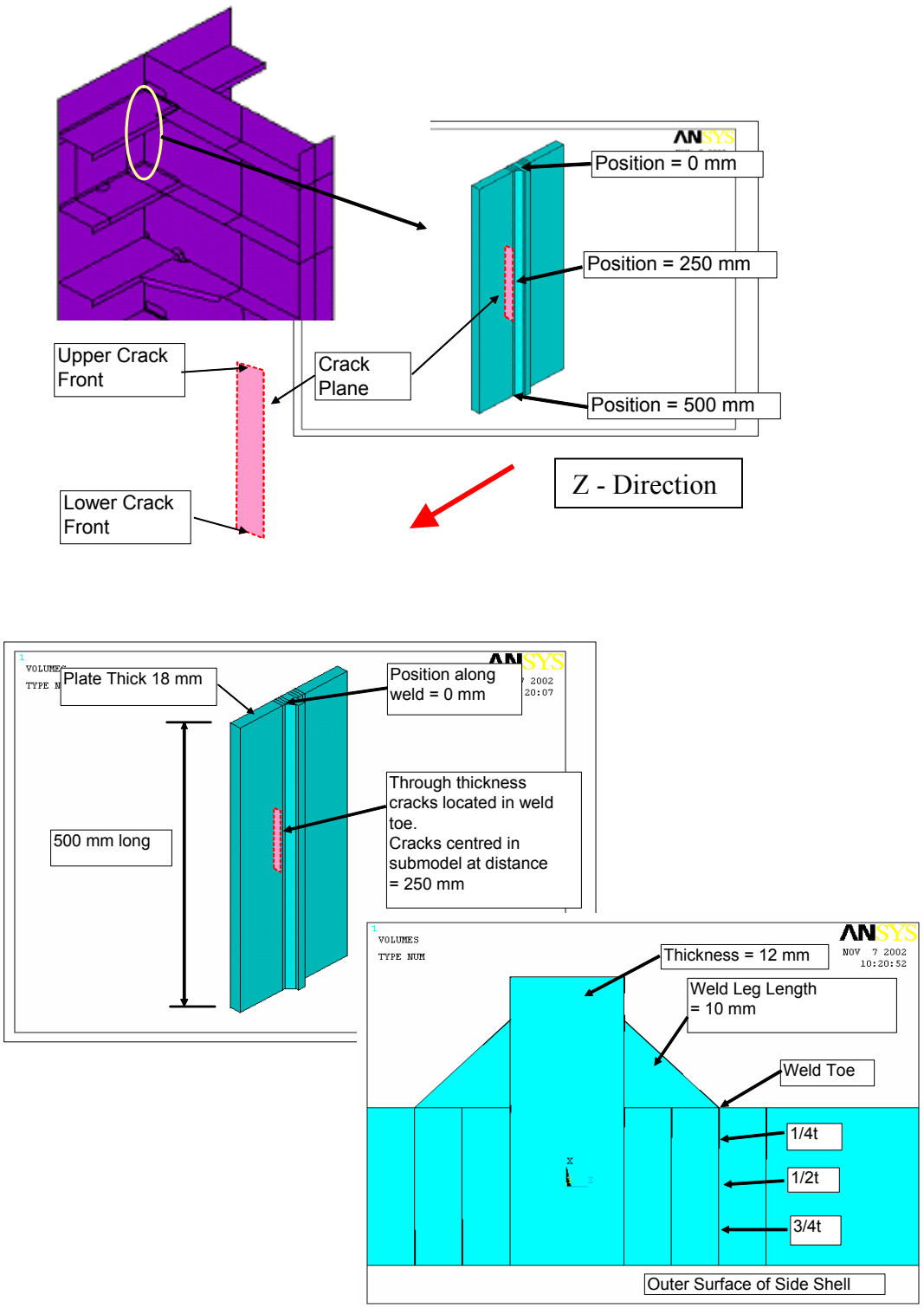

Figure 2.17: Coarse Meshed Model Geometry for the Through Thickness Calibration Example Crack Location

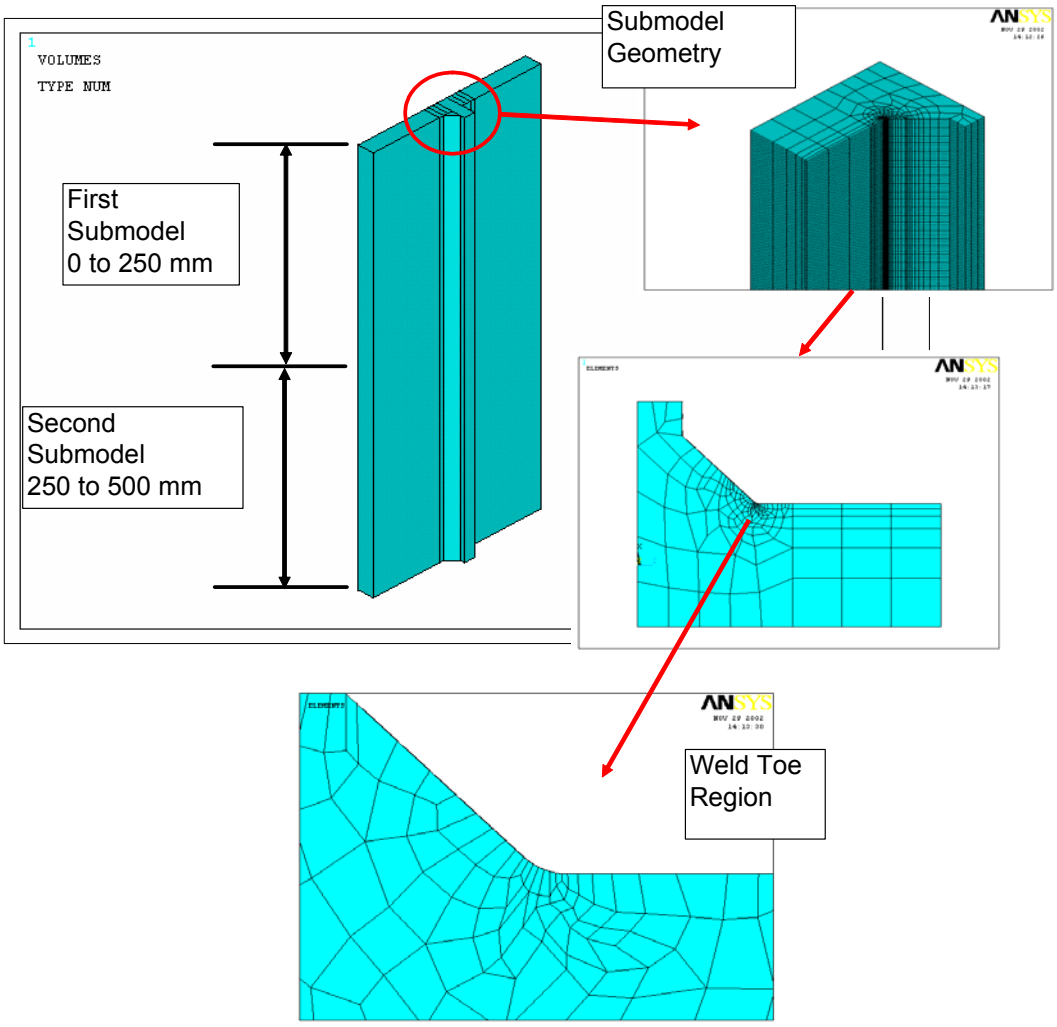

Figure 2.18: Uncracked Refined Mesh Submodel Details for the Through Thickness Crack Location

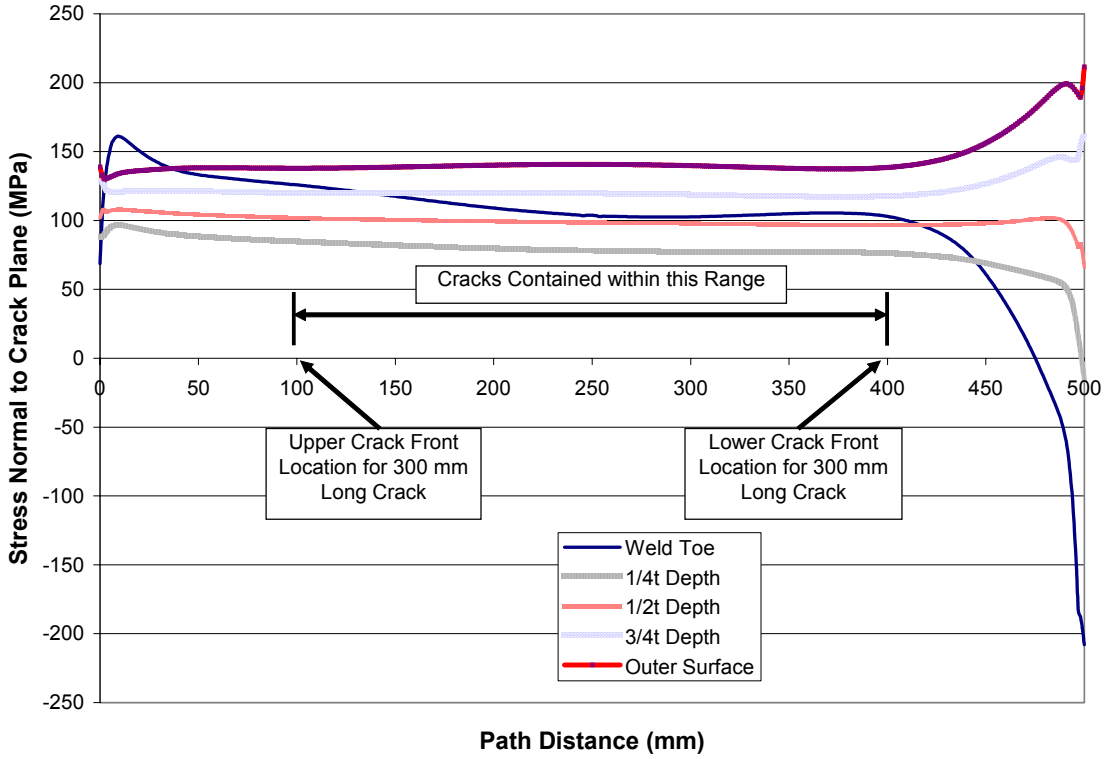

Figure 2.19: Through Thickness Stress Estimates Perpendicular to the Crack Plane for the Through Crack Calibration Model

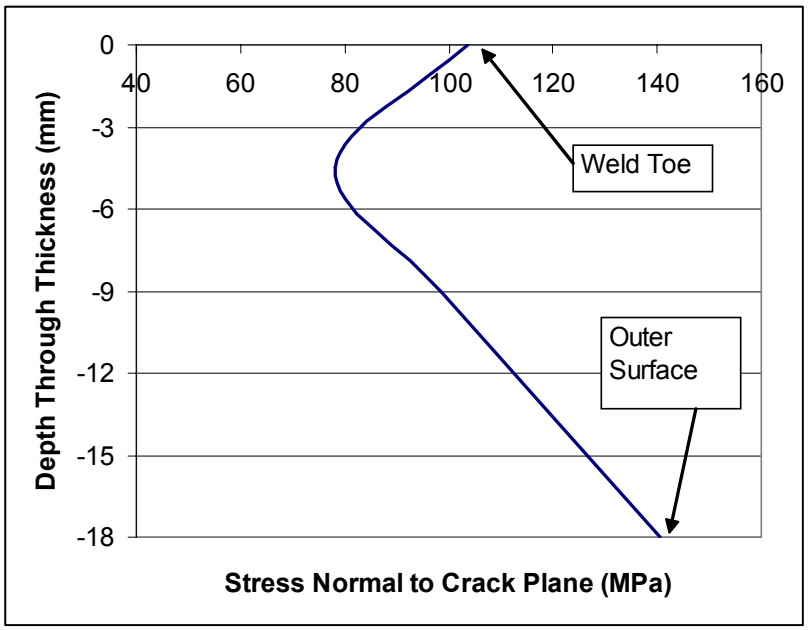

Figure 2.20: Through Thickness Stress Profile for Through Crack Calibration Model at Path Distance = 250 mm

2.3.2 Through Thickness Cracked Calibration Models

The through crack models also required two submodeling steps. As shown in Figure 2.21, Tada et. al. [1] indicated that the length of the plate containing the through crack will have an effect on the stress intensity factor with the application of displacement-controlled boundary conditions. The correction factor F_1 must be applied to the analytical solution of a through crack in an infinitely wide plate for values of h less than being about 4a (a being the half crack length) to achieve a K_I estimate to within about 10% of the actual value. With this in mind, the initial submodel was generated with a length in the Z-direction almost equivalent to the total length of the global structure (h = 4.9a for the largest crack, 2a = 300 mm).

Cracks were introduced into the larger submodels to permit local crack opening displacement behavior under the applied remote loading, but because of restrictions on the number of degrees of freedom that can be accommodated by BMT FTL computing capabilities, crack tip elements were not used in these models. The larger submodel geometry is illustrated in Figure 2.22.

The second stage of submodeling used boundary conditions extracted from the larger submodels applied to geometrically smaller models containing crack tip elements (Figure 2.23). Six crack sizes were chosen with surface lengths, 2a, of 50 mm, 100 mm, 150 mm, 200 mm, 250 mm, and 300 mm. The upper (Figure 2.23) and lower crack fronts were meshed with ANSYS Solid95 crack tip elements and were assumed to be straight through the side shell thickness.

Estimates for K_I were taken at the mid thickness positions (Figure 2.17) on the upper and lower crack fronts and are presented in Table 2.2. There are slight differences in the K_I estimates for the upper and lower crack fronts. The bending load from the sagging condition resulted in a slightly higher stress at the lower crack front.

Table 2.2: K_I Estimates for Through Cracked Calibration Models at the Mid-Thickness of the Upper and Lower Crack Fronts (see Figure 2.17)

Crack Length, 2a (mm)	ANSYS Stress Intensity Factor Estimates $MPa(mm)^{1/2}$			
	Upper Crack Front		Lower Crack Front	
	Plane Strain	Plane Stress	Plane Strain	Plane Stress
50	853	776	861	784
100	1138	1036	1158	1036
150	1359	1237	1393	1267
200	1493	1358	1540	1401
250	1576	1435	1638	1490
300	1617	1471	1691	1539

$$s = \frac{a}{a+h} = \frac{a/h}{1+a/h} = \frac{1}{1+h/a}$$

$$K_I = \sigma\sqrt{\pi a}\cdot F_1(s)$$

$$= \sigma\sqrt{h}\cdot F_2(s)$$

$$s \to 0 (a/h \to 0) : F_1 = 1, F_2 \to \sqrt{\frac{\pi a}{h}}$$

$$s \to 1 \left(\frac{a}{h} \to \infty\right) : \quad F_2 = \sqrt{1-\nu^2}$$

$$F_1 \to \sqrt{1-\nu^2}\sqrt{\frac{h}{\pi a}}$$

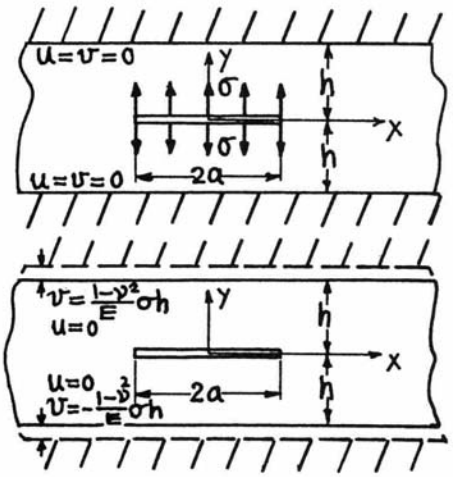

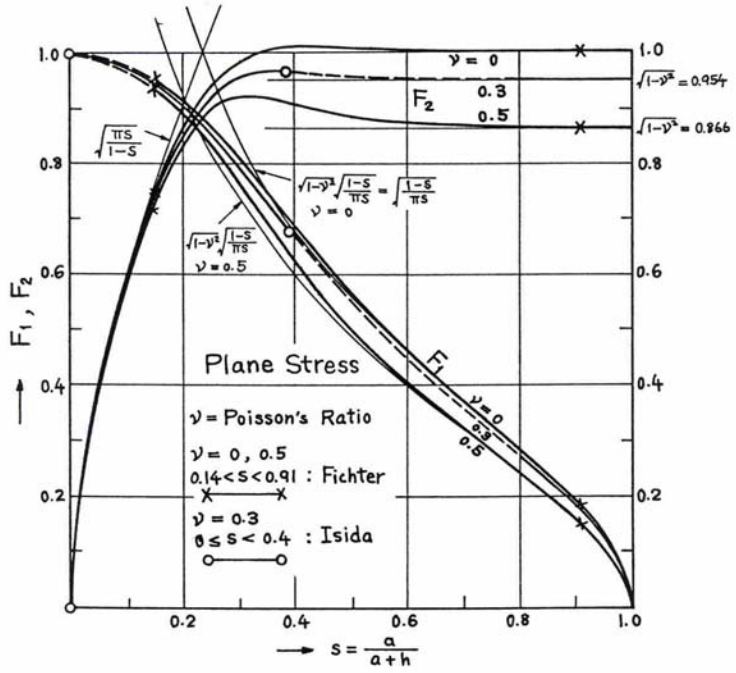

Methods: Expansions of Complex Stress Potentials (Isida), Fourier Transform (Fichter), $s \to 0$: Solution for Infinite Plate, $s \to 1$: Energy Balance (Rice)

Accuracy: Order of 1%

References: **Fichter 1967; Rice 1967; Isida 1971a**

NOTE: For plane strain $F_2(s \to 1) = \sqrt{1-2\nu}/(1-\nu)$, etc.

Figure 2.21: Correction Factors for Through Cracks in Plate Strips Subjected to Uniform Displacements or Stresses Applied to Cracks in Plate Strips with Restrained Edges [1]

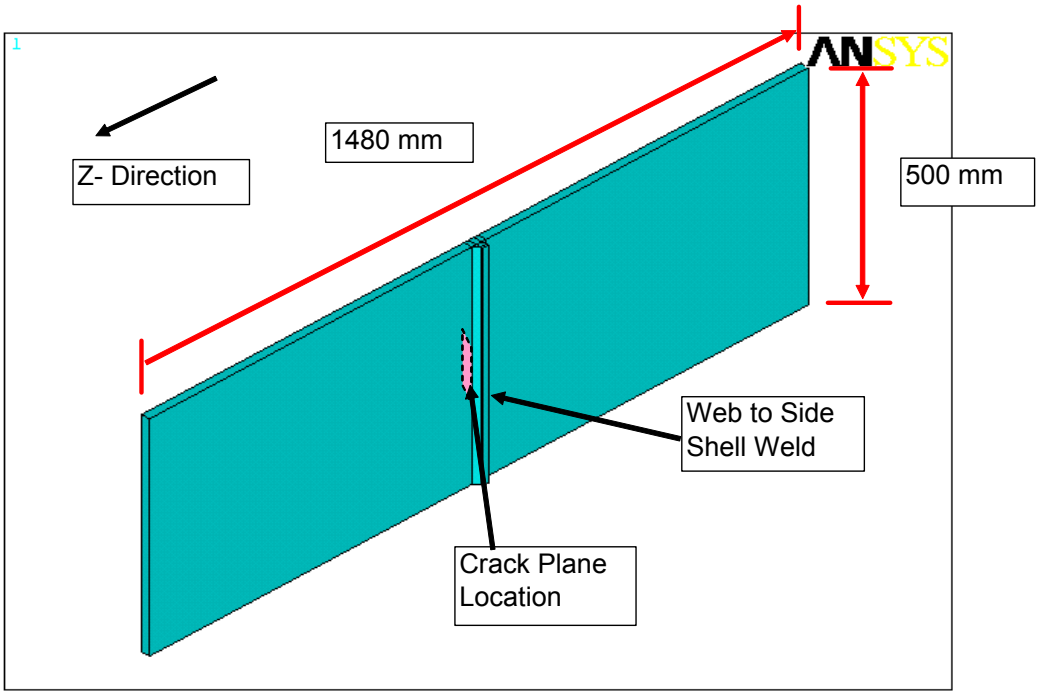

Figure 2.22: Geometry of First Stage Submodels for Through Crack Calibration Examples

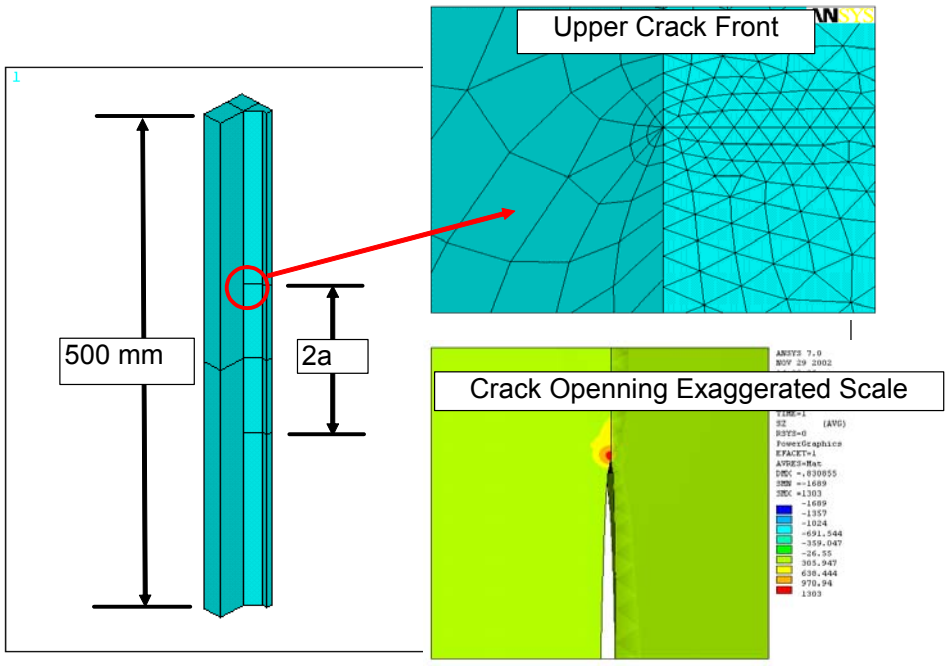

Figure 2.23: Through Cracked Calibration Example Geometry

At the mid thickness location for the shortest crack length, the through thickness stress component is approximately zero. The magnitude of the through thickness stress increases giving a value of approximately 9.8 MPa for the 300 mm long crack or about 10% of the stress perpendicular to the crack. The plane strain results should provide a conservative estimate of K_I for all cracks analyzed so the weight function results will be compared to the ANSYS plane strain estimates later in this report.

Initially, the larger submodels were not used and displacement boundary conditions from the global model were applied to the smaller submodel directly. These early models resulted in plane strain KI values between 608 and 611 MPa(mm)$^{1/2}$ and plane stress values from 553 to 555 MPa(mm)$^{1/2}$. The application of the displacement controlled boundary conditions so close to the crack plane did not accurately model the local crack opening behavior. It was decided therefore to use the larger submodels, almost the same size as the global model to ensure that the crack opening behaviour was modeled more accurately.

2.4 Surface Crack Location Submodels

2.4.1 Uncracked Model for Surface Crack Weight Function Calibration

The location of the surface crack is shown in Figure 2.24. Submodeling was performed in two stages to allow a sufficient number of elements in the weld toe region. Figure 2.25 shows the geometry of the coarsely mesh submodel with detailed dimensions given in Figure 2.26. The cracking plane extends into the web from the toe of the fillet weld joining the clip to the side shell stiffener. The fillet weld was assumed to have a 6 mm weld leg with a 1 mm root gap between the clip and the web.

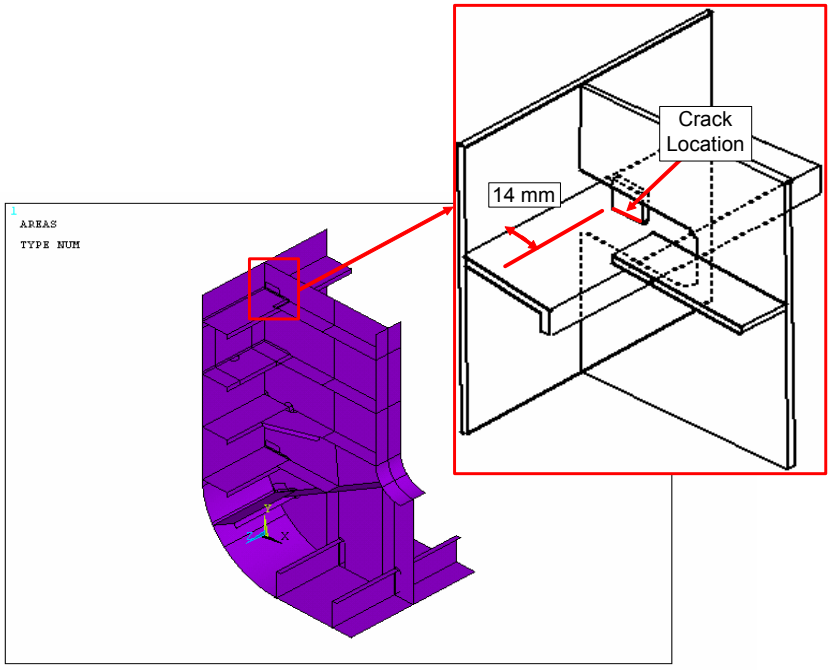

Figure 2.24: Position of Semi-Elliptical Crack Calibration Example in Global Model Geometry

Figure 2.27 shows the weld profile used to join the clip to the side shell stiffener in the coarsely meshed submodel. A 1 mm radius was assumed for the fillet weld toe. Meshing of the submodel was performed using 20 noded ANSYS Solid95 bricks. Five brick elements were placed along the weld toe radius. Through the thickness of the web bricks were set to have a 1 mm edge length and along the length of the weld a 1.5 mm element edge length was specified.

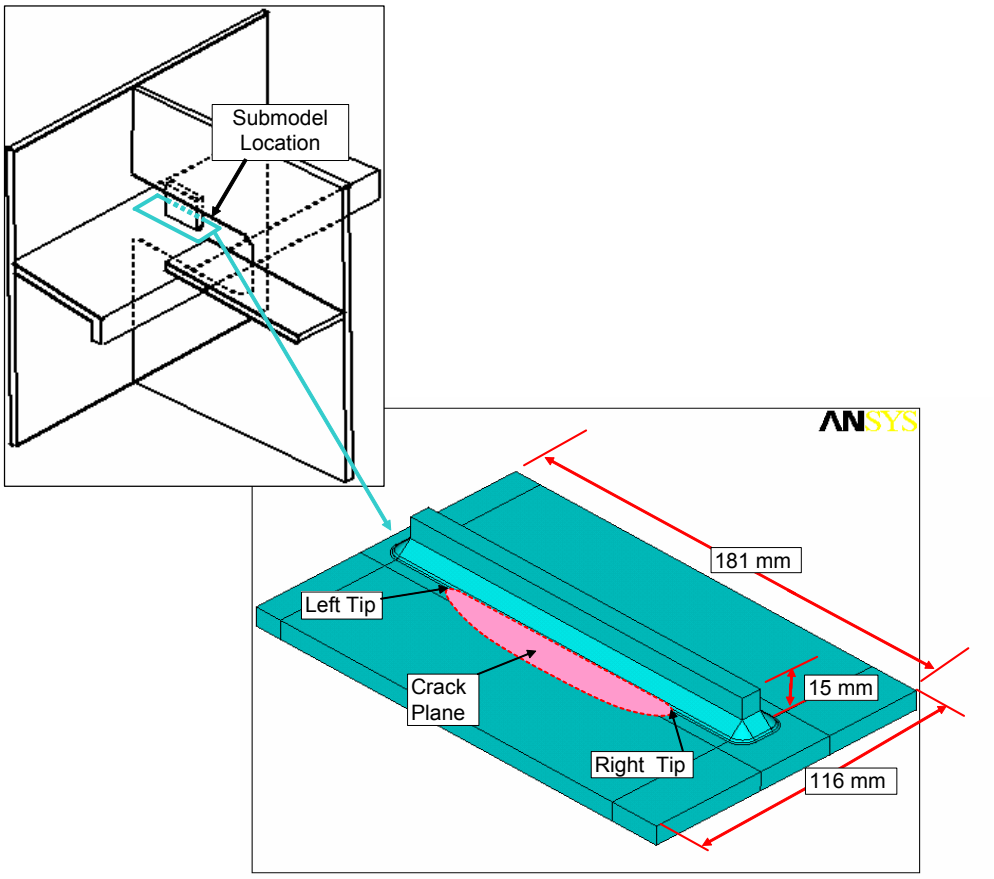

Figure 2.25: Semi-Elliptical Crack Calibration Example Submodel and Location in Global Model

The coarsely meshed model was further refined to ensure a sufficient number of elements in the through thickness direction in the region just below the weld toe to capture the peak stress and the weld toe stress concentration effects. The element mesh was reset to 0.25 mm in the through thickness direction. Using boundary constraints from the coarsely meshed submodel, the fine meshed model (Figure 2.28) was used to generate the through thickness stress profile shown in Figure 2.29.

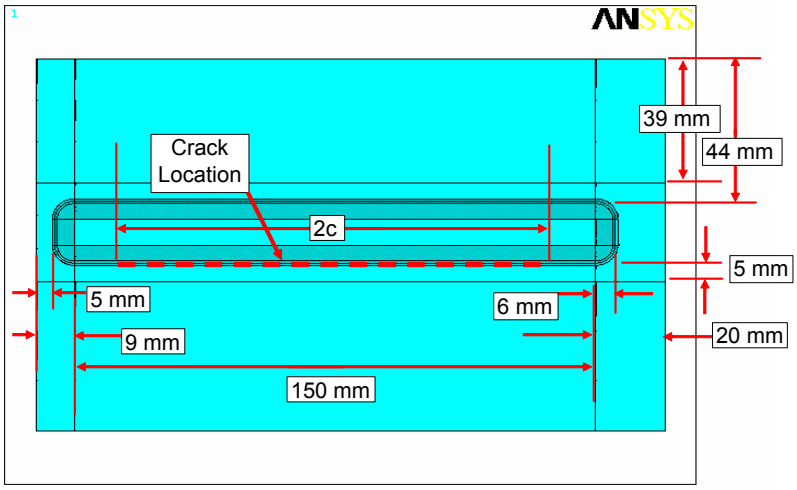

Figure 2.26: Top View of Uncracked Semi-Elliptical Calibration Example with Dimensions

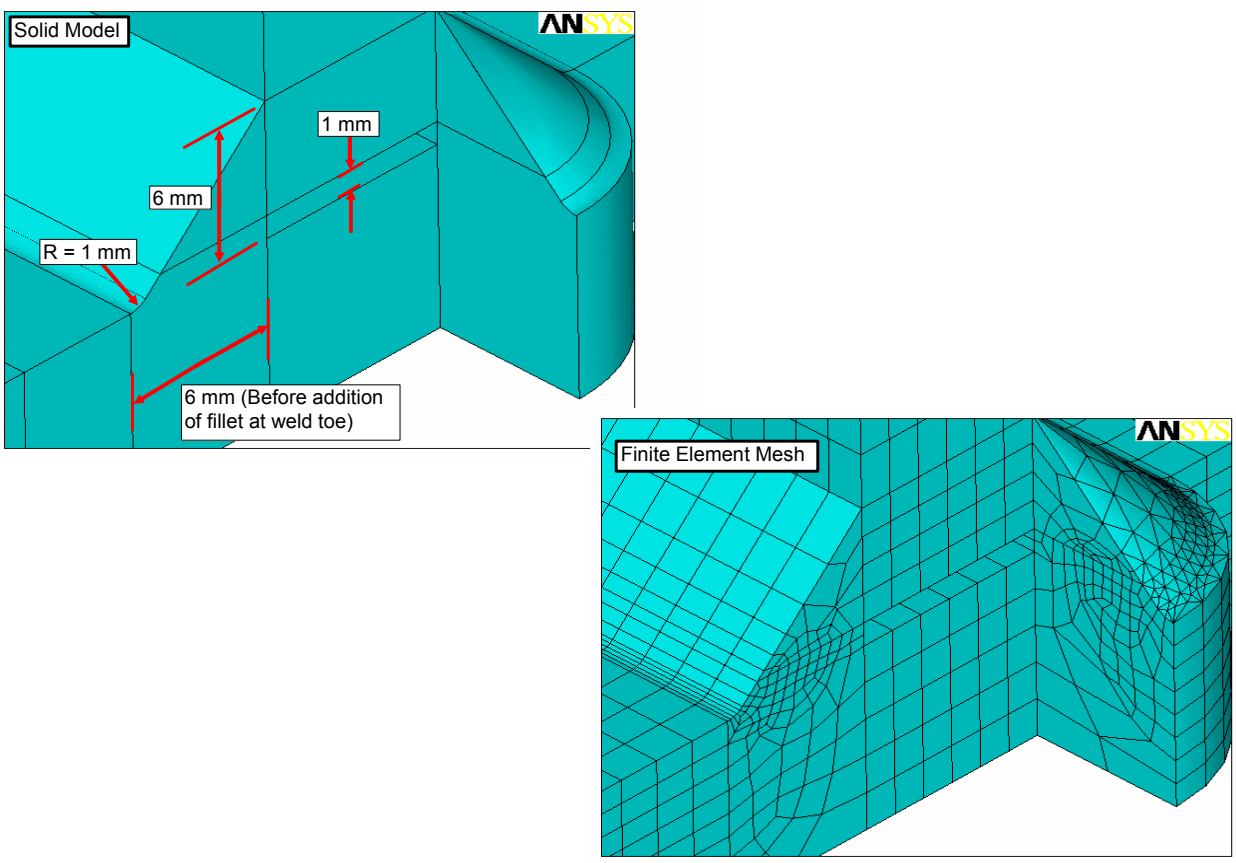

Figure 2.27: Detail of Weld Profile in Solid Model (top left) and Finite Element Mesh (below right) for the Coarsely Meshed Surface Crack Calibration Model

Figure 2.29 shows the distribution of stress oriented perpendicular to the crack plane at mid-length along the crack. This distribution is oriented in the through thickness direction starting at the weld toe at Y = 0 mm.

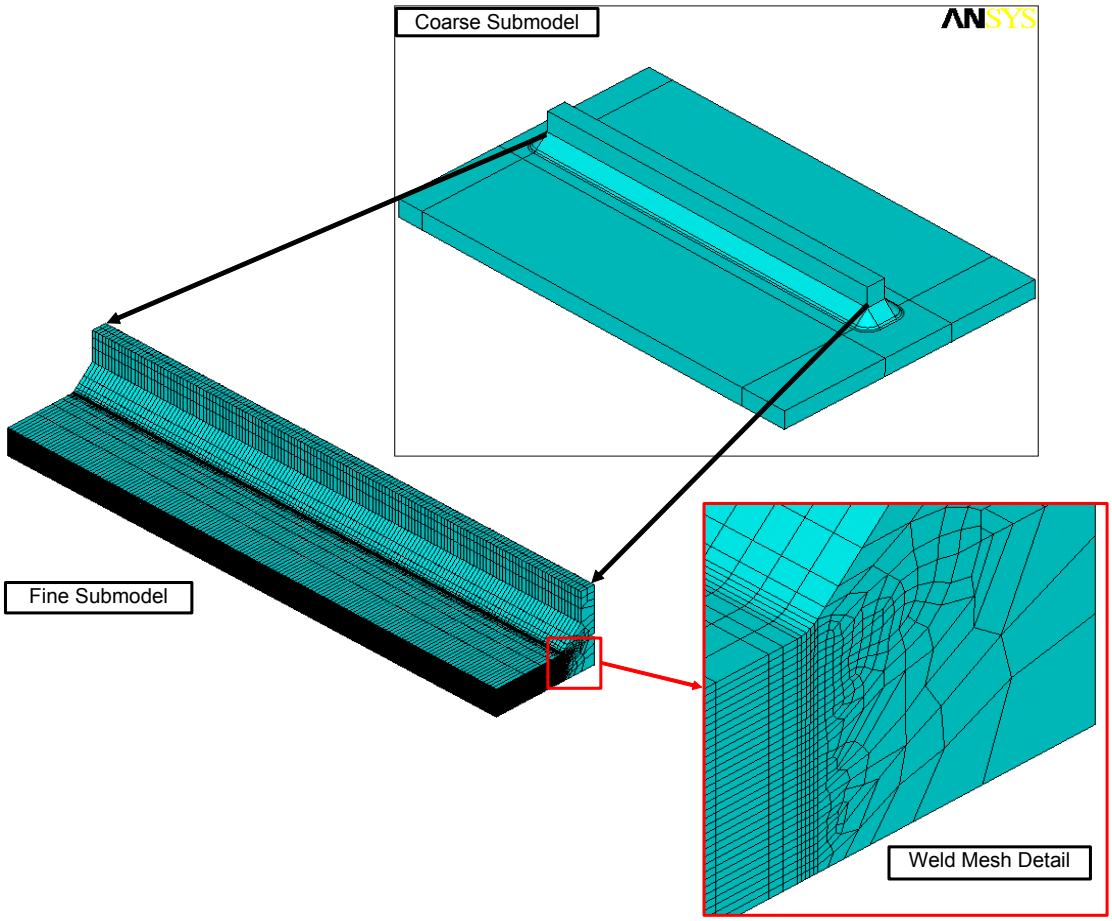

Figure 2.28: Weld Mesh Details in Fine Meshed Submodel for the Surface Crack Calibration Example

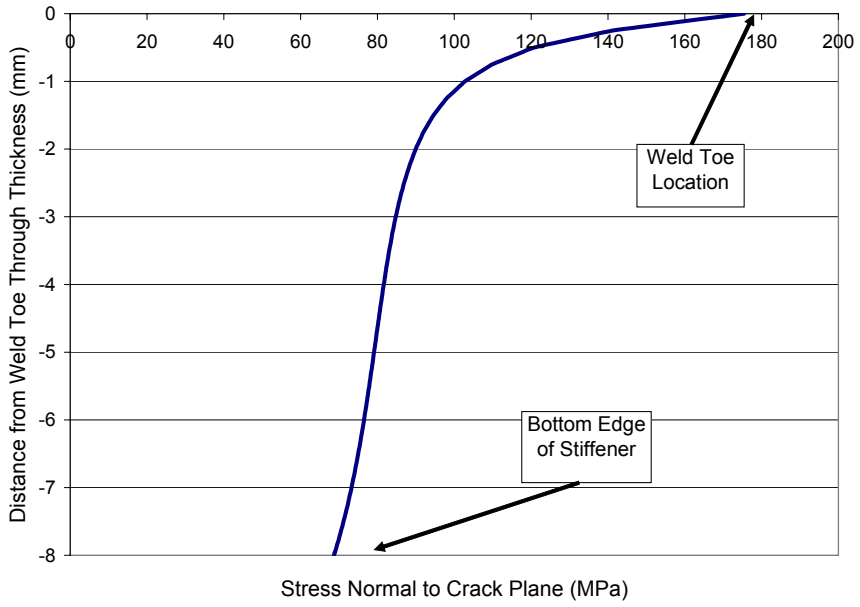

Figure 2.29: Through-Thickness Stress Distribution at Middle of Crack Normal to the Crack Plane in the Surface Crack Calibration Model

2.4.2 Semi-Elliptical Cracked Calibration Submodels

The cracked submodel geometry is shown in Figure 2.30. The model extended 40 mm ahead of the weld toe containing the crack. The entire model was meshed using ANSYS Solid95 brick elements, with crack tip elements used along the crack front. The degree of freedom boundary conditions were extracted from the global model and applied to the edges of this mode. Estimates for K_I were initially taken at the center of the crack (i.e., the deepest point along the crack front) and are presented in Table 2.3 along with the crack dimensions used.

Table 2.4 presents the K_I estimates for the end of the crack identified in Figure 2.30. The method employed in FE model calculations for K_I do not accurately account for free surface effects at the ends of cracks and therefore some researchers have used extrapolation techniques to determine K_I at the surface points. K_I was determined at points along the crack front leading up to the free surface and these values were used to extrapolate to the surface location. Another possible method would be to use K_I values for a set angle (i.e. 5^o) below the surface.

As an example, Figure 2.31 shows the results of the K_I estimates for the 1.6 mm deep, 50 mm long crack along the crack front leading up to the surface. In this case, X = 0 is the surface point of the crack. Setting X = 0 in the polynomials gives the K_I estimate at the crack surface; in this case $K_I = 150$ MPa$(mm)^{1/2}$ at the surface for the plane stress assumption.

An example of the crack tip element mesh used for the 50 mm long and 4.8 mm deep crack is show in Figure 2.32. Along the maximum curvature near the ends of the crack, the element edge length was set to 0.5 mm. For the 1.6 mm deep cracks, the element edge length near the surface was reduced to about 0.2 mm.

At the deepest point of the crack, the stress parallel to the crack plane varies from about 20 MPa at a depth of 1.6 mm to about 13.7 MPa at a depth of 4.8 mm which is 20% and 18%, respectively, of the stress normal to the crack plane. The stress state for the deepest points on the semi-elliptical crack front would be more conservatively estimated assuming a state of plain strain. At the free surface point, the stress state will be plane stress. The weight function estimates will therefore be compared to the ANSYS plane strain values at the deepest point and the ANSYS plane stress values at the surface point.

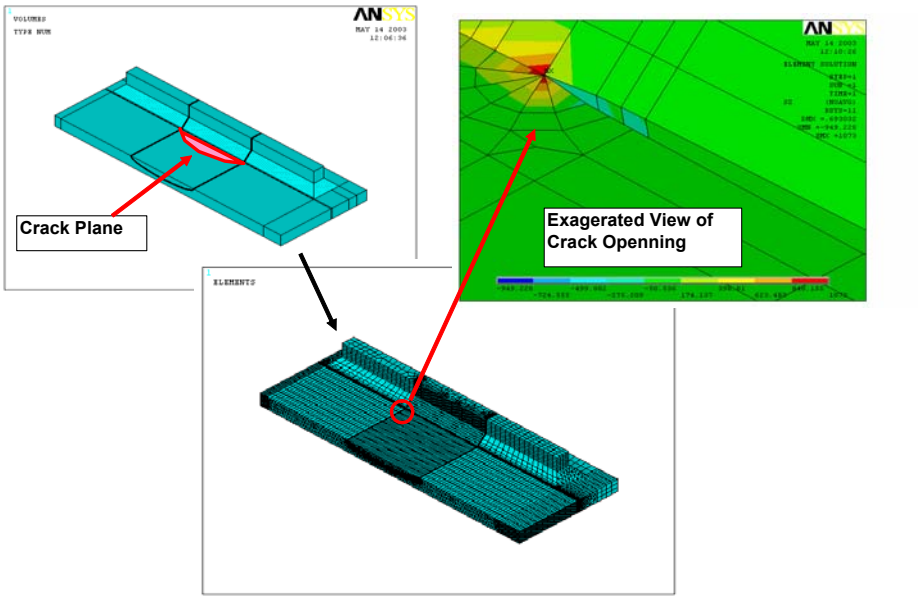

Figure 2.30: Semi-Elliptical Calibration Crack Submodel Containing Crack Tip Elements

Table 2.3: K_I Estimates for the Deepest Point of the Semi-Elliptical Cracks

Crack Length, 2c (mm)	Crack Depth, a (mm)	ANSYS K_I Estimates MPa(mm)$^{1/2}$	
		Plane Strain	Plane Stress
50	**1.6**	254	
100	**1.6**	272	
50	**3.2**	330	300
100	**3.2**	359	327
50	**4.8**	389	354
100	**4.8**	442	402

KI estimates in Table 2.4 from this End

Table 2.4: K_I Estimates for the Surface Point of the Semi-Elliptical Cracks Shown in Figure 2.26

Crack Length, 2c (mm)	Crack Depth, a (mm)	ANSYS K_I Estimates $MPa(mm)^{1/2}$
		Plane Stress
50	**1.6**	150
100	**1.6**	262
50	**3.2**	188
100	**3.2**	161
50	**4.8**	277
100	**4.8**	242

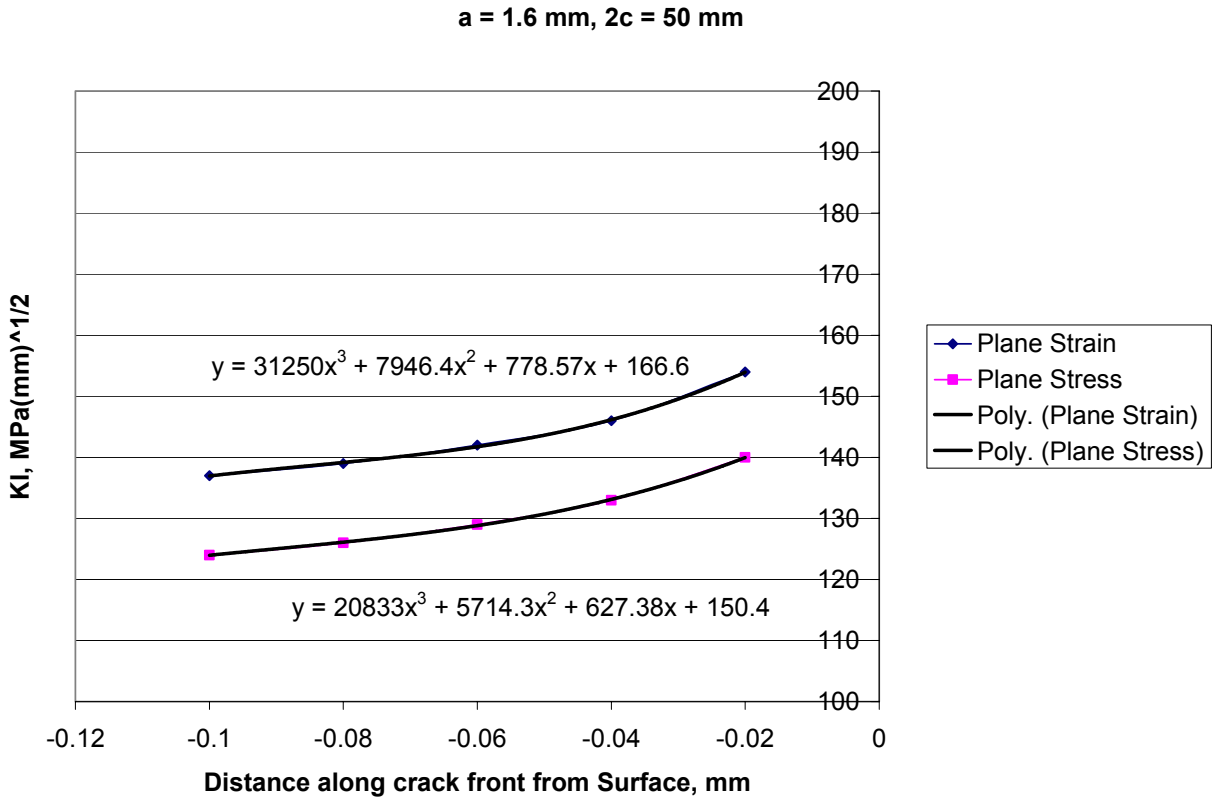

Figure 2.31: Sub-Surface K_I Estimates Along Crack Front used to Estimate K_I at the Surface of the Semi-Elliptical Calibration Crack with a = 1.6 mm and 2c = 50 mm

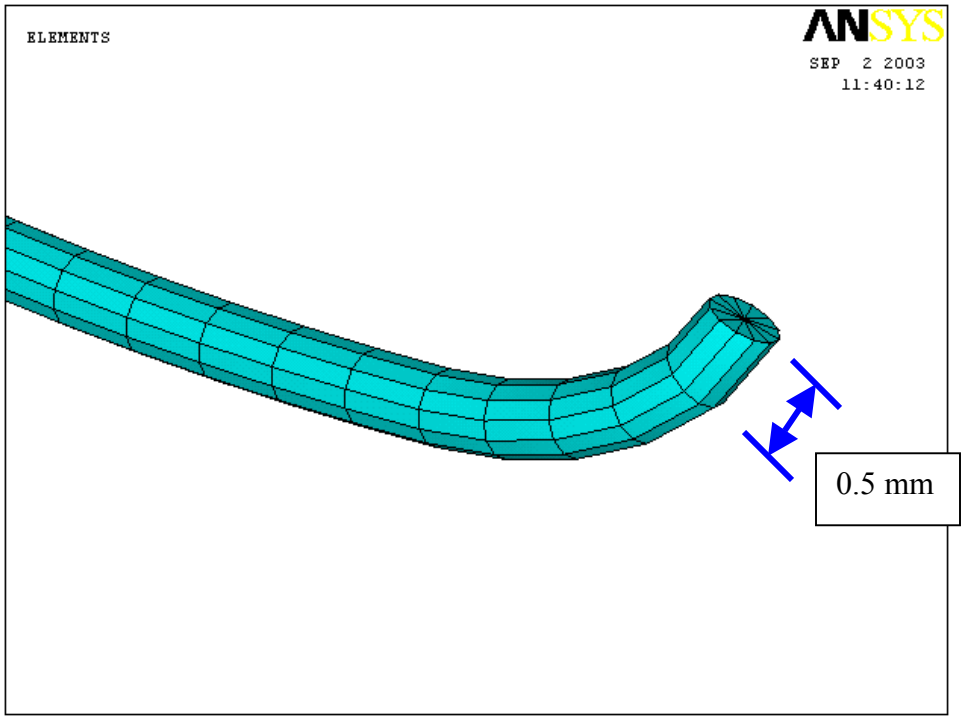

Figure 2.32: Element Mesh Along the Crack Front for the 4.8 mm Deep, 50 mm Long Surface Crack

3. WEIGHT FUNCTION SOLUTIONS FOR CALIBRATION MODELS

The following section describes the weight function theory, and documents the results of the application of the weight function solutions to the calibration models described in Section 2. The standard weight function solutions for edge, through-thickness and semi-elliptical cracks are presented first, followed by a discussion of how they were applied to the calibration examples to obtain estimates of the stress intensity factor for the crack sets.

3.1 Calculation of Stress Intensity Factors Using the Weight Function Approach

The calculation of stress intensity factors accounting for non-uniform stress distributions in welded joints requires the derivation of a special method enabling the analysis of cracks growing through a high gradient stress field. Figure 3.1 illustrates the definition of the stress perpendicular to the crack plane required for the weight function approach for edge crack and through thickness crack examples. The required stress profile for a surface crack is shown in Figure 3.2.

In general, the stress distribution is extracted from the mid-point along the crack front with X = 0 and the crack mouth for an edge or surface crack, or the mid-length of a through thickness crack. X = a is located at the crack front. The primary assumption is that the stress is uniform over the crack plane. The Shen-Glinka weight functions presented in this report do not specifically account for out of plane bending. Under such loading conditions K_I would vary along the crack front and to obtain estimates for the variation in K_I, the stress profile corresponding to the specific location on the crack front can be used.

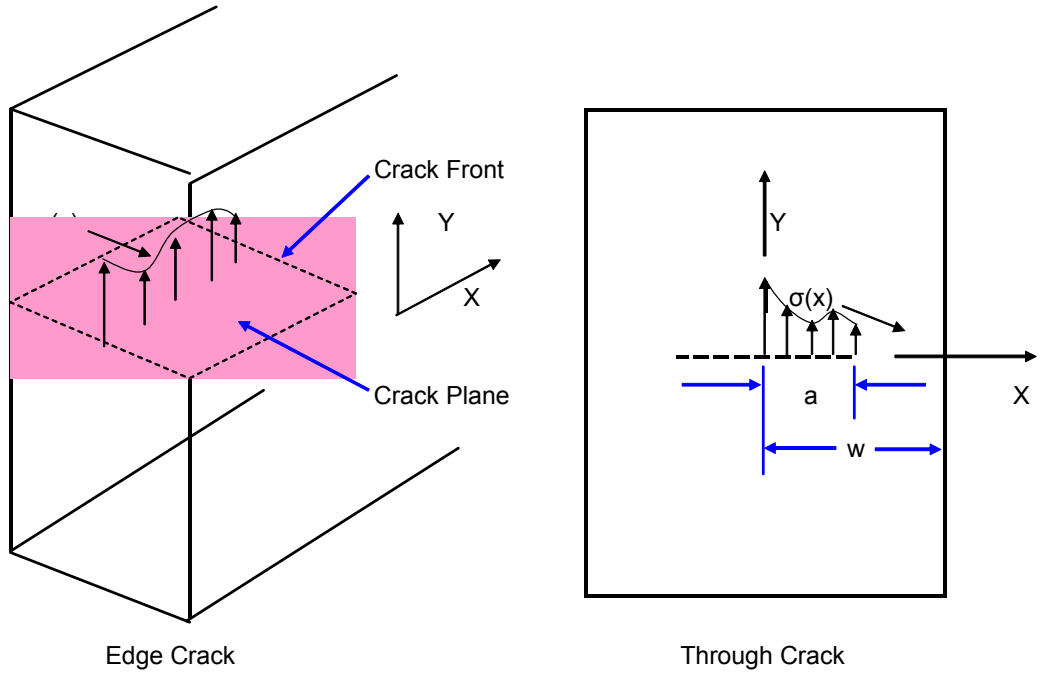

Figure 3.1: Required Stress Profiles for Weight Function Solutions for Edge and Through Cracks

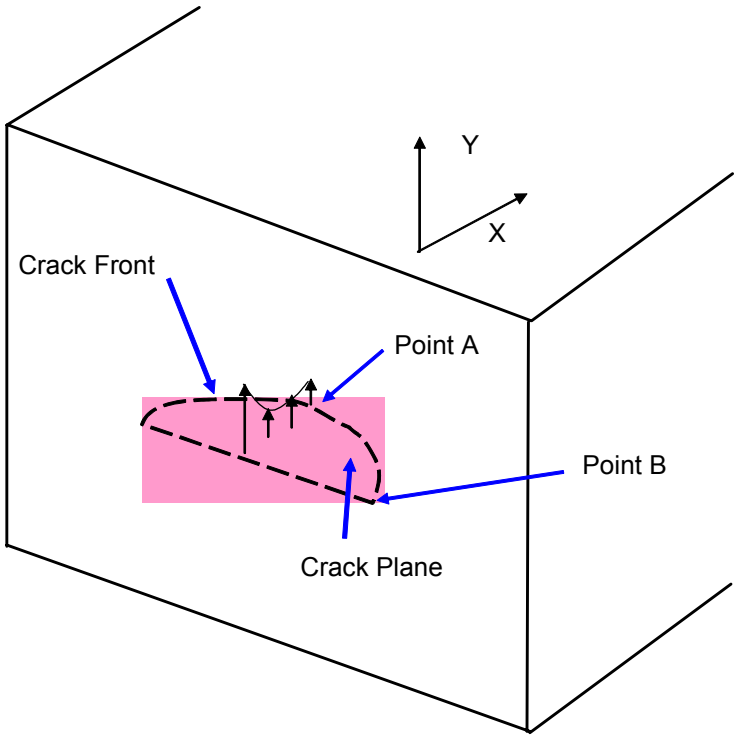

Figure 3.2: Require Stress Profile for Weight Function Solution for a Semi-elliptical Surface Crack

The weight function technique [2, 3] has been used in this project and the weight functions for edge and through cracks were derived in the form of one general expression, Eqn. 3.1 [4, 5].

$$m(x,a)=\frac{2}{\sqrt{2\pi(a-x)}}\left[1+M_1\left(1-\frac{x}{a}\right)^{\frac{1}{2}}+M_2\left(1-\frac{x}{a}\right)^{1}+M_3\left(1-\frac{x}{a}\right)^{\frac{3}{2}}\right] \qquad (3.1)$$

The weight function for the deepest point in a semi-elliptical surface crack (referred to as Point A in the context of this report) is given by Eqn 3.2, while the weight function for the surface point (referred to as Point B) is given by Eqn 3.3.

$$m_A(x,a)=\frac{2}{\sqrt{2\pi(a-x)}}\left[1+M_{1A}\left(1-\frac{x}{a}\right)^{\frac{1}{2}}+M_{2A}\left(1-\frac{x}{a}\right)^{1}+M_{3A}\left(1-\frac{x}{a}\right)^{\frac{3}{2}}\right] \qquad (3.2)$$

$$m_B(x,a)=\frac{2}{\sqrt{\pi x}}\left[1+M_{1B}\left(\frac{x}{a}\right)^{\frac{1}{2}}+M_{2B}\left(\frac{x}{a}\right)^{1}+M_{3B}\left(\frac{x}{a}\right)^{\frac{3}{2}}\right] \qquad (3.3)$$

The specifics related to the geometries of the cracks and base plates will be discussed later in this section.

Parameters M_1, M_2, and M_3 appropriate for the crack geometries covered in the scope of this project will be discussed shortly. They were derived using two reference stress intensity factors [5] and properties of the weight function. The form of the equations and number of terms in the series expansions are sufficient to provide K_I estimates in agreement with comparable analytical solutions to an accuracy usually better than 3%.

The stress intensity factor for a one dimensional crack can be obtained by multiplying the weight function, m(x,a), and the internal stress distribution, σ(x), in the prospective crack plane and integrating the product over the crack length 'a' (Eqn. 3.4) as depicted schematically in Figure 3.1.

$$K = \int_0^a \sigma(x) m(x,a) dx \qquad (3.4)$$

In order to calculate stress intensity factors using the weight function technique the following tasks need to be carried out:

- Determine the stress distribution, σ(x), in the prospective crack plane using linear elastic analysis of the un-cracked body, i.e. perform the stress analysis ignoring the crack and determine the stress distribution $\sigma(x) = \sigma_0 f(S,x)$;
- Apply the "un-cracked" stress distribution, σ(x), to the crack surfaces as a traction,
- Choose the appropriate generic weight function,
- Integrate the product of the stress function, σ(x), and the weight function, m(x,a), over the entire crack length or crack surface, Eqn.(3.2).

This approach can be used for calculating stress intensity factors for any non-linear stress distribution providing that the stress function, σ(x), is known. Very often the stress distribution is obtained numerically by using the finite element or the boundary element method and the closed form stress function describing the stress distribution is unknown. Therefore, special methods of integration of Eqn.3.2 have been developed, enabling calculation of stress intensity factors for any stress field given by a series of discrete stress points (such as the nodal stress values for example).

3.1.1 Numerical Integration Methods

The calculation of a stress intensity factor from a weight function requires integration of the product "σ(x) m(x,a)" along the crack length according to Eqn. 3.2. The weight function itself can always be written in the general form of Eqn. 3.1. However, the stress distribution "σ(x)" can take any form depending on the problem of interest. If the stress distribution is given in the form of a closed mathematical expression, analytical integration can be performed and closed form integrals of Eqn.3.2 are sometimes feasible. However, when the stress distribution "σ(x)" is obtained from finite element calculations, the results are given as a series of stress values corresponding to a range of points of the coordinate "x".

Therefore, a numerical integration technique is needed for the integration and the calculation of stress intensity factors. Two methods of efficient integration are described in this document.

a) Integration by using the centroids of areas under the weight function curve.

The integration method using the area centroids is based on the following theorem:

If m(x,a) and σ(x) are monotonic and linear functions respectively and both depend on variable x only, (Figure 3.3), then the integral in Eqn. 3.2 can be calculated from Eqn. 3.5, representing the product of the area, S, under the curve m(x,a) and the value of the stress function, σ(X), at the co-ordinate x = X corresponding to the centroid, C.

$$K = S \times \sigma(X) \qquad (3.5)$$

The weight functions, m(x,a), are monotonic and non-linear. The stress functions, σ(x), are usually non-linear as well. Therefore, in order to apply the theorem above to the integral, the integration interval is divided into "n" sub-intervals in such a way that the stress function, σ(x), is approximated by the secant line drawn between the end points of each sub-interval as illustrated in Figure 3.4. Thus, the approximate stress function, σ(x), over the sub-interval 'i', may be written in the form of Eqn. 3.6.

$$\sigma_i(x) = A_i x + B_i \quad for \quad x_{i-1} \le x \le x_i \qquad (3.6)$$

where:

$$A_i = \frac{\sigma(x_i) - \sigma(x_{i-1})}{x_i - x_{i-1}} \; and \; B_i = \sigma(x_i) - A_i x_i \qquad (3.6a)$$

After substitution of Eqn. 3.6 into Eqn. 3.4 and summation over all sub-intervals, the Eqn. 3.7 can be derived.

$$K = \sum_{i=1}^{n} \int_{x_{i-1}}^{x_i} (A_i x + B_i)\, m(x,a)dx \qquad (3.7)$$

Each integral in Eqn.3.5 can be computed by using the simplified integration method given in the form of Eqn. 3.3. Thus, the stress intensity factor, K, can be finally written in the form of Eqn 3.8.

$$K = \sum_{i}^{n} S_i * \sigma(X_i), \qquad where \quad i = 1,2,...,n \qquad (3.8)$$

In order to calculate the stress intensity factor given in the form of Eqn. 3.8, it is necessary to calculate the areas, S_i, under the weight function curve, m(x,a), and the co-ordinates of their centroids, X_i. The area, S_i, and the centroid co-ordinate, X_i, for each sub-interval need to be calculated only once in a general form based on the generalized weight functions Eqn. 3.1 to 3.3. However, the end results are too lengthy for efficient hand calculations. Fortunately, further simplification of the integration routine is possible due to the fact that the weight functions are smooth within their ranges of integration. Therefore, the procedure can be reversed by calculating first the areas, S_i^*, under the stress function, σ(x), and the co-ordinates, X_i^*, of their centroids.

Then the appropriate values, $m(X^*,a)$, of the weight function, m(x,a), can be calculated from Eqn. 3.1 to 3.3 for the crack of interest. It is worth noting that in the case of the piece-wise approximation of the stress function, σ(x), the areas, S_i^*, and the co-ordinates, X_i^*, of their centroids can be easily calculated from Eqn. 3.9 and Eqn. 3.10 respectively.

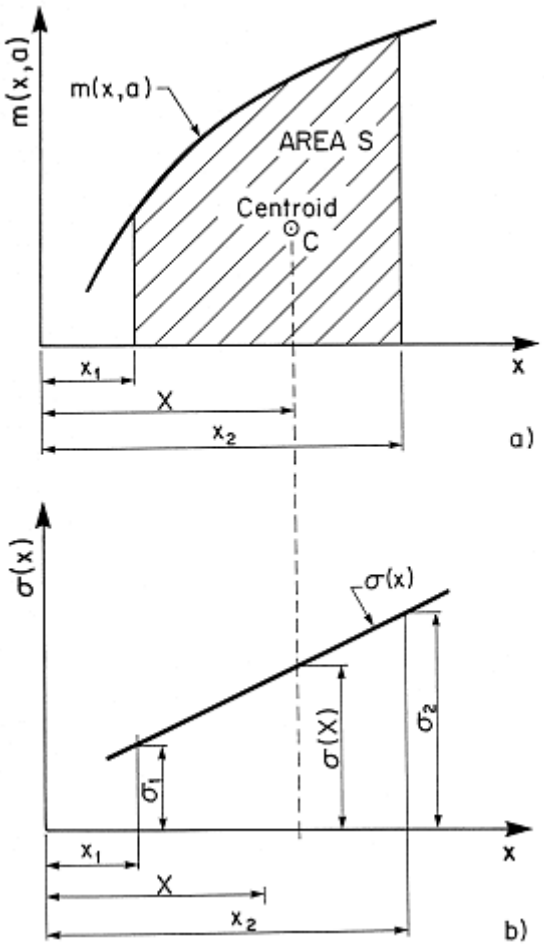

Figure 3.3: Graphical Explanation of the Simplified Numerical Integration Method Using Centroids of the Areas under the Nonlinear Weight Function with a Linear Stress Function

$$S_i^* = \frac{1}{2}\left[\sigma(x_i)+\sigma(x_{i-1})\right](x_i - x_{i-1}) \tag{3.9}$$

$$X_i^* = x_i - \frac{(x_i - x_{i-1})\left[2\sigma(x_{i-1})+\sigma(x_i)\right]}{3\left[\sigma(x_{i-1})+\sigma(x_i)\right]} \tag{3.10}$$

Finally the stress intensity factor, K, is calculated from Eqn. 3.11.

$$K = \sum_{i=1}^{n} S_i^* \times m\left(X_i^*, a\right) \tag{3.11}$$

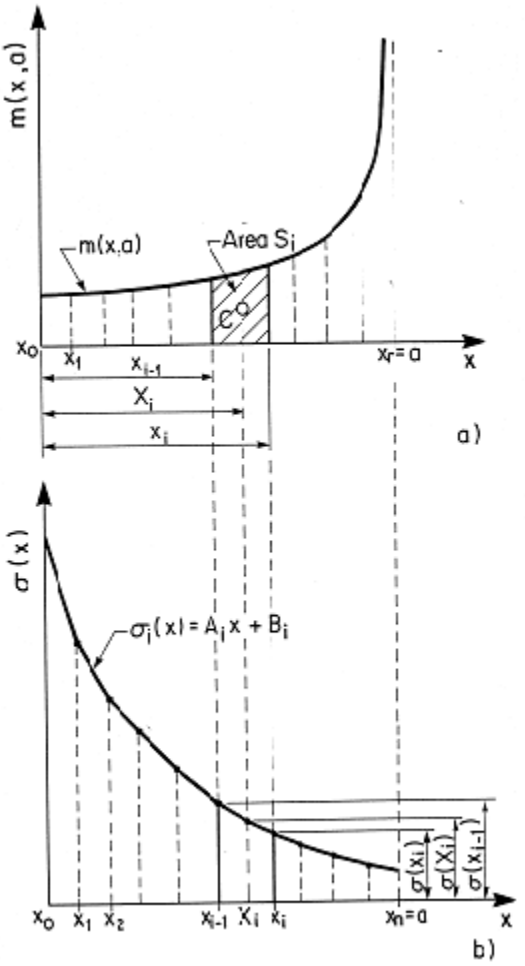

Figure 3.4: Graphical Explanation of the Simplified Numerical Integration Method Using Centroids of the Areas under the Nonlinear Weight Function with a Nonlinear Stress Function

Thus, the numerical procedure for calculating the stress intensity factor using the integration method described above requires the calculation of appropriate parameters using equations 3.1 to 3.3 and 3.9 to 3.11. The method described above is recommended for quick approximate calculations with the help of hand calculator.

(b) Analytical integration of the linearized piecewise stress distribution and the weight function:

The integration technique described above is convenient for a hand calculator calculation when a few linear segments can approximate the stress distribution. However, the segments adjacent to the crack tip cannot be large because the weight function tends to infinity near the crack tip and if the stress is the highest near the crack tip, the method described above might be inaccurate. Moreover, in the case of stress distributions characterized by high gradients, accurate approximation of the stress distribution requires a relatively large number of linear segments and the integration has to be carried out with the help of a computer. However, the computer integration routine can also be significantly simplified because closed form solutions to the integral can be derived analytically for each linear piece of the stress function $\sigma(x)$.

The stress function, $\sigma(x)$, over the linear segment 'i' can be given in the form of the linear equation, Eqn. 3.6. Thus, the contribution to the stress intensity factor associated with the stress segment 'i' can be calculated from Eqn. 3.4 after substituting appropriate expressions for the stress and the weight function.

$$K_i = \int_{x_{i-1}}^{x_i} (A_i x + B_i) \frac{2}{\sqrt{2\pi a\left(1-\frac{x}{a}\right)}} \left[1 + M_1\left(1-\frac{x}{a}\right)^{\frac{1}{2}} + M_2\left(1-\frac{x}{a}\right)^{1} + M_3\left(1-\frac{x}{a}\right)^{\frac{3}{2}}\right] dx \qquad (3.12)$$

The closed form expression resulting from the integration of Eqn. 3.12 is given below.

$$K_i = \sqrt{\frac{2}{\pi a}}\left[\begin{array}{l}\alpha_i\left(C_{i1} + M_1 C_{i2} + M_2 C_{i3} + M_3 C_{i4}\right) \\ \qquad + \beta_i\left(C_{i3} + M_1 C_{i4} + M_2 C_{i5} + M_3 C_{i6}\right)\end{array}\right] \qquad (3.13)$$

Where:

$$\alpha_i = B_i + aA_i \qquad \text{and} \qquad \beta_i = -aA_i$$

$$C_{i1} = 2a\left[\left(1-\frac{x_{i-1}}{a}\right)^{\frac{1}{2}} - \left(1-\frac{x_i}{a}\right)^{\frac{1}{2}}\right] \qquad C_{i2} = a\left[\left(1-\frac{x_{i-1}}{a}\right)^{1} - \left(1-\frac{x_i}{a}\right)^{1}\right]$$

$$C_{i3} = \frac{2a}{3}\left[\left(1-\frac{x_{i-1}}{a}\right)^{\frac{3}{2}} - \left(1-\frac{x_i}{a}\right)^{\frac{3}{2}}\right] \qquad C_{i4} = \frac{a}{2}\left[\left(1-\frac{x_{i-1}}{a}\right)^{2} - \left(1-\frac{x_i}{a}\right)^{2}\right]$$

$$C_{i5} = \frac{2a}{5}\left[\left(1-\frac{x_{i-1}}{a}\right)^{\frac{5}{2}} - \left(1-\frac{x_i}{a}\right)^{\frac{5}{2}}\right] \qquad C_{i6} = \frac{a}{3}\left[\left(1-\frac{x_{i-1}}{a}\right)^{3} - \left(1-\frac{x_i}{a}\right)^{3}\right]$$

Equation 3.13 can be used for calculating stress intensity contributions due to each linear piece of the stress distribution function by substituting appropriate values for a, x_{i-1}, x_i, A_i and B_i. The stress intensity factor K can be finally calculated as the sum of all contributions K_i associated with all linear pieces within the range of $0 \le x \le a$.

$$K = \sum_{1}^{n} K_i \tag{3.14}$$

Thus, the integration can be reduced to the substitution of appropriate parameters into Eqn. 3.13 and summation according to Eqn. 3.14. Such a method makes it possible to develop a very efficient numerical integration routine, applicable to lengthy fatigue crack growth analyses.

3.2 Weight Function for an Edge Crack in a Finite Width Plate

The following equations provide the expressions for M_1, M_2 and M_3 required for the weight function solution for an edge crack in a finite width plate valid for $0 < {}^{a}/_{w} < 0.9$. The geometry is described in Figure 3.5.

$$M_1 = \frac{-0.029207 + \frac{a}{w}\left(0.213074 + \frac{a}{w}\left(-3.029553 + \frac{a}{w}\left(5.901933 + \frac{a}{w}\left(-2.657820\right)\right)\right)\right)}{1.0 + \frac{a}{w}\left(-1.259723 + \frac{a}{w}\left(-0.048475 + \frac{a}{w}\left(0.481250 + \frac{a}{w}\left(-0.526796 + \frac{a}{w}\left(0.345012\right)\right)\right)\right)\right)}$$

$$M_2 = \frac{0.451116 + \frac{a}{w}\left(3.462425 + \frac{a}{w}\left(-1.078459 + \frac{a}{w}\left(3.558573 + \frac{a}{w}\left(-7.553533\right)\right)\right)\right)}{1.0 + \frac{a}{w}\left(-1.496612 + \frac{a}{w}\left(0.764586 + \frac{a}{w}\left(-0.659316 + \frac{a}{w}\left(0.258506 + \frac{a}{w}\left(0.114568\right)\right)\right)\right)\right)}$$

$$M_3 = \frac{0.427195 + \frac{a}{w}\left(-3.730114 + \frac{a}{w}\left(16.276333 + \frac{a}{w}\left(-18.799956 + \frac{a}{w}\left(14.112118\right)\right)\right)\right)}{1.0 + \frac{a}{w}\left(-1.129189 + \frac{a}{w}\left(0.033758 + \frac{a}{w}\left(0.192114 + \frac{a}{w}\left(-0.658242 + \frac{a}{w}\left(0.554666\right)\right)\right)\right)\right)}$$

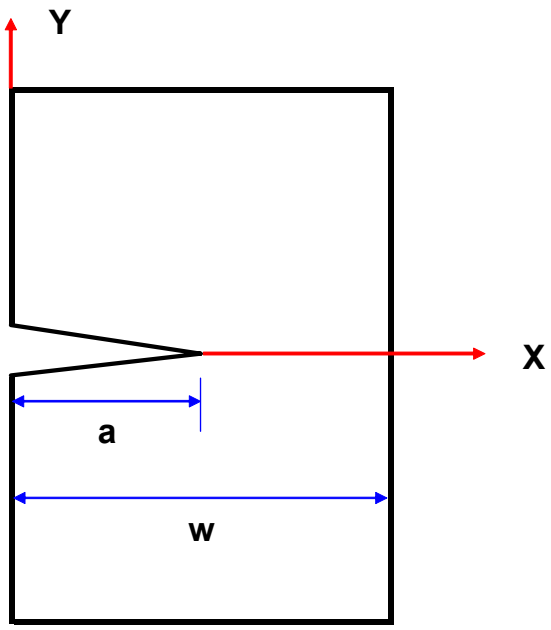

Figure 3.5: Edge Crack in a Finite Width Plate

3.3 Weight Function for a Through-Thickness Crack in a Finite Width Plate

The following equations give M1, M2 and M3 applicable to a weight function solution for a central through-thickness crack in a finite width plate subjected to symmetric loading, valid for $0 < {}^{a}/_{w} < 0.9$. The geometry is illustrated in Figure 3.6.

$$M_1 = 0.06987 + 0.40117\left(\frac{a}{w}\right) - 5.5407\left(\frac{a}{w}\right)^2 + 50.0886\left(\frac{a}{w}\right)^3 - 200.699\left(\frac{a}{w}\right)^4 + 395.552\left(\frac{a}{w}\right)^5 - 377.939\left(\frac{a}{w}\right)^6 + 140.218\left(\frac{a}{w}\right)^7$$

$$M_2 = -0.09049 - 2.14886\left(\frac{a}{w}\right) + 22.5325\left(\frac{a}{w}\right)^2 - 89.6553\left(\frac{a}{w}\right)^3 + 210.599\left(\frac{a}{w}\right)^4 - 239.445\left(\frac{a}{w}\right)^5 - 111.128\left(\frac{a}{w}\right)^6$$

$$M_3 = 0.427216 + 2.56001\left(\frac{a}{w}\right) - 29.6349\left(\frac{a}{w}\right)^2 + 138.40\left(\frac{a}{w}\right)^3 - 347.255\left(\frac{a}{w}\right)^4 + 457.128\left(\frac{a}{w}\right)^5 - 295.882\left(\frac{a}{w}\right)^6 + 68.1575\left(\frac{a}{w}\right)^7$$

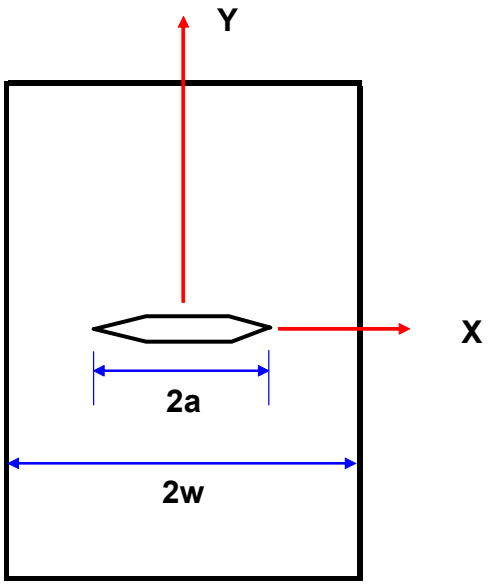

Figure 3.6: Central Through-Thickness Crack in a Finite Width Plate

3.4 Weight Function for a Surface Crack in a Finite Thickness Plate

The weight function solution for the deepest point in a semi-elliptical surface crack in a finite thickness plate (Point A in Figure 3.7) uses the following values of M_1, M_2 and M_3 for $0 < {}^{a}/_{t} \leq 0.8$ and $0 < {}^{a}/_{c} \leq 1.0$.

$$M_{1A} = \frac{2\pi}{\sqrt{2Q}}\left(2Y_0 - 3Y_1\right) - \frac{24}{5}$$

$$M_{2A} = 3$$

$$M_{3A} = \frac{6\pi}{\sqrt{2Q}}\left(2Y_1 - Y_0\right) + \frac{8}{5}$$

Where:

$$Q = 1 + 1.464\left(\frac{a}{c}\right)^{1.65}$$

$$Y_0 = A_0 + A_1\left(\frac{a}{t}\right)^2 + A_2\left(\frac{a}{t}\right)^4 + A_3\left(\frac{a}{t}\right)^6$$

$$A_0 = 1.0929 + 0.2581\left(\frac{a}{c}\right) - 0.7703\left(\frac{a}{c}\right)^2 + 0.4394\left(\frac{a}{c}\right)^3$$

$$A_1 = 0.456 - 3.045\left(\frac{a}{c}\right) + 2.007\left(\frac{a}{c}\right)^2 + \frac{1}{0.147 + \left(\frac{a}{c}\right)^{0.688}}$$

$$A_2 = 0.995 - \frac{1}{0.027 + \left(\frac{a}{c}\right)} + 22.0\left[1 - \left(\frac{a}{c}\right)\right]^{9.953}$$

$$A_3 = -1.459 + \frac{1}{0.014 + \left(\frac{a}{c}\right)} - 24.211\left[1 - \left(\frac{a}{c}\right)\right]^{8.071}$$

and

$$Y_1 = B_0 + B_1\left(\frac{a}{t}\right)^2 + B_2\left(\frac{a}{t}\right)^4 + B_3\left(\frac{a}{t}\right)^6$$

$$B_0 = 0.4537 + 0.1231\left(\frac{a}{c}\right) - 0.7412\left(\frac{a}{c}\right)^2 + 0.460\left(\frac{a}{c}\right)^3$$

$$B_1 = -1.652 + 1.665\left(\frac{a}{c}\right) - 0.534\left(\frac{a}{c}\right)^2 + \frac{1}{0.198 + \left(\frac{a}{c}\right)^{0.846}}$$

$$B_2 = 3.418 - 3.126\left(\frac{a}{c}\right) - \frac{1}{0.041 + \left(\frac{a}{c}\right)} + 17.259\left[1 - \left(\frac{a}{c}\right)\right]^{9.286}$$

$$B_3 = -4.228 + 3.643\left(\frac{a}{c}\right) + \frac{1}{0.020 + \left(\frac{a}{c}\right)} - 21.924\left[1 - \left(\frac{a}{c}\right)\right]^{9.203}$$

For the surface, Point B, the following equations apply:

$$M_{1B} = \frac{3\pi}{\sqrt{Q}}\left(5F_1 - 3F_0\right) - 8$$

$$M_{2B} = \frac{15\pi}{\sqrt{Q}}\left(2F_0 - 3F_1\right) + 15$$

$$M_{3B} = \frac{3\pi}{\sqrt{Q}}\left(10F_1 - 7F_0\right) - 8$$

Where:

$$Q = 1 + 1.464\left(\frac{a}{c}\right)^{1.65}$$

$$F_0 = \left[C_0 + C_1\left(\frac{a}{t}\right)^2 + C_2\left(\frac{a}{t}\right)^4\right]\sqrt{\frac{a}{c}}$$

$$C_0 = 1.2972 - 0.1548\left(\frac{a}{c}\right) - 0.0185\left(\frac{a}{c}\right)^2$$

$$C_1 = 1.5083 - 1.3219\left(\frac{a}{c}\right) + 0.5128\left(\frac{a}{c}\right)^2$$

$$C_2 = -1.101 + \frac{0.879}{0.157 + \left(\frac{a}{c}\right)}$$

and

$$F_1 = \left[D_0 + D_1\left(\frac{a}{t}\right)^2 + D_2\left(\frac{a}{t}\right)^4\right]\sqrt{\frac{a}{c}}$$

$$D_0 = 1.2687 - 1.0642\left(\frac{a}{c}\right) + 1.4646\left(\frac{a}{c}\right)^2 - 0.7250\left(\frac{a}{c}\right)^3$$

$$D_1 = 1.1207 - 1.2289\left(\frac{a}{c}\right) + 0.5876\left(\frac{a}{c}\right)^2$$

$$D_2 = 0.190 - 0.608\left(\frac{a}{c}\right) + \frac{0.199}{0.035 + \left(\frac{a}{c}\right)}$$

For $0 \le {}^{a}/_{t} \le 0.8$ and $1.0 < {}^{a}/_{c} \le 2.0$ at the deepest Point A:

$$M_{1A} = \frac{2\pi}{\sqrt{2Q}}\left(2Y_0 - 3Y_1\right) - \frac{24}{5}$$

$$M_{2A} = 3$$

$$M_{3A} = \frac{6\pi}{\sqrt{2Q}}\left(2Y_1 - Y_0\right) + \frac{8}{5}$$

Where:

$$Q = \begin{cases} 1 + 1.464\left(\frac{a}{c}\right)^{1.65} & for\ 0 \le {}^{a}/_{c} \le 1.0 \\ \left[1 + 1.464\left(\frac{c}{a}\right)^{1.65}\right]\left(\frac{a}{c}\right)^{2} & for\ {}^{a}/_{c} > 1.0 \end{cases}$$

$$Y_0 = A_0 + A_1\left(\frac{a}{t}\right)^2 + A_2\left(\frac{a}{t}\right)^4$$

$$A_0 = 1.13047 - 0.12945\left(\frac{a}{c}\right) + 0.03526\left(\frac{a}{c}\right)^2$$

$$A_1 = 1.08461 - 1.01106\left(\frac{a}{c}\right) + 0.2454\left(\frac{a}{c}\right)^2$$

$$A_2 = 0.7855 + 0.5517\left(\frac{a}{c}\right) - 0.0934\left(\frac{a}{c}\right)^2$$

and

$$Y_1 = B_0 + B_1\left(\frac{a}{t}\right)^2 + B_2\left(\frac{a}{t}\right)^4$$

$$B_0 = 0.5044 - 0.2609\left(\frac{a}{c}\right) + 0.0529\left(\frac{a}{c}\right)^2$$

$$B_1 = 0.7259 - 0.6352\left(\frac{a}{c}\right) + 0.1492\left(\frac{a}{c}\right)^2$$

$$B_2 = -0.6459 + 0.4177\left(\frac{a}{c}\right) - 0.0731\left(\frac{a}{c}\right)^2$$

For $0 \le {}^{a}/_{t} \le 0.8$ and $1.0 < {}^{a}/_{c} \le 2.0$ at the surface Point B:

$$M_{1B} = \frac{3\pi}{\sqrt{Q}}\left(5F_1 - 3F_0\right) - 8$$

$$M_{2B} = \frac{15\pi}{\sqrt{Q}}\left(2F_0 - 3F_1\right) + 15$$

$$M_{3B} = \frac{3\pi}{\sqrt{Q}}\left(10F_1 - 7F_0\right) - 8$$

Where:

$$Q = \begin{cases} 1 + 1.464\left(\dfrac{a}{c}\right)^{1.65} & for\ 0 \le {}^{a}/_{c} \le 1.0 \\ \left[1 + 1.464\left(\dfrac{c}{a}\right)^{1.65}\right]\left(\dfrac{a}{c}\right)^{2} & for\ {}^{a}/_{c} > 1.0 \end{cases}$$

$$F_0 = \left[C_0 + C_1\left(\frac{a}{t}\right)^2 + C_2\left(\frac{a}{t}\right)^4\right]\sqrt{\frac{a}{c}}$$

$$C_0 = 1.33469 - 0.29091\left(\frac{a}{c}\right) + 0.08125\left(\frac{a}{c}\right)^2$$

$$C_1 = 1.75673 - 1.5275\left(\frac{a}{c}\right) + 0.37185\left(\frac{a}{c}\right)^2$$

$$C_2 = 0.08429 - 0.4423\left(\frac{a}{c}\right) + 0.1894\left(\frac{a}{c}\right)^2$$

and

$$F_1 = \left[D_0 + D_1\left(\frac{a}{t}\right)^2 + D_2\left(\frac{a}{t}\right)^4\right]\sqrt{\frac{a}{c}}$$

$$D_0 = 1.11855 - 0.2065\left(\frac{a}{c}\right) + 0.07817\left(\frac{a}{c}\right)^2$$

$$D_1 = 1.15312 - 0.98743\left(\frac{a}{c}\right) + 0.23315\left(\frac{a}{c}\right)^2$$

$$D_2 = 0.2246 - 0.4784\left(\frac{a}{c}\right) + 0.1864\left(\frac{a}{c}\right)^2$$

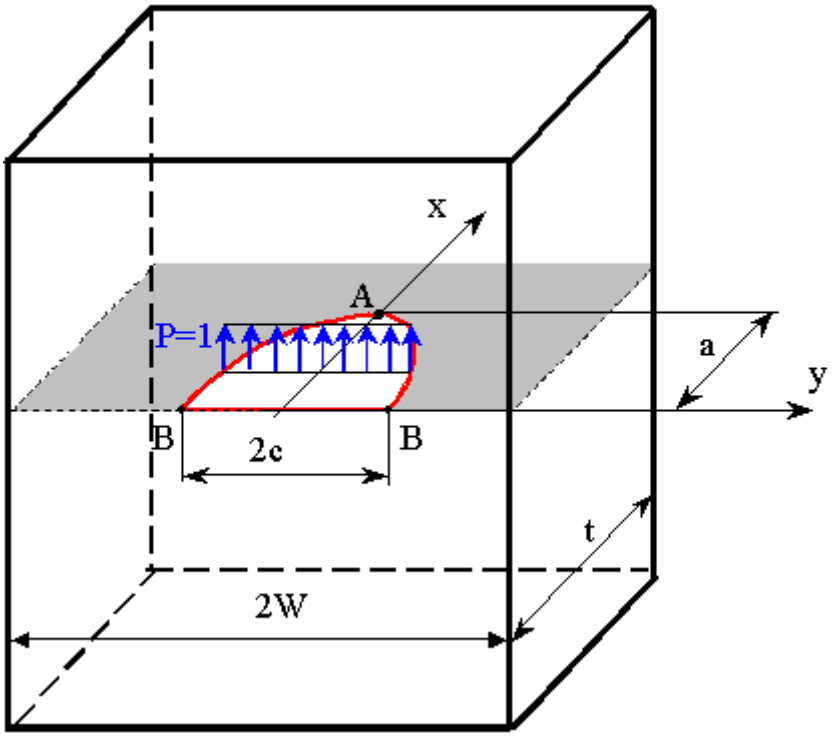

Figure 3.7: Geometric Description of a Surface Crack in a Finite Thickness Plate

3.5 Comparison of Weight Function Solution and FE Model Results for the Edge Crack Calibration Example

It became apparent quickly that the weight function solutions presented in Section 3.2 did not agree with the FE model prediction of the stress intensity factor for the 6 crack models described in Section 2.2 for the cracks larger than 10 mm in length. Table 3.1 presents the comparison of the stress intensity factors calculated from the six FE models along with the initial weight function results.

In the first attempt at a weight function calculation of K_I, the width of the crack member was assumed to be equal to the height of the flange to the underside of the web which was 46 mm. As indicated in Table 3.1, this resulted in a significant overestimation of K_I as the crack depth increased compared to the FE model estimates.

As a check to determine if the FE model results were providing reasonable estimates of K_I, the Gross [6] and Brown [7] solution for an edge crack in a finite width plate [1] was used and the results are also presented in Table 3.1.

$$K_I = Y\left(\frac{a}{w}\right)\cdot \sigma\sqrt{\pi a}$$

Where:

$$Y\left(\frac{a}{w}\right)=1.122-0.231\left(\frac{a}{w}\right)+10.550\left(\frac{a}{w}\right)^2-21.710\left(\frac{a}{w}\right)^3+30.382\left(\frac{a}{w}\right)^4$$

For the application of the Gross and Brown solution which requires a uniform nominal stress, the applied stress was assumed to be the average stress acting at the mid-thickness of the flange in the longitudinal (Z) direction (approximately 88 MPa). The Gross and Brown solution overestimated K_I compared to both the FE and weight function solutions.

Table 3.1: Comparison of Stress Intensity Factor Estimates Using the Standard Edge Crack Weight Function Solution

Crack Length, a (mm)	FE Model K_I Estimate MPa(mm)$^{1/2}$	Standard Weight Function K_I Estimate MPa(mm)$^{1/2}$	Gross and Brown Solution K_I Estimate MPa(mm)$^{1/2}$
	Plane Stress		
5	366	367	417
10	557	595	698
15	744	930	1063
20	938	1303	1616
25	1130	1897	2557
30	1296	2921	4214

SaFFD [8] has suggested that the differences in the K_I estimates may be attributable to features of the stiffener geometry. The single edge crack weight function was derived for the geometrical configuration illustrated in Figure 3.5. However, the actual stiffener geometry is different because of the web effect and it was proposed that the web could be treated as extra stiffening element on the upper edge of the cracked flange.

The use of the displacement boundary conditions extrapolated from the global model, results in a displacement controlled loading scenario for the cracked models, especially given that the global model does not explicitly contain cracks. Standard weight functions (as in the case of those presented in this document) are generally derived for load control scenarios for single path loading.

The implications of the load versus displacement controlled assumption can be illustrated with the use of a simple example as shown in Figure 3.8. If the load, P, is applied to the structure as shown (assuming that the cross member is infinitely rigid), then simple mechanics will show that the load transferred to Bar B is equal to the load transferred to Bar A.

If the load is replaced by a uniform deflection of the cross-member, δ, the load in Bar B is actually ½ of the load in Bar A. Compare this to a scenario where two identical stiffeners are located in a ship structural detail under a constant displacement loading. If the cross-sectional area of the stiffener is reduced due to the presence of a crack, but the global displacement of that detail remains constant because of redundancies elsewhere in the structure, the load in the cracked stiffener actually reduces and more of the load is transferred to the uncracked stiffener.

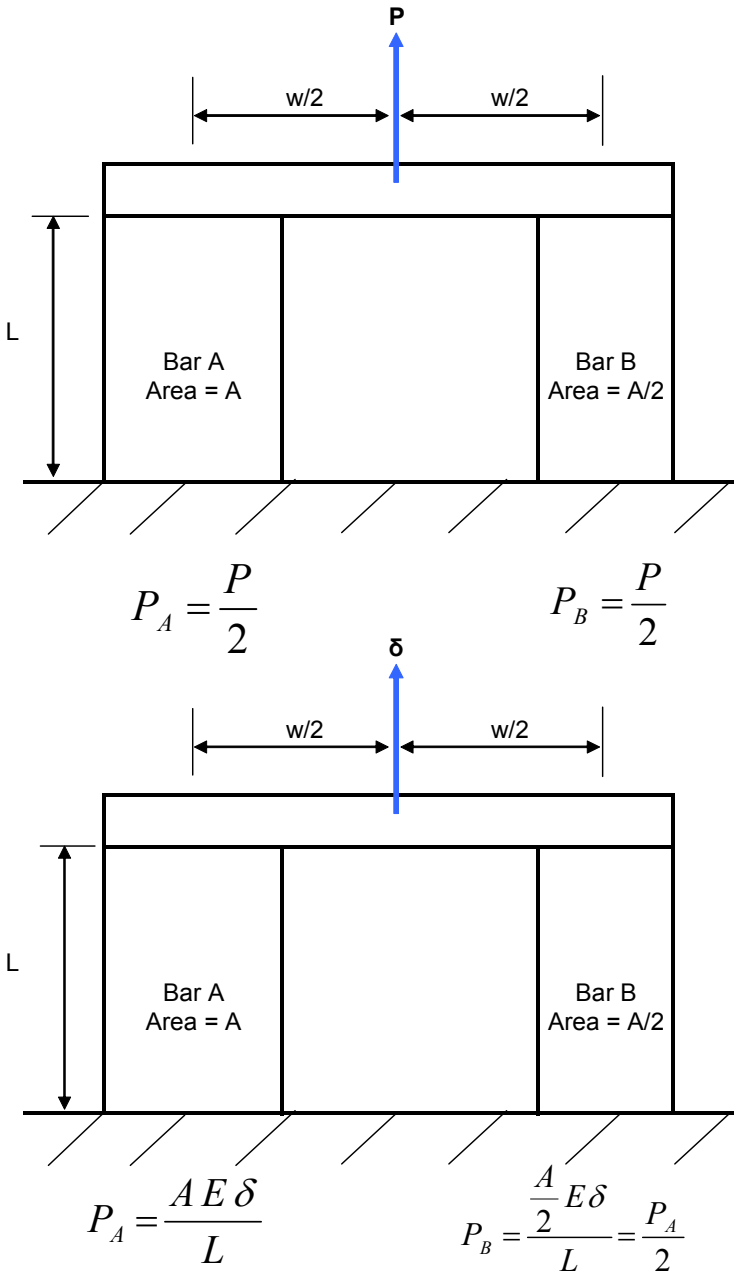

Figure 3.8: Comparison of Load vs. Displacement Controlled Scenarios

Weight function solutions derived for load controlled scenarios would be based on the assumption that the load remains constant in the presence of the crack (i.e. the stress in the component increases proportionally to the decrease in cross-sectional area). Under displacement control in a redundant structure, the increase in stress (if any) will not be directly proportional to the change in cross-section (i.e. load shedding may occur).

A couple of attempts were made to develop correction factors to account for differences in stiffness and the displacement versus load controlled boundary conditions. While a set of correction factors did appear to be valid for the calibration example, the application of these factors to the validation edge cracks was not successful. The details are presented in Appendix A.

3.6 Comparison of Weight Function Solutions and FE Model Results for the Through-Thickness Crack Calibration Example

As illustrated in Tables 3.2 and 3.3, there was also a significant disagreement between the ANSYS K_I estimates and the application of the weight function solution to the through crack calibration models for all cracks with the exception of the two shortest cracks. The standard weight function solution requires the input of the stress profile over half of the crack length, the crack half-length, a, and the plate half width, w (refer to Figures 3.1 and 3.6). For this example, the plate width was assumed to be 600 mm, which is the vertical distance between the side-shell stiffeners on either side of the crack location. The stress profile was taken from the mid-thickness of the side-shell (Figure 2.17).

The distance from the crack plane to the leading and trailing edges of the global model was approximately 750 mm. The distance to the leading edge incorporated in the first stage submodel (Figure 2.22) was approximately 740 mm. Based upon the information provided in Figure 2.21, the global model dimensions are such that a correction factor, F_1, for the plate half-width, h, could be applied to the weight function results to account for the geometry effects under the displacement controlled boundary conditions. As indicated in Tables 3.2 and 3.3, this correction factor was not sufficient to describe the differences between the FE model and weight function estimates of K_I.

Table 3.2: Upper Crack Front Mid-Thickness Weight Function Solution Comparison for Through Crack Calibration Example

Crack Length a (mm)	ANSYS Solutions MPa(mm)$^{1/2}$ Plane Strain	Weight Function Solution MPa(mm)$^{1/2}$	F_1	Weight Function Solution Modified by F_1 MPa(mm)$^{1/2}$
50	853	876	0.99	867
100	1138	1253	0.98	1228
150	1359	1572	0.98	1541
200	1493	1872	0.97	1816
250	1576	2178	0.94	2047
300	1617	2522	0.93	2345

Table 3.3: Lower Crack Front Mid-Thickness Weight Function Solution Comparison for Through Crack Calibration Example

Crack Length a (mm)	ANSYS Solutions $MPa(mm)^{1/2}$ Plane Strain	Weight Function Solution $MPa(mm)^{1/2}$	F_1	Weight Function Solution Modified by F_1 $MPa(mm)^{1/2}$
50	861	961	0.99	951
100	1158	1371	0.98	1343
150	1393	1711	0.98	1676
200	1540	2028	0.97	1967
250	1638	2339	0.94	2198
300	1691	2662	0.93	2475

The reason for the discrepancy between the ANSYS and weight function solutions again seems to be a result of the displacement versus load controlled boundary conditions. A discussion of attempts made to generate correction factors other than F_1, are presented in Appendix A. In the simple case of a through crack in flat plate (discussed later in Section 5), SaFFD was able to generate correction factors to convert K_I estimated from load controlled boundary conditions to displacement controlled boundary conditions. The application of the correction factors to the ship structure models was not successful, however.

3.7 Comparison of Weight Function Solution and FE Model Results for the Surface Crack Calibration Example

The geometry used in generating the surface crack weight function solutions is provided in Figures 3.9 and 3.10. The results of the comparison between the weight function estimates and the ANSYS plane strain K_I estimates for the deepest point along the crack front is provided in Table 3.4. The results for the surface point are presented in Table 3.5.

Table 3.4: Comparison of Stress Intensity Factor Estimates for the Deepest Point in the Surface Crack Calibration Example

Crack Depth, a (mm)	Crack Length, 2c (mm)	FE Model K_I Estimate $MPa(mm)^{1/2}$ Plane Strain	Weight Function K_I Estimate $MPa(mm)^{1/2}$
1.6	**50**	254	315
	100	272	324
3.2	**50**	330	478
	100	359	549
4.8	**50**	389	600
	100	442	817

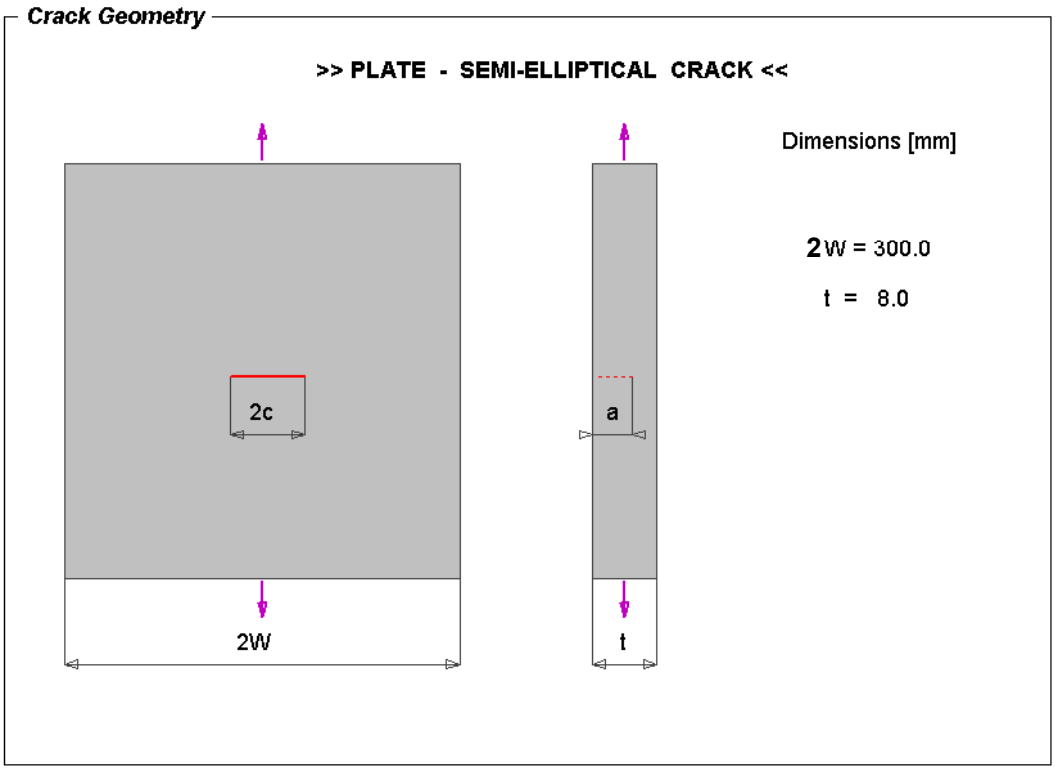

Figure 3.9: Geometry of Plate for Semi-Elliptical Surface Crack Weight Function Solution

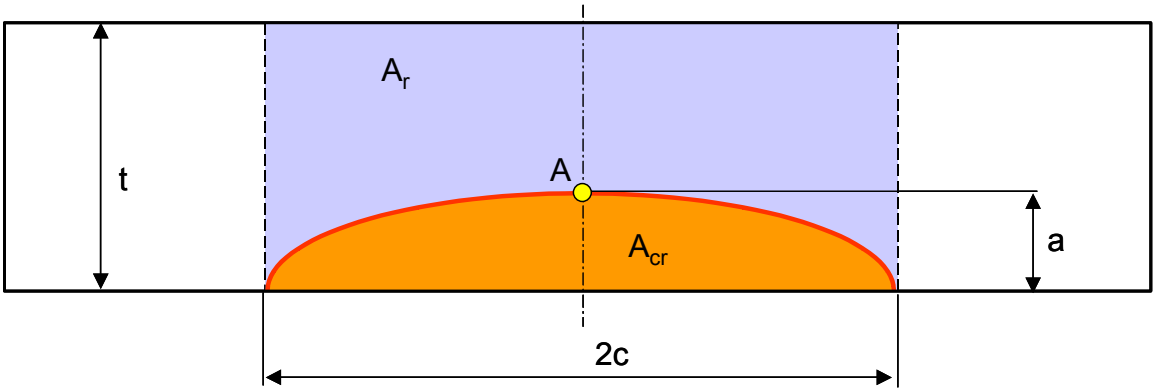

Figure 3.10: Parameters Required for Stiffness Correction Factors Applied to Semi-Elliptical Crack Weight Function Solutions for Displacement Controlled Loading Scenarios

Once again, the weight function solution overestimated the value of K_I compared to the ANSYS results, which is likely attributed primarily to the displacement controlled boundary conditions used in the FE models. The attempt to apply a correction factor is discussed in Appendix A.

Table 3.5: Comparison of Stress Intensity Factor Estimates for the Surface Crack Calibration Example at the Surface Location

Crack Depth, a (mm)	Crack Length, 2c (mm)	FE Model K_I Estimate $MPa(mm)^{1/2}$	Weight Function K_I Estimate $MPa(mm)^{1/2}$
		Plane Stress	
1.6	**50**	167	123
	100	290	90
3.2	**50**	206	243
	100	180	187
4.8	**50**	305	393
	100	264	323

4. VALIDATION EXAMPLES

In addition to the calibration models, six additional locations in the ship structure detail presented in Figure 4.1 were selected and submodeled in cracked and uncracked configurations. The weight function solutions described in Section 3 were applied to these crack cases without the input of SaFFD to check that the equations and proposed correction factors (presented in Appendix A) could be applied to different geometric configurations to explore the universality of the proposed weight function solutions.

The locations of the validation crack submodels are provided in Figure 4.1 and described in Table 4.1. Two edge cracks, two semi-elliptical surface cracks and two through thickness cracks were considered.

The validation models were used to evaluate the attempt to develop correction factors to account for geometry effects and the displacement controlled boundary conditions. As discussed in Appendix A, the validation models indicated that proposed correction factors were not universally applicable to the structural details. The results presented in this section will focus primarily on the uncorrected weight function solutions for K_I.

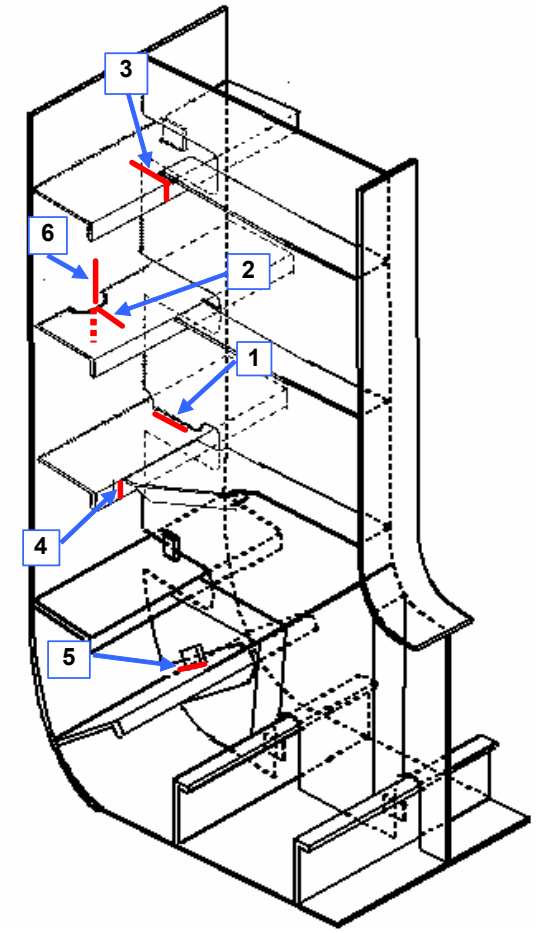

Figure 4.1: Locations of Validation Cracks

Table 4.1: Validation Crack Description

Crack No.	Type	Crack Depth (mm)	Crack Length (mm)	Description
1	Surface	4	50	Surface crack in toe of web to side-shell stiffener fillet weld toe
2	Edge	N/A	75	Edge crack extending from rat hole in side shell stiffener
3	Edge	N/A	60 (into web)	Edge crack extending into web of side shell stiffener
4	Surface	10	30	Surface crack extending from weld between web stiffener and side shell stiffener
5	Through	N/A	100	Through crack at toe of fillet weld joining clip to side shell stiffener
6	Through	N/A	100	Through crack in side shell under rat hole in side shell stiffener

4.1 Validation Crack 1: Surface Crack

Dimensioned pictures of the Validation Crack 1 submodel geometry used to estimate K_I are shown in Figure 4.2. The model length in the forward direction was set to 140 mm in an attempt to minimize the effects of the submodel geometry on the K_I estimate.

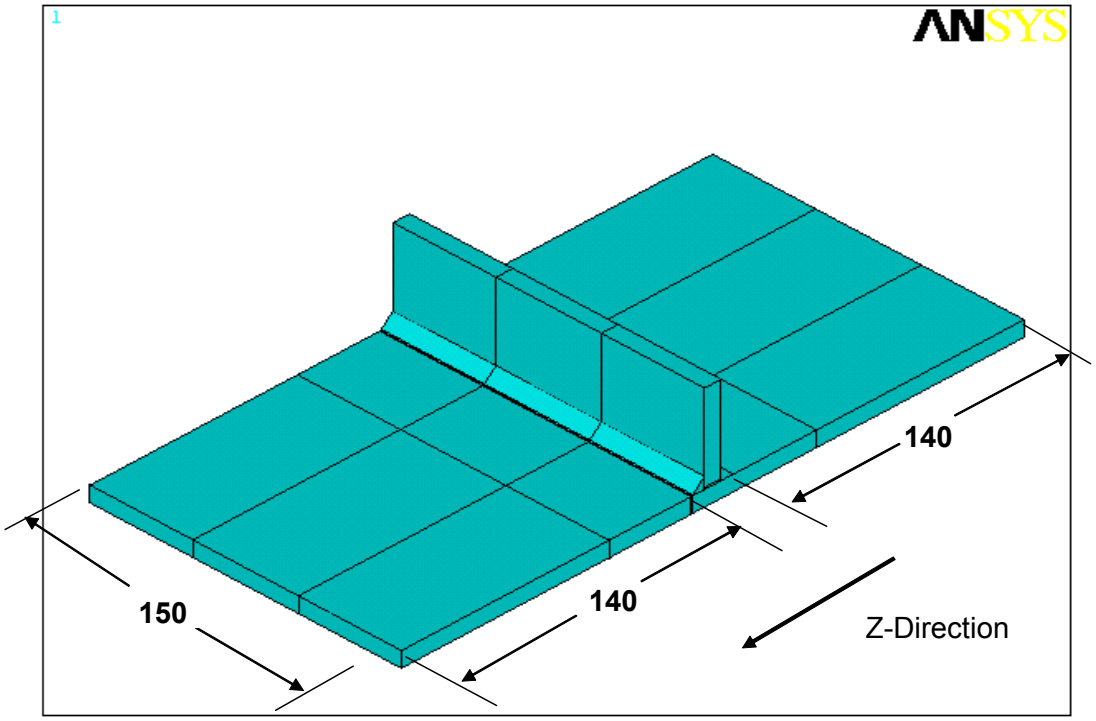

Figure 4.2: Dimensions of Validation Crack 1 Submodel used to Estimate K_I

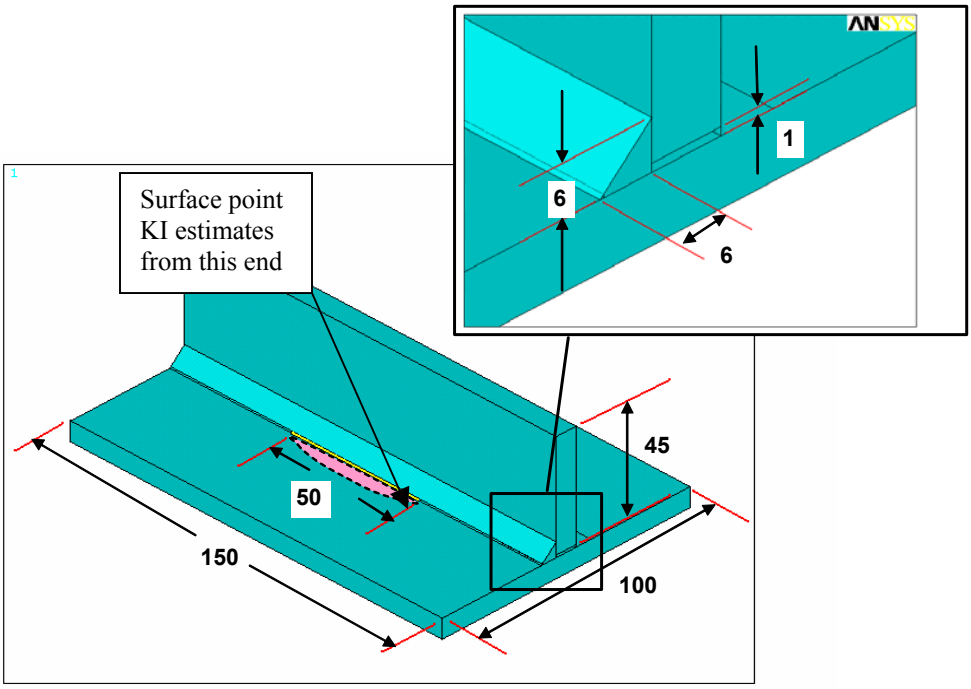

Figure 4.3: Local Details of the Geometry of the Validation Crack 1 Submodel used to Calculate K_I (all dimensions in mm)

The model was meshed using ANSYS Solid95 crack tip elements along the crack front. The crack depth was 4 mm and its length was 50 mm and the crack plane was located in the global X-Y plane. The fillet weld used to connect the web to the side shell stiffener was assumed to have a 6 mm leg length and a 1 mm root gap.

The uncracked geometry model is shown in Figure 4.4. Once again the model was meshed with ANSYS Solid95 elements. The weld details were identical to the cracked model except the weld toe radius was assumed to be 1 mm and 5 elements were placed along the weld toe curvature.

The stress distribution at the crack mid-point is shown in Figure 4.5. The stress concentration effect of the weld toe at Depth = 0 is quite apparent. A comparison of the FE model and weight function K_I estimates is provided in Table 4.2. As with the calibration models, the deepest point K_I estimate is compared assuming a state of plane strain and the surface point a state of plane stress. The surface point K_I estimates from the ANSYS model were determined at the end farthest from the side shell using the extrapolation technique discussed in Section 2.4.2.

For the deepest and surfaces points, the K_I estimates agree to within 2.5% and 21% respectively. These results indicate that the geometry is possibly less affected by the displacement versus load control boundary conditions. In this example h/a = 140/25 = 5.6.

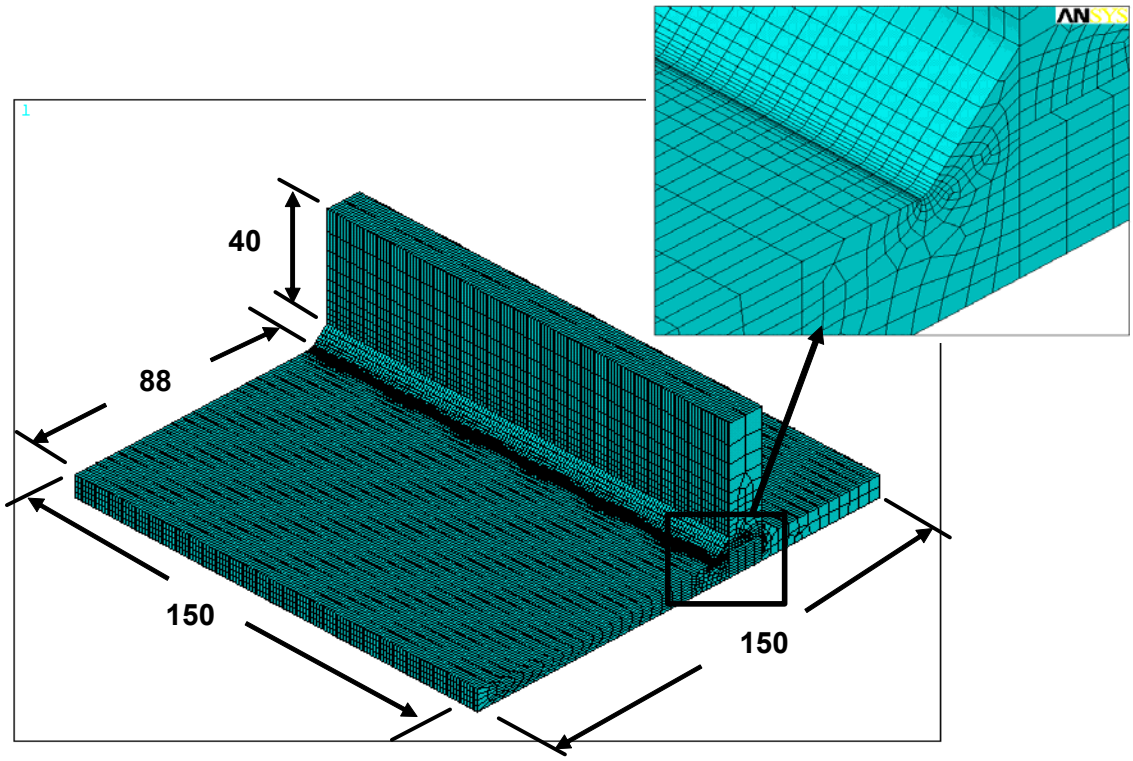

Figure 4.4: Details of the Uncracked Submodel for Validation Crack 1

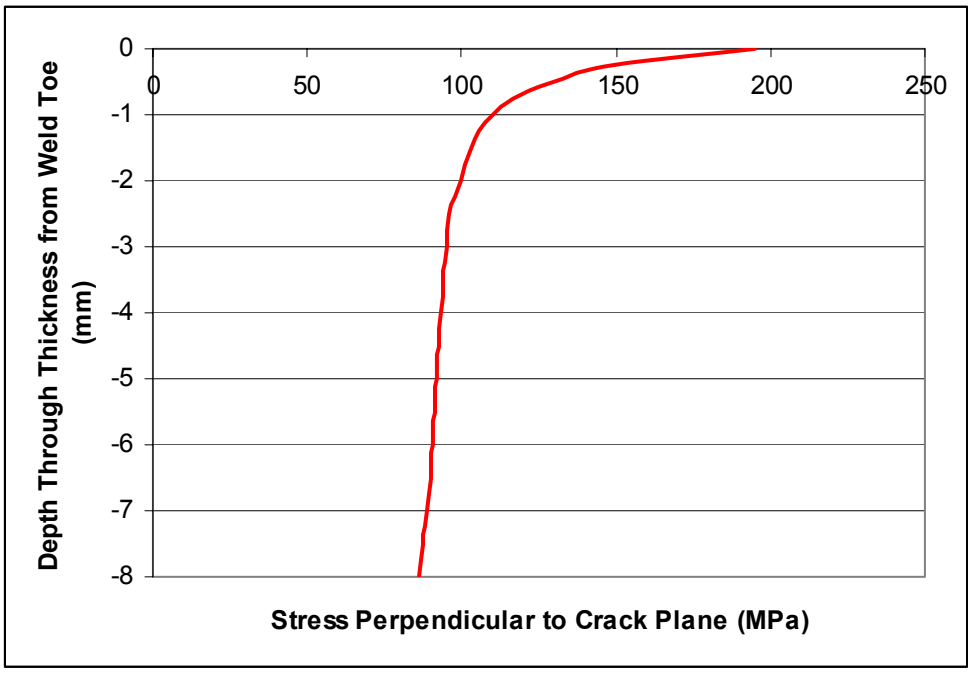

Figure 4.5: Mid-Crack Length Stress Distribution Perpendicular to the Crack Plane for Validation Crack 1

Table 4.2: Comparison of Weight Function and FE Model Estimates of K_I for Validation Crack 1 (Surface Crack)

Crack Depth, a mm	Crack Length, 2C mm	Weight Function K_I Estimates MPa(mm)$^{1/2}$		ANSYS K_I Estimates MPa(mm)$^{1/2}$	
		Deepest Point	Surface Point	Deepest Point Plane Strain	Surface Point Plane Stress
4	50	605	270	590	214

4.2 Validation Crack 2: Edge Crack

The geometry of the Validation Crack 2 submodel used to calculate K_I is shown in Figure 4.6. The crack extends from the center of the rat hole for 75 mm into the web of the side shell stiffener and the crack plane is again oriented in the X-Y plane. The length of the model is sufficient to satisfy the requirements for a nominal remote load outlined in Tada et. al. [1].

The uncracked geometry for Validation Crack 2 was modeled in both ANSYS and NASTRAN to compare the results using both FE modeling packages in generating the weight function K_I estimates. The ANSYS model geometry was identical to the cracked model geometry shown in Figure 4.6. ANSYS Solid95 elements were used to mesh the model. Element edge lengths in the refined mesh region measured 1 mm.

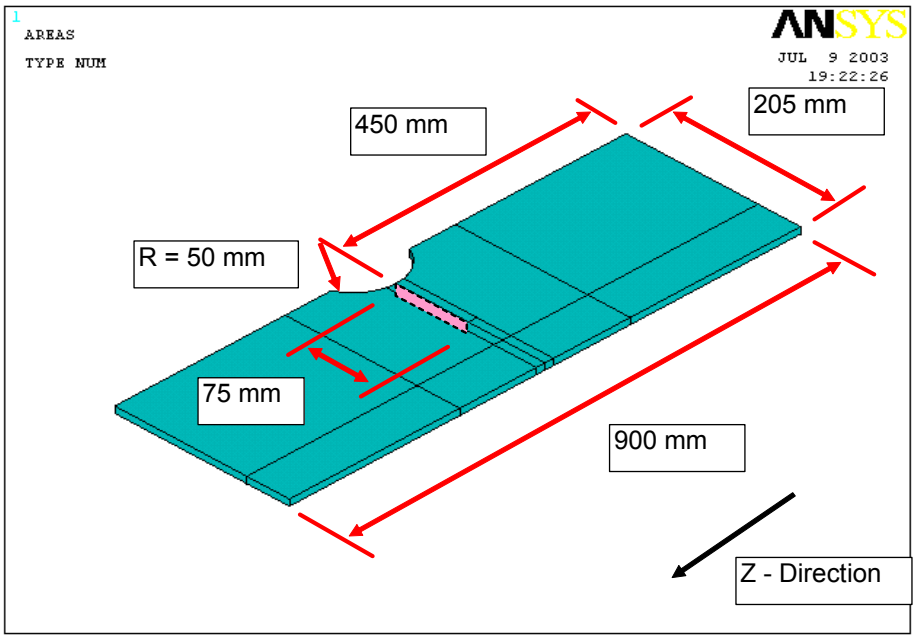

Figure 4.6: Geometry of Validation Crack 2 Submodel used to Calculate K_I (all dimensions in mm)

NASTRAN does not offer the ANSYS option of interpolating the degree of freedom solutions for nodes on the edges of the submodel boundary between the global model shell elements and the submodel solid elements. To overcome this difficulty, solid model elements were inserted in the NASTRAN global model at the location of Validation Crack 2 (Figure 4.7). At the boundary between the shell and solid element meshes, constraint equations were used to prevent rotation along the edges of the shells. Triangular CTRIA3 and Rectangular CQUAD4 plate elements and CHEXA solid elements were used in the NASTRAN model. The refined mesh solid elements had 1 mm element edge lengths similar to the elements in the ANSYS model.

Figure 4.8 shows the stress estimates along the mid thickness of the side shell stiffener from both the ANSYS and NASTRAN models. There is a maximum difference of about 7% in the variation in the results generated from both FE packages with ANSYS predicting a peak stress of 239.25 MPa at the edge of the rat hole and NASTRAN predicting a peak stress of 222.5 MPa.

To generate the weight function K_I estimates, the crack length used included the radius of the rat hole so the total crack depth was 125 mm (Figure 4.9). Over the first 50 mm zero stress was applied. The results are presented in Table 4.3.

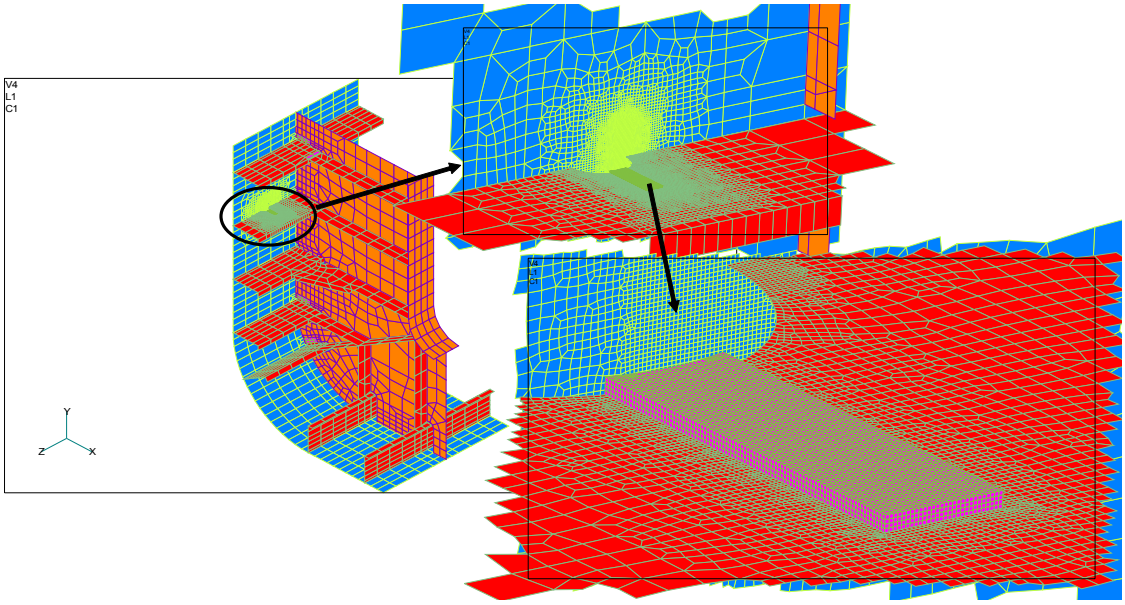

Figure 4.7: NASTRAN Model used to Generate the Uncracked Stress Distribution for Validation Crack 2

The single edge crack solution results in an overestimation of K_I compared to the FE model results by a factor of about 3. The connection to the side shell would impact the opening of the crack and affect the rotation of the stiffener as the crack opened. This additional restraint would not be accounted for in a single edge crack solution. The stress results were also used in a double edge crack weight function solution (see Appendix A) to try and add some of this rotational stiffness. The overestimate in K_I was reduced to less than a factor of 2.

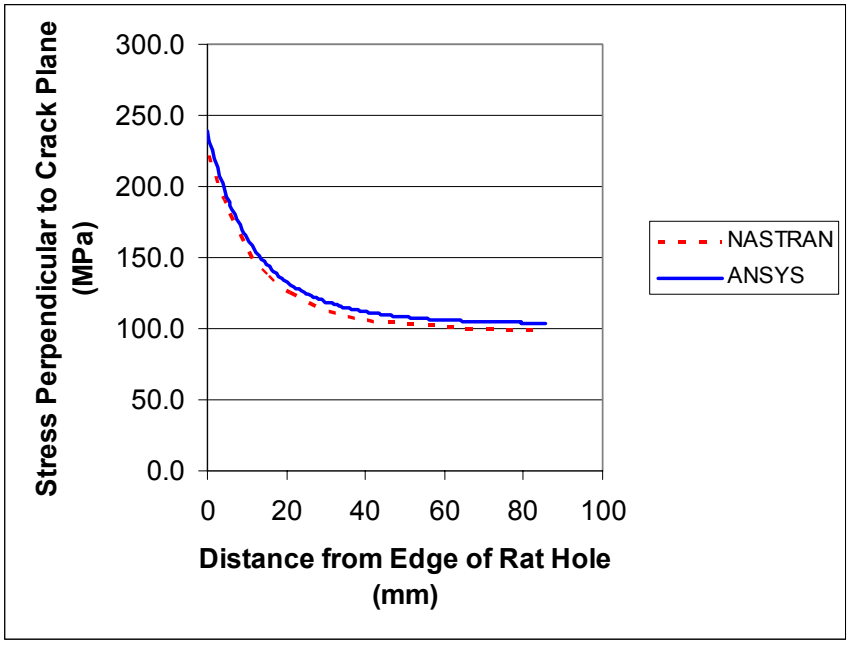

Figure 4.8: Comparison of NASTRAN and ANSYS Mid-Thickness Stress Estimates Perpendicular to the Crack Plane in Validation Example 2

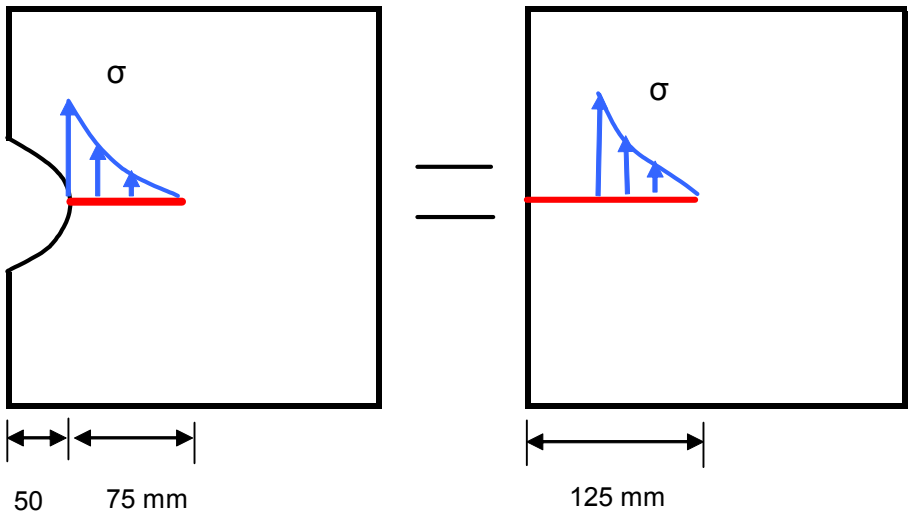

Figure 4.9: Crack Length Description Required for Validation Crack 2

Table 4.3: Comparison of Weight Function and FE Model K_I Estimates for Validation Crack 2

Crack Length, a (mm)	Plate Width, w (mm)	FE Model K_I Estimate MPa(mm)$^{1/2}$		Weight Function K_I Estimate MPa(mm)$^{1/2}$			
				Single Edge Crack		Double Edge Crack	
		Plane Strain	Plane Stress	ANSYS	NASTRAN	ANSYS	NASTRAN
125	**295**	1198	1091	3226	3052	1951	1851

4.3 Validation Crack 3: Edge Crack

The geometry for the edge crack submodel, Validation Crack 3, used to determine K_I is shown in Figure 4.10. The crack coincides with the toe of the lap weld between the web stiffener and the side shell stiffener. It was assumed that the crack had propagated completely through the flange in the side shell stiffener and extends 60 mm into the web. The crack is again located in the global X-Y plane.

The model was extended as far as possible in the forward and aft directions to minimize the effects of the length of the plate on the K_I estimate [1]. In order to do so, details of the web stiffener lap weld connection were included in the model. The leg length of the lap welds was assumed to be 6 mm with a 1 mm gap between the stiffeners as shown in Figure 4.11.

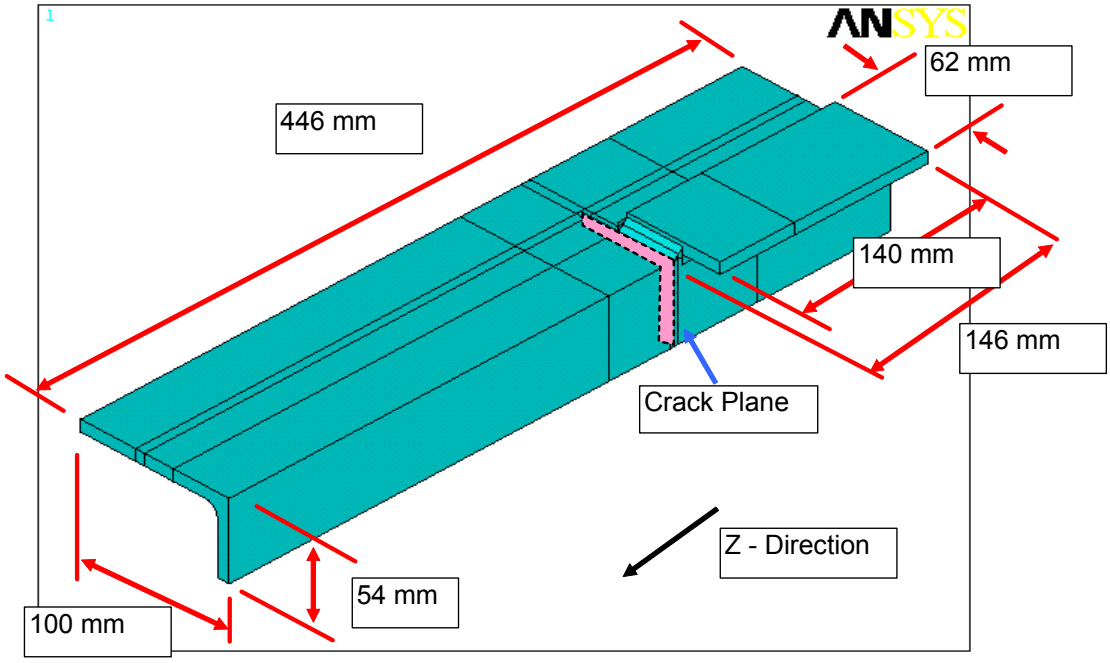

Figure 4.10: Geometry of the Validation Crack 3 Submodel used to Calculate K_I (all dimensions in mm)

The geometry of the uncracked model was identical to the cracked model, except a weld toe radius of 1 mm was assumed for the perimeter of the lap weld. Five elements were placed along the fillet to ensure the weld toe stress concentration effects were properly modeled.

The resulting Z-direction stress profile was extracted from the mid-thickness of the web of the side shell stiffener (Figure 4.12). It was not necessary to include the stress in the flange since it had been completely detached and no longer supported any load.

The comparison of the weight function and ANSYS K_I estimates is provided in Table 4.4. In this case the through thickness stresses were non-zero so the weight function solution is compared to the ANSYS plane strain estimate and results in a overestimation by a factor of 1.55.

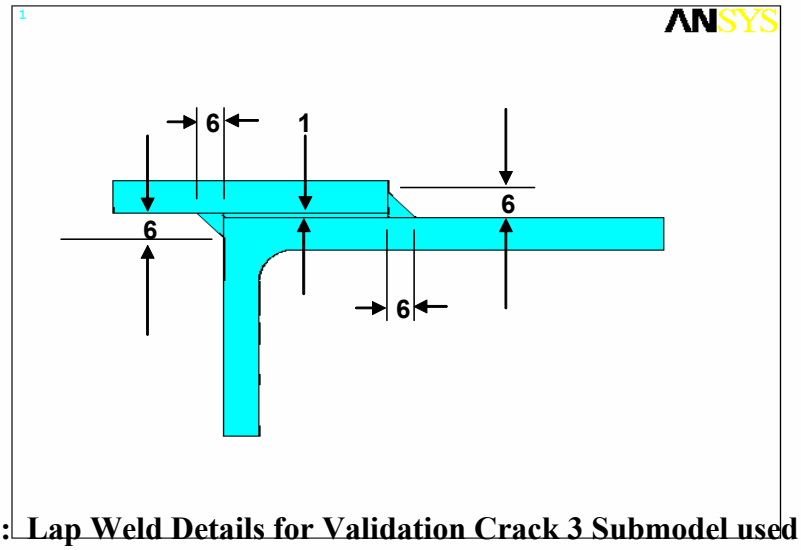

Figure 4.11: Lap Weld Details for Validation Crack 3 Submodel used to Calculate K_I (Additional Volumes Removed for Clarity)

Table 4.4: Comparison of Weight Function and FE Model K_I Estimates for Validation Crack 3

Crack Length, a (mm)	Plate Width, w (mm)	FE Model K_I Estimate MPa(mm)$^{1/2}$		Single Edge Crack Weight Function K_I Estimate MPa(mm)$^{1/2}$
		Plane Strain	Plane Stress	
60	**295**	904	823	1403

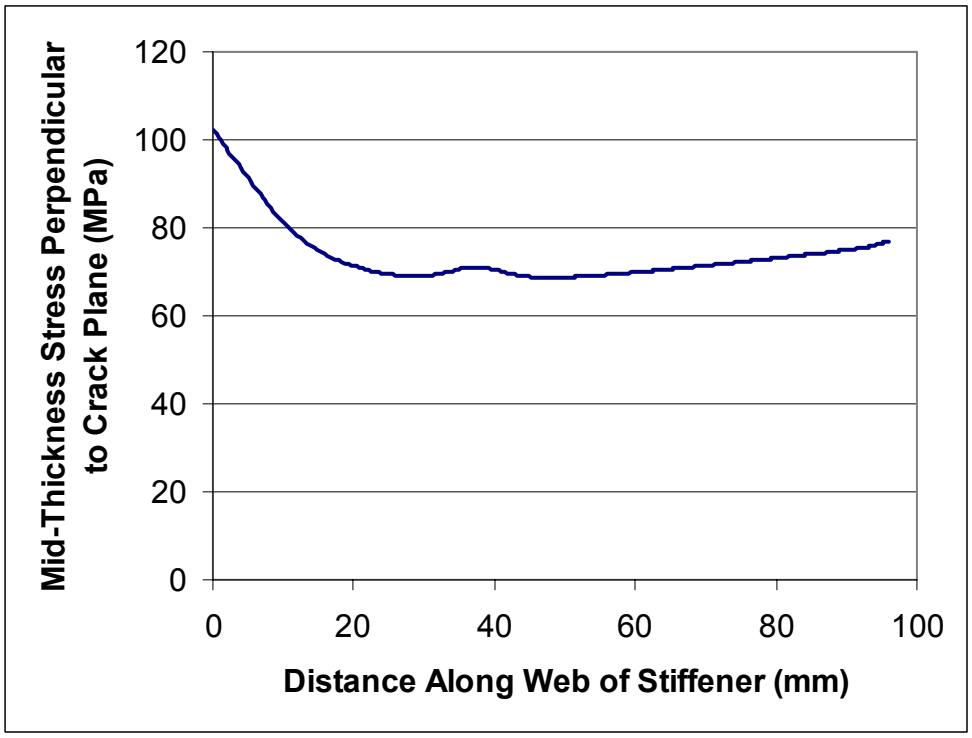

Figure 4.12: Mid-Thickness Stress Profile Perpendicular to Crack Plane used for the Weight Function Solution for Validation Crack 3

4.4 Validation Crack 4: Surface Crack

The geometry of the Validation Crack 4 submodel used to determine the stress profile for the uncracked component is shown in Figure 4.13. A 1 mm element edge length was used at the refined mesh location and ANSYS Solid95 were used in both the crack and uncracked submodels. The crack depth was assumed to be 10 mm at its deepest point and the crack length was 30 mm along the surface of the upset bulb section. To simplify the modeling and permit sufficient mesh refinement in the crack region, the profile of the butt weld between the stiffeners was not explicitly modeled. It is assumed that the weld would have been generated using a single sided groove weld preparation from the top of the stiffeners and that the root penetration would not have extended significantly below the bottom of the web stiffener. The cap on the top side of the stiffeners would add very little additional stiffness to the geometry.

The crack is assumed to be semi-elliptical in shape extending from the bottom edge of the butt weld between the upset bulb section and the web stiffener. It is acknowledge that a surface crack in the location shown in Figures 4.1 and 4.13 may be unlikely to occur in practice in the position and orientation selected. The global model loading discussed in Section 2.1 resulted in compressive stresses in some of the locations originally selected for validation crack example locations and several of the cracks were relocated after discussions with and approval from the Project Technical Committee. While this example may not represent a common cracked component in a structural detail, it is useful in determining the applicability of the weight function solutions to complex geometries and flaw orientations. A future investigation into the use of the corner crack weight function solution may be of interest for this structural detail.

The stress through the bulb section at the location coinciding with the deepest point on the crack front is shown in Figure 4.14. Based upon this stress distribution, the weight function estimates for K_I at the deepest point and the end of the semi-elliptical crack nearest the bottom of the bulb section are compared to the FE model results in Table 4.5. The bulb section thickness 15 mm below the bottom surface of the web stiffener was 41.3 mm and this value was used as the section thickness for the weight function calculations. The surface point K_I value was taken from the crack tip 30 mm below the web.

The weight function K_I estimates at the deepest point and surface point were 1.17 and 1.27 times the ANSYS estimates, respectively.

Table 4.5: Comparison of Weight Function and FE Model Estimates of KI for Validation Crack 4 (Surface Crack)

Crack Depth, a mm	Crack Length, 2C mm	Weight Function K_I Estimates MPa(mm)$^{1/2}$		ANSYS K_I Estimates MPa(mm)$^{1/2}$			
				Deepest Point		Surface Point	
		Deepest Point	Surface Point	Plane Strain	Plane Stress	Plane Strain	Plane Stress
10	30	411	415	351	319	361	328

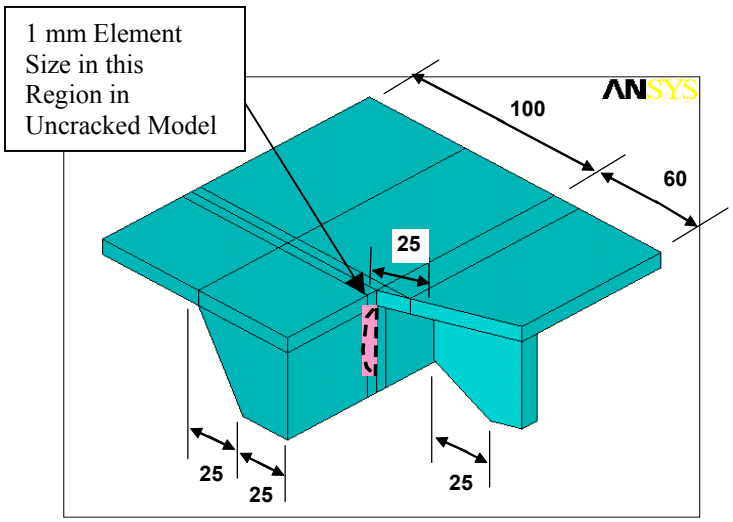

(a)

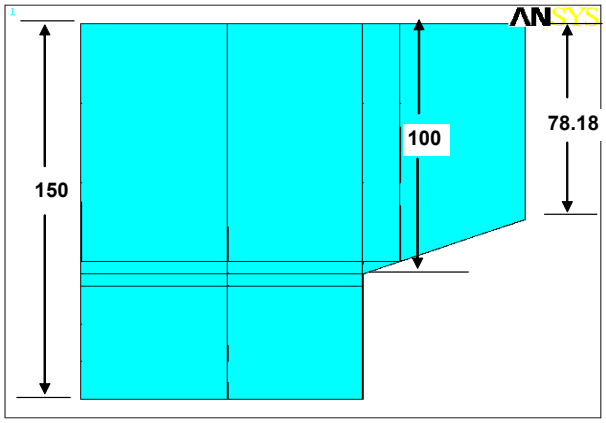

(b)

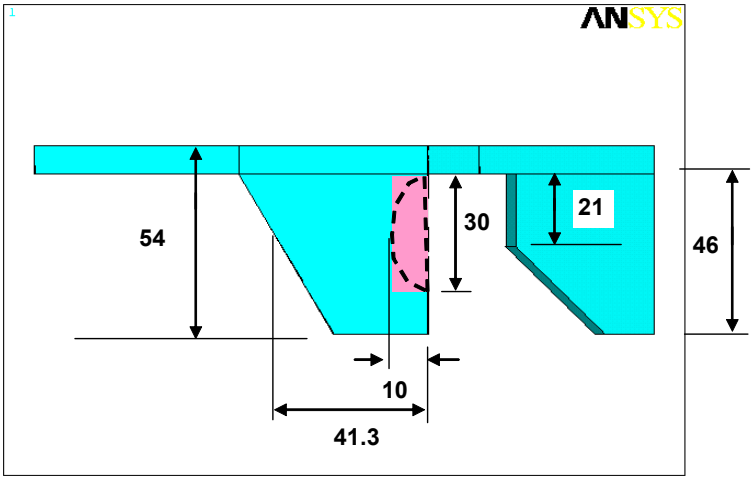

(c)

Figure 4.13: (a) Isometric, (b) Top and (c) Side Views of the submodel geometry for the Validation Crack 4 Surface Crack (all dimensions in mm)

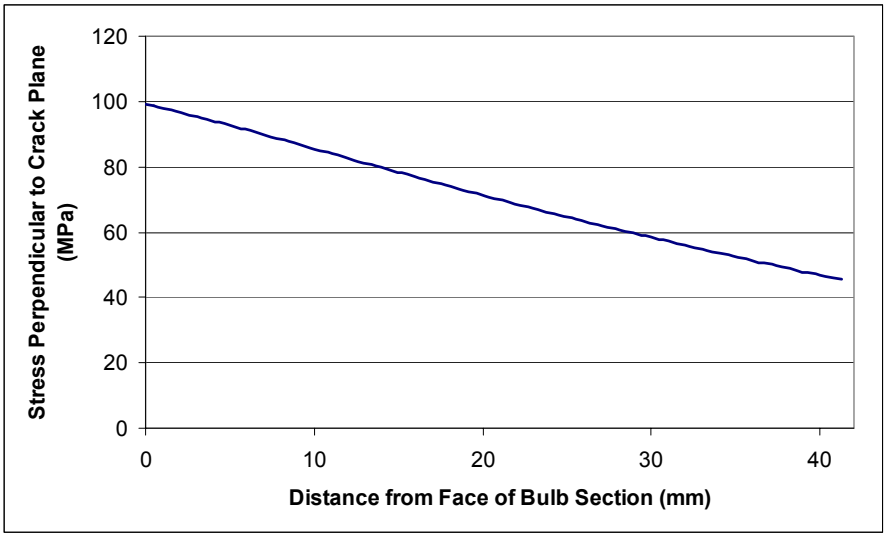

Figure 4.14: Stress Through the Bulb Section Perpendicular to the Crack Plane at the Deepest Point of Validation Crack 4

4.5 Validation Crack 5: Through Thickness Crack

The geometry of the Validation Crack 5 submodel used to estimate K_I is shown in Figures 4.15 and 4.16. The 100 mm long through thickness crack was oriented in the X-Y plane and located in the toe of the fillet weld joining the clip to the stiffener. The leg length for the fillet weld was once again assumed to be 6 mm with a 1 mm root gap. Both the cracked and uncracked submodels were meshed with ANSYS Solid95 elements.

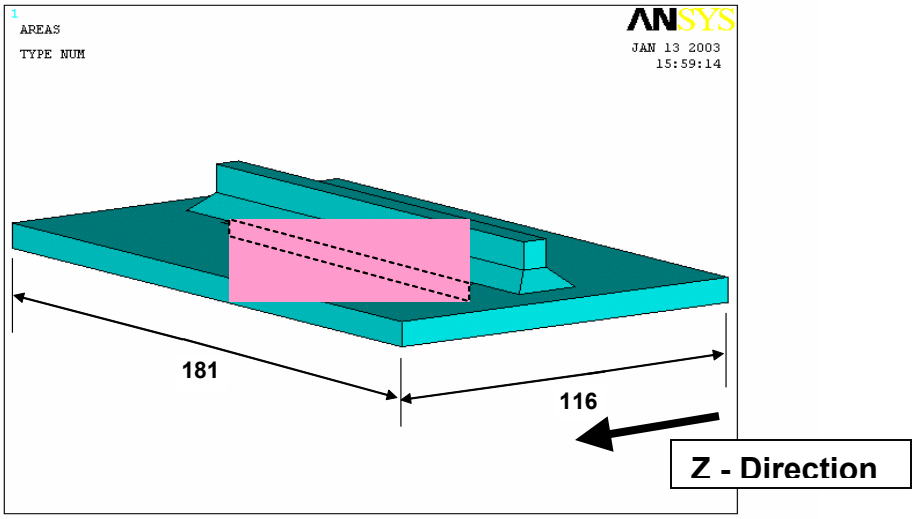

Figure 4.15: Through Crack in the Web Stiffener Coinciding with the Fillet Weld for the Clip

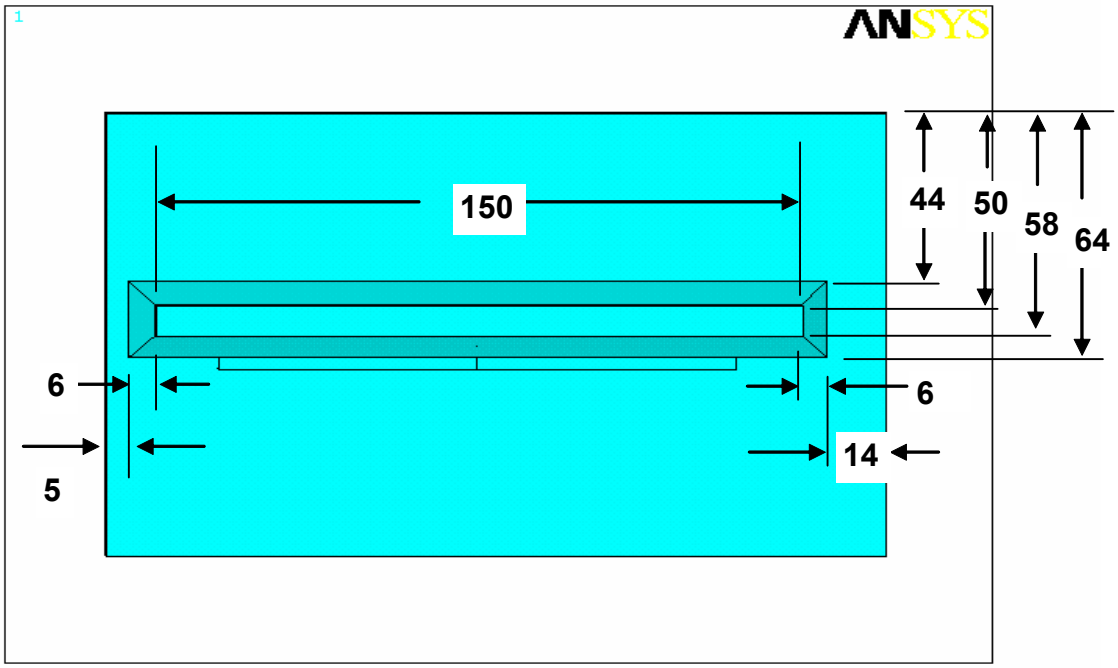

Figure 4.16: Geometry of Validation Crack 5 Submodel used to Calculate K_I (all dimensions in mm)

As shown in Figure 4.17, a 1 mm weld toe radius and 1 mm weld root gap were used. Five elements were placed along the fillet. The resulting mid-thickness stress distribution perpendicular to the crack plane in the stiffener is shown in Figure 4.18.

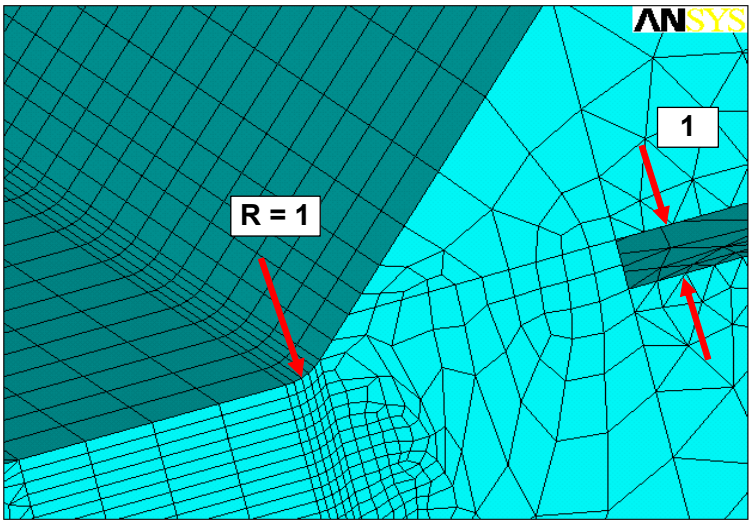

Figure 4.17: Weld Details for Uncracked Submodel for Validation Crack 5 (all dimensions in mm)

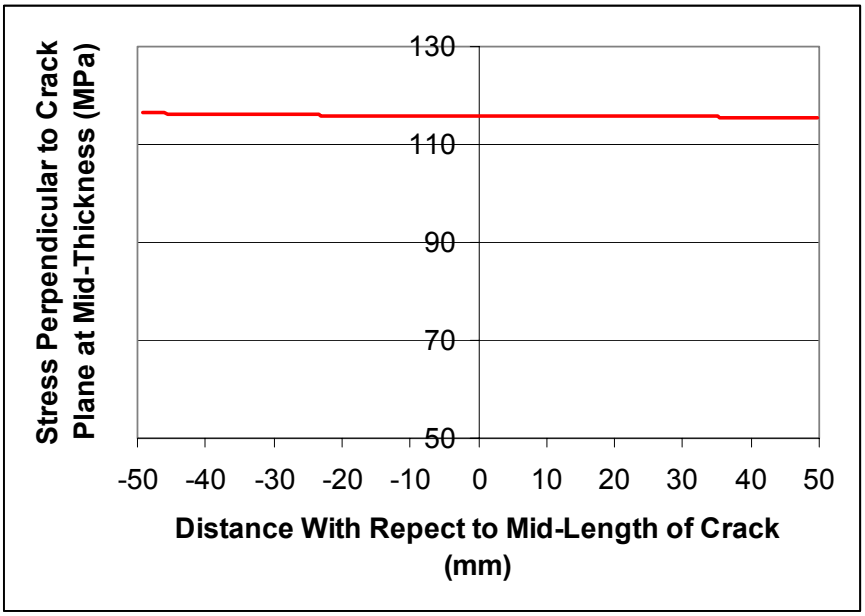

Figure 4.18: Mid-Thickness Stress Distribution in Side Shell Stiffener Perpendicular to the Crack Plane (X = 0 at center of clip, negative X values towards side shell)

Because of the uniform nature of the loading, the FE model K_I estimates were virtually identical at either end of the crack. These results are compared to the weight function estimate using half of the stress profile shown in Figure 4.18, X= 0 to X = 50mm, (crack front farthest from the side shell) and presented in Table 4.6. The plate width was assumed to be the width of the web (295 mm).

The through thickness stress at mid thickness was essentially negligible and therefore the weight function solution is compared to the ANSYS plane stress solution. In this example there is only a 3.6% difference between the weight function and ANSYS K_I estimates even though the h/a value was approximately equal to 1.

Table 4.6: Comparison of FE Model K_I Estimates and Weight Function Solution for Validation Crack 5

Crack Length, a (mm)	Plate Width, w (mm)	ANSYS Solutions MPa(mm)$^{1/2}$		Weight Function Solution MPa(mm)$^{1/2}$
		Plain Strain	Plain Stress	
100	295	1664	1515	1570

4.6 Validation Crack 6: Through Thickness Crack

The uncracked model geometry for Validation Crack 6, a through thickness crack in the side shell associated with the stiffener rat hole, was again modeled in both ANSYS and NASTRAN.

As with Validation Crack 2, NASTRAN did not permit a simple means of transferring the global plate element boundary conditions to a solid element submodel, so the solid elements were inserted into the global model geometry (Figure 4.19) using constraint equations at the plate to solid intersections.

The details of the side shell stiffener to side shell weld from the NASTRAN model geometry is shown in Figure 4.20. Unlike the previous model, the level of detail associated with the welded connection did not permit the use of 20 noded brick elements. In order to minimize the number of degrees of freedom associated with the model, 8 noded CHEXA brick elements were used. Triangular CTRIA3 and Rectangular CQUAD4 plate elements were used to construct the remainder of the structure. In the refined region at the crack location the brick elements have 1 mm edge lengths.

The uncracked ANSYS model used 20 noded solid 95 elements and had a through thickness element size of 0.5 mm. The geometry was essentially the same as the ANSYS model containing the crack (Figure 4.21) with the exception of the refinement in the weld toe region shown in Figure 4.22.

For both the uncracked ANSYS and NASTRAN models a 6 mm weld leg length was assumed, with a 1 mm weld toe radius. The root gap was reduced to zero for these models and the stiffener was assumed to be rigidly attached to the side shell.

The ANSYS cracked model was meshed with Solid95 elements and contained a 100 mm long through thickness crack in the side shell oriented in the X-Y plane.

Figure 4.23 compares the stress estimates from the ANSYS and NASTRAN Models at the mid-thickness location in the side shell perpendicular to the crack plane. The ANSYS model predicts stresses ranging between 10% and 20% than the NASTRAN model. This is likely partially the result of differences in meshing and the higher order elements used in ANSYS.

The comparison of the K_I estimates from the FE model and the weight function solutions are given in Table 4.7 for the lower crack tip (X = 0 mm to X = 50 mm in Figure 4.25) . The plate width was assumed to be the distance between the stiffeners above and below the stiffener containing the rat-hole (1200 mm). In this model there are through thickness stresses present at the mid thickness location of the crack tip and therefore comparisons were made using the ANSYS plane strain results.

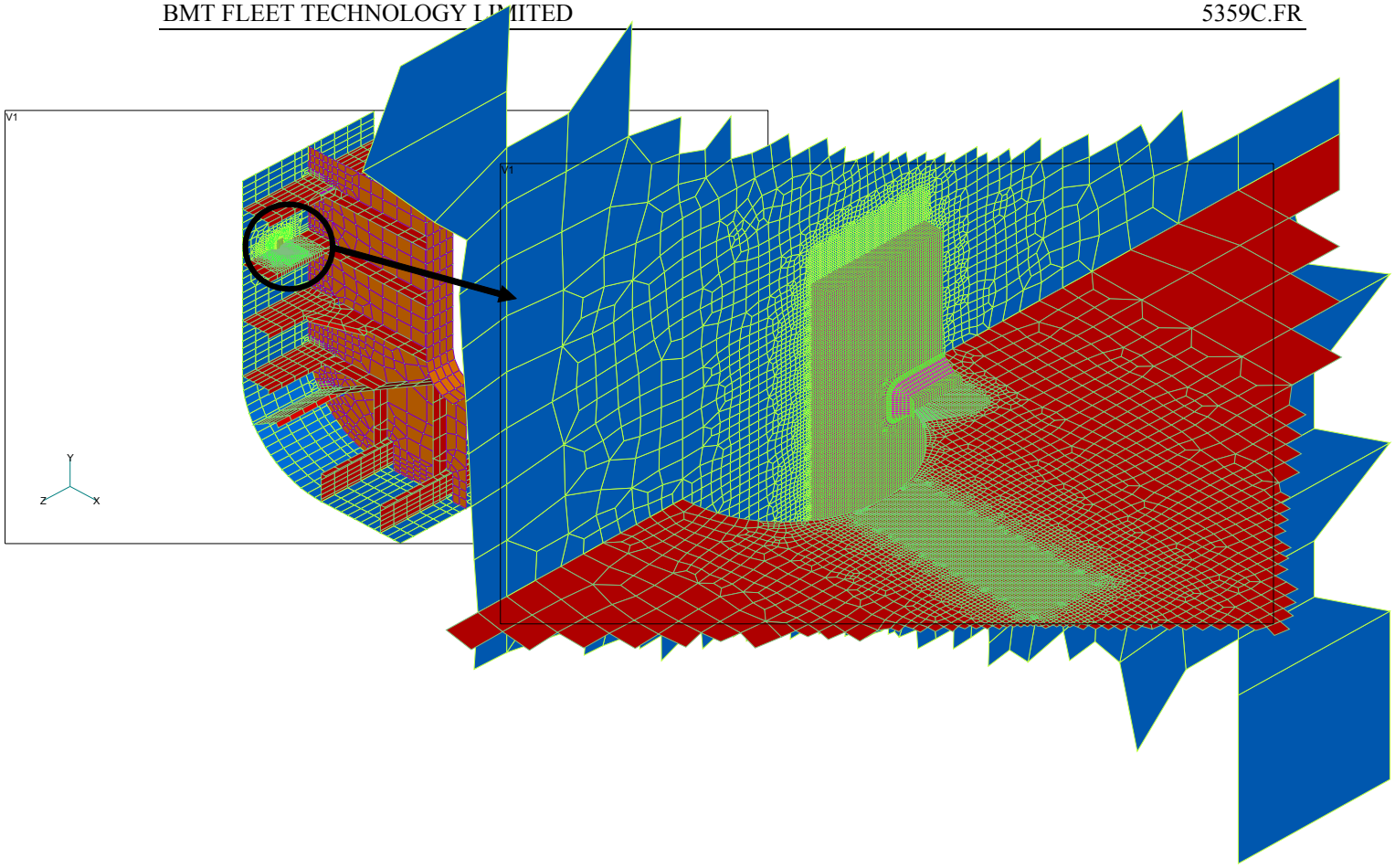

Figure 4.19: NASTRAN Model for the Uncracked Geometry for Validation Crack 6

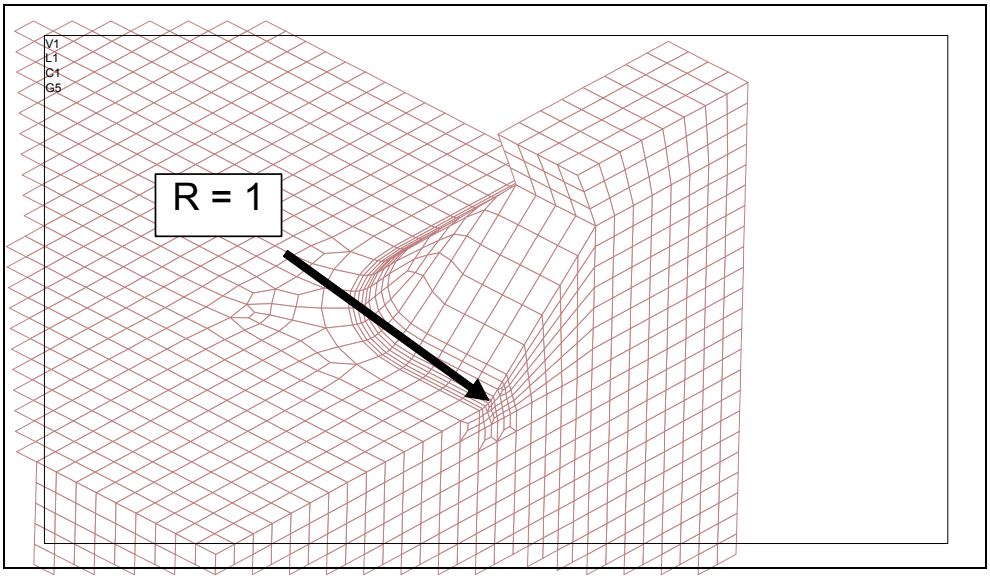

Figure 4.20: Detail of Stiffener to Side Shell Weld Used in the NASTRAN Model (rotated about the Z-axis)

As expected, from the difference in the stress profiles, the weight function solution based upon the NASTRAN stress profile is lower than then result using the ANSYS stress profile. The NASTRAN-based weight function solution is 1.49 times higher than the FE model estimate, while the ANSYS-based weight function solution is 1.77 times higher.

Table 4.7: Comparison of FE Model and Weight Function KI Estimates for Validation Crack 6

FE Package used to Estimate Stresses	Crack Length, a (mm)	Plate Width, w (mm)	FE Model Estimates MPa(mm)$^{1/2}$		Weight Function Solution MPa(mm)$^{1/2}$
			Plain Strain	Plain Stress	
ANSYS	100	1200	782	711	1381
NASTRAN					1165

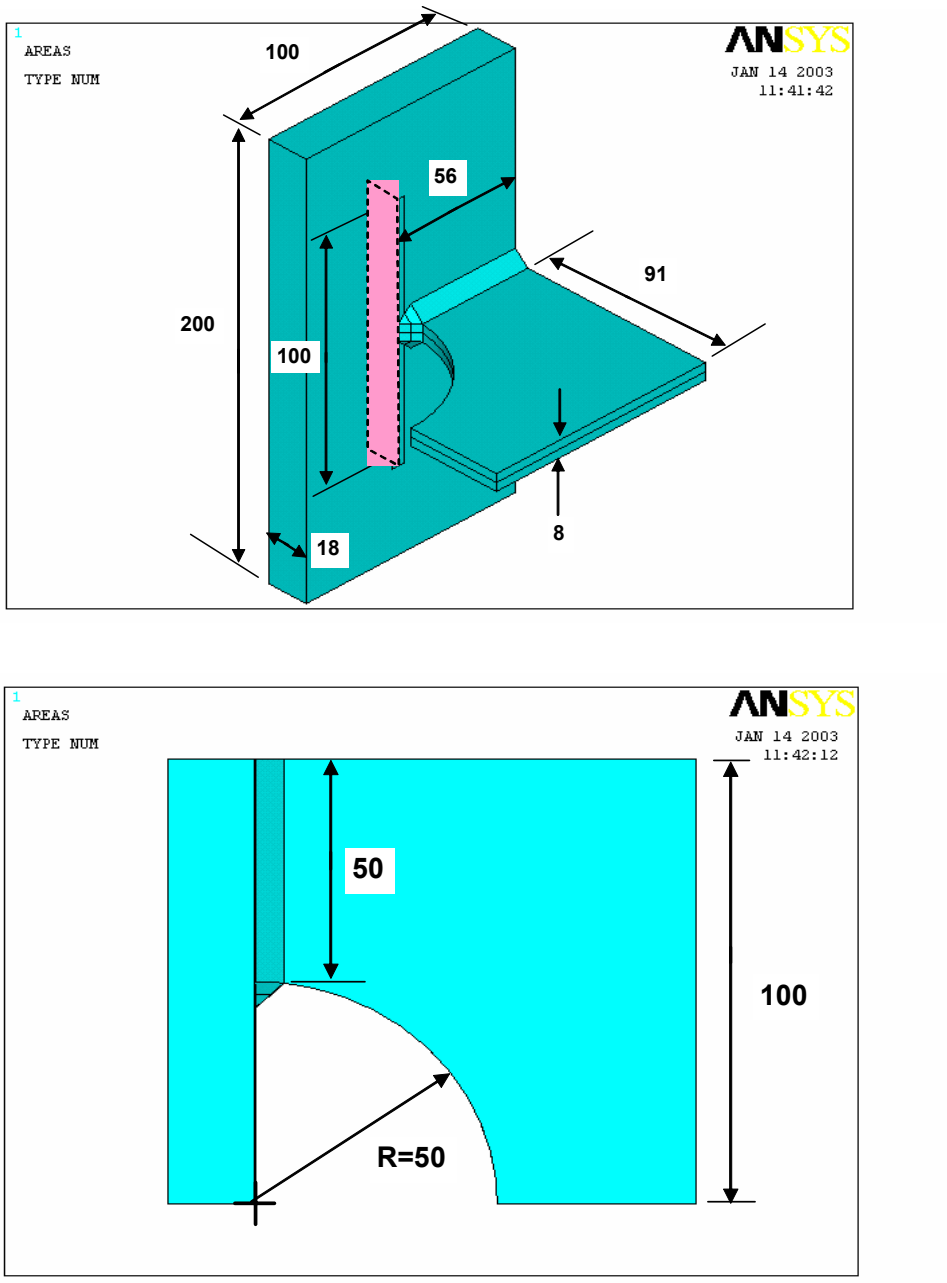

Figure 4.21: Geometry of Validation Crack 6 Submodel used to Calculate K_I (all dimensions in mm)

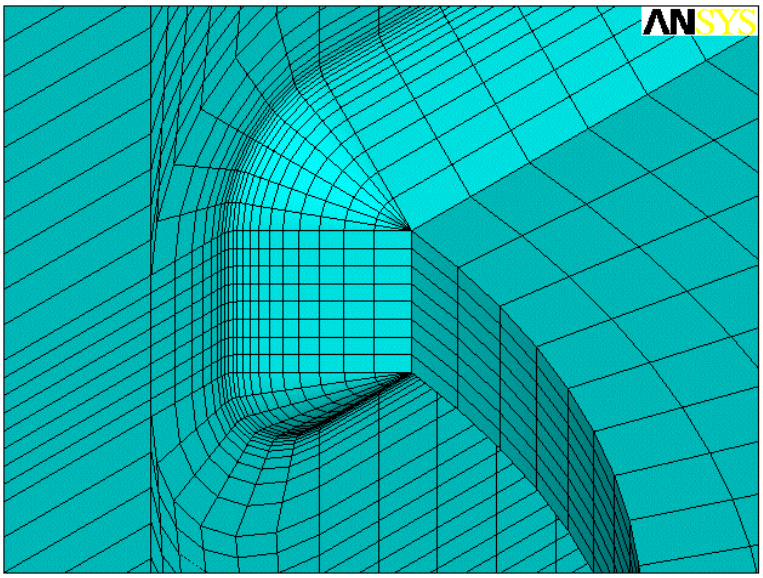

Figure 4.22: ANSYS Model Weld Geometry for the Uncracked Submodel for Validation Crack 6

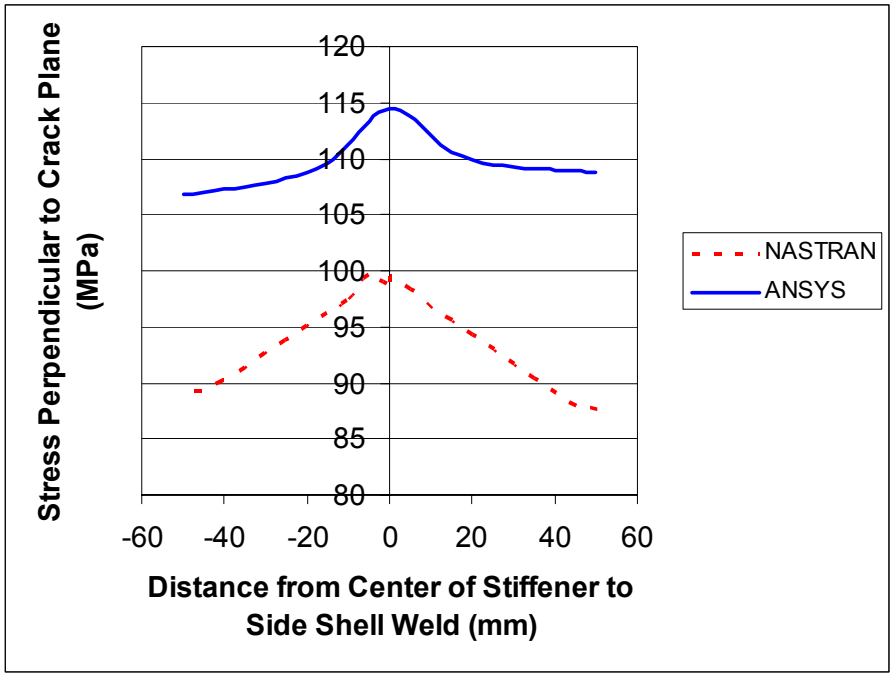

Figure 4.23: Comparison of Stress Perpendicular to the Crack Plane in the ANSYS and NASTRAN Models

5. MODELING OF SIMPLE CRACKED PLATE GEOMETRIES

There was an obvious disagreement between some of the weight function K_I estimates and the ANSYS results for both the calibration and validation model data sets and inconsistencies associated with the application of the corrections proposed by SaFFD [8] to account for section geometries and displacement controlled boundary conditions (see Appendix A). This led BMT FTL to examine other possible explanations for the disagreements observed. Three concepts were explored using simpler cracked plate geometries than those presented in Sections 3 and 4:

- Modeling to ensure that the crack tip element geometries did not significantly impact the ANSYS K_I estimates
- Modeling to examine the effects of displacement versus load control boundary conditions on K_I estimates
- Modeling to examine the effects of restrained and unrestrained plate stiffeners on K_I estimates

5.1 Examination of Crack Tip Element Geometry for a Surface Crack in a Finite Width Plate

Modeling semi-elliptical surface cracks tends to be the most difficult crack geometry to mesh in ANSYS. To ensure that the modeling approach used at BMT FTL produced K_I estimates consistent with handbook solutions and standard weight function estimates, the cracked plate geometry presented in Figure 5.1 was modeled. Note the geometric parameters depicted in Figure 5.1 are based upon the handbook solution for a surface flaw in a finite width plate used in this analysis.

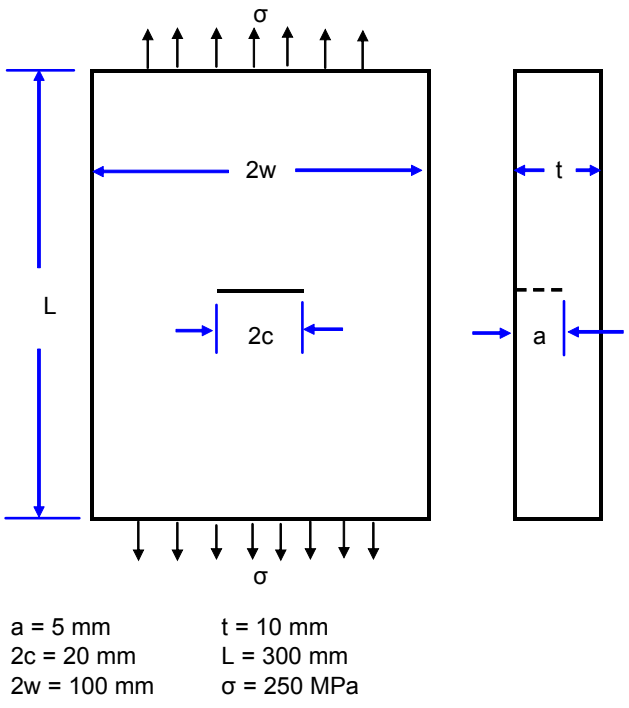

Figure 5.1: Geometry of Simple Surface Cracked Plate Example

The results of the ANSYS modeling was compared to the weight function solutions presented in Section 3.3 and the Raju and Newman solution [12] as presented in British Standards BS 7910, "Guide on methods for assessing the acceptability of flaws in metallic structures" [13]. For an axially loaded plate with a/2c ≤ 0.5, the Raju and Newman formulation is:

$$K_I = Y \sigma \sqrt{\pi a}$$

Where:

$$Y \sigma = f_w M_m P_m$$

P_m is the primary membrane stress applied to the plate (in this example 250 MPa) and f_w is the finite width correction factor. M_m is the membrane loading shape function based upon the flaw and plate size.

$$f_w = \left\{ \sec\left[\left(\frac{\pi c}{W} \right) \left(\frac{a}{B} \right)^{0.5} \right] \right\}^{0.5}$$

$$M_m = \frac{\left\{ M_1 + M_2 \left(\frac{a}{B} \right)^2 + M_3 \left(\frac{a}{B} \right)^4 \right\} g f_\theta}{\phi}$$

$$M_1 = 1.13 - 0.09 \left(\frac{a}{c} \right)$$

$$M_2 = \left[\frac{0.89}{0.2 + \frac{a}{c}} \right] - 0.54$$

$$M_3 = 0.5 - \frac{1}{0.65 + \frac{a}{c}} + 14 \left\{ 1 - \left(\frac{a}{c} \right) \right\}^{24}$$

$$\phi = \left\{ 1 + 1.464 \left(\frac{a}{c} \right)^{1.65} \right\}^{0.5}$$

At the deepest point g = 1, f_θ = 1. At the surface point:

$$g = 1.1 + 0.35 \left(\frac{a}{B} \right)^2$$

$$f_\theta = \left(\frac{a}{c} \right)^{0.5}$$

The ANSYS model crack tip was meshed in a manner similar to the models used in the calibration and validation studies ensuring that the elements met the requirements specified in the ANSYS help manuals [14]. The element edge aspect ratio was less than 4:1 with the radius of the crack tip elements less than a/8. One element was positioned every 30^o around the crack tip so that 12 wedged shaped elements surrounded the stress singularity. Along the length of the crack front an element was positioned for, at most, every 15^o change in curvature of the semi-elliptical profile. To satisfy the later criteria and maintain elements with as close to straight sides as possible, near the intersection of the crack front and the surface, elements were placed every 0.2 mm along the crack front.

The comparison of the results between the ANSYS, Raju and Newman and weight function K_I estimates is presented in Table 5.1. The surface point K_I estimate from the ANSYS models was estimated using the extrapolation method discussed in Section 2.4.2. For the deepest point, the ANSYS plane strain solution is within 5% of the Raju and Newman solution. Similarly, the ANSYS plane stress solution for the surface point is also within 5% of the Raju and Newman solution. The weight function solution is within 2% and 0.5% of the handbook solution for the deepest and surface points, respectively. The results indicate that the meshing used in the ANSYS models is adequate for determining K_I to a reasonable accuracy and would not explain the larger discrepancies reported for the ship structural details.

Table 5.1: Comparison of ANSYS, Handbook and Weight Function Solutions for a Surface Crack in a Plate

Crack Depth, a [mm]	Crack Length, 2c [mm]	ANSYS KI Estimate [MPa(mm)$^{1/2}$]				Raju and Newman KI Estimate [MPa(mm)$^{1/2}$]		Weight Function KI Estimate [MPa(mm)$^{1/2}$]	
		Deepest Point		Surface		Deepest Point	Surface	Deepest Point	Surface
		Plane Strain	Plane Stress	Plane Strain	Plane Stress				
5	**20**	967	880	880	815	1019	856	998	852

5.2 Effects of Load vs. Displacement Control on a Simple Through Crack in a Finite Width Plate Example

To examine the effects of load versus displacement control on K_I estimates, the simple through cracked plate geometry shown in Figure 5.2 was modeled for a series of crack lengths (2a) and compared to handbook and weight function solutions.

The handbook solution by Koiter [15] was used in this example, which is reportedly accurate to within 1% for any value of a/b [1]:

$$K_I = \sigma \sqrt{\pi a}\, F\left(a/b\right)$$

$$F\left(a/b\right)=\frac{1-0.5\left(a/b\right)+0.370\left(a/b\right)^2-0.044\left(a/b\right)^3}{\sqrt{1-a/b}}$$

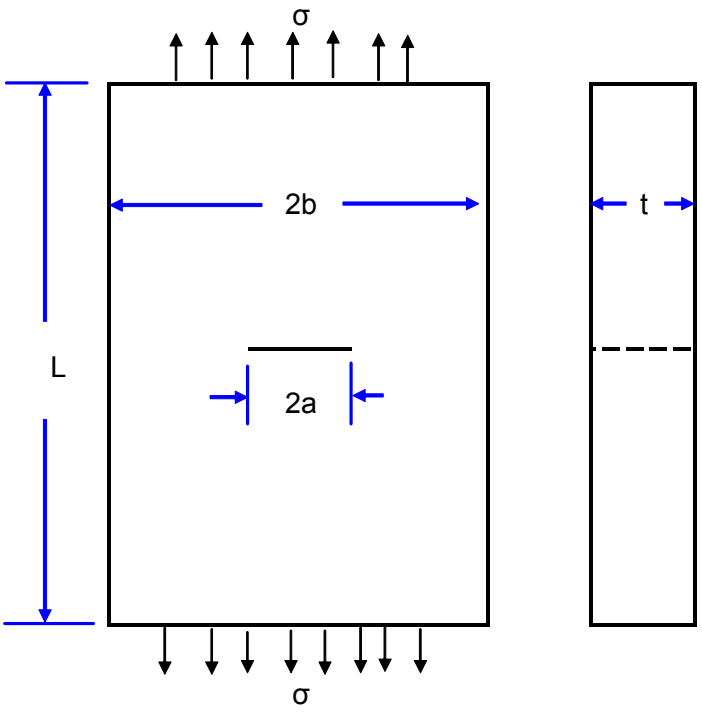

σ = 290 MPa t = 10 mm
2b = 100 mm L = 1000 mm

Figure 5.2: Simple Through Crack in a Finite Width Plate Geometry used to Compare Load versus Displacement Control

For the load control cases, a nominal remote stress of 290 MPa was applied to the FE models and used in the Koiter and weight function solutions. The load was kept constant and the crack length (2a) increased from 10 mm to 80 mm. In reduce the effects of the plate length on the K_I estimate as discussed previously, the plate was made very long (1000 mm) with respect to the plate width and crack size. Thus, the h/a values ranged from 12.5 to 100.

For the displacement controlled models, the displacement (ΔL) required to achieve a nominal stress of 290 MPa in an uncracked plate geometry was calculated assuming linear elastic loading and a Young's modulus of 207 GPa. For these models, the displacement was held constant while the crack length increased. The model mesh was exactly the same in both the load and displacement controlled models.

$$\Delta L = L\frac{\sigma}{E}=(1000)\left(\frac{290}{207000}\right)=1.4\,mm$$

The results are presented in Table 5.2 and Figure 5.3 for the mid-thickness location. The Koiter and weight function solutions agree to within 1% while the ANSYS plane stress K_I load control estimates agree to within 5% of the weight function solutions. The weight function solution estimates were always between the load control plane strain and plane stress estimates from ANSYS. However, in the displacement controlled boundary conditions models, as the crack length increases, the difference between the K_I obtained from ANSYS plane stress estimate and the weight function solution increases from about 3% to about 17%.

The effects of displacement controlled boundary conditions can be clearly identified in this example and it has ramifications when submodeling in ANSYS from a global model that does not explicitly contain a crack, even for very long plate lengths.

Table 5.2: Effects of Load and Displacement Controlled Boundary Conditions of K_I Estimates for a Simple Through Crack Model

Crack Half Length, a [mm]	Plate Half Width, b [mm]	ANSYS K_I Estimates [MPa(mm)$^{1/2}$]				Koiter K_I Estimate [MPa(mm)$^{1/2}$]	Weight Function K_I Estimate [MPa(mm)$^{1/2}$]	% Difference ANSYS Load Control Plane Stress to Weight Function	% Difference ANSYS Disp Control Plane Stress to Weight Function
		Load Control		Disp. Control					
		Plane Strain	Plane Stress	Plane Strain	Plane Stress				
5	**50**	1234	1123	1232	1121	1155	1155	2.8	2.9
10		1745	1588	1734	1578	1659	1670	4.9	5.5
20		2687	2445	2614	2379	2528	2565	4.7	7.3
25		3216	2927	3074	2797	3021	3064	4.5	8.7
30		3870	3522	3607	3282	3637	3684	4.4	10.9
35		4775	4346	4294	3908	4494	4512	3.7	13.4
40		6232	5671	5304	4827	5876	5825	2.6	17.1

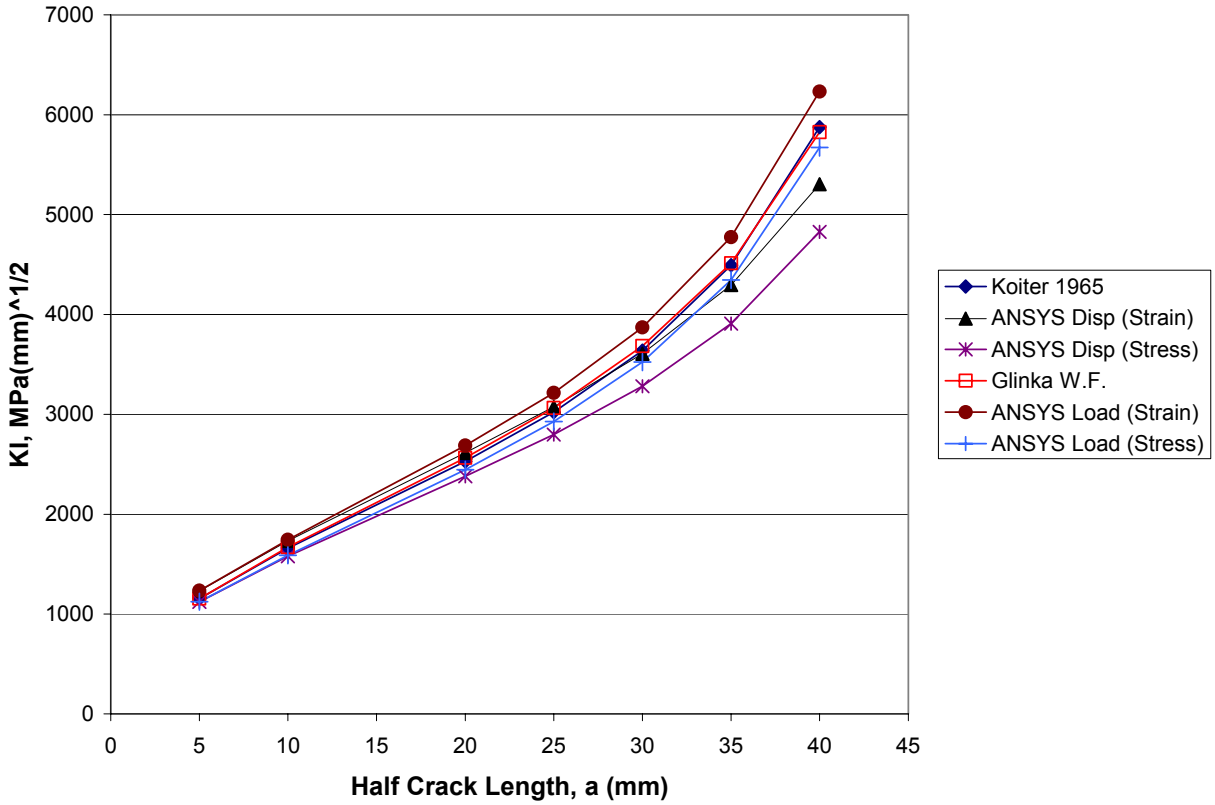

Figure 5.3: Results of Load vs. Displacement Control Investigation for the Simple Through Crack Example

5.3 Effects of Stiffened Elements on K_I Estimates

The third simplified geometry considered was similar to that shown in Figure 5.2 except a stiffening element was added on either side of the crack plane as indicated in Figure 5.4. Eight models were run in all. Four were run under displacement control and four under load control with the following scenarios:

- Uncracked with the stiffening elements unrestrained in the load application direction
- Uncracked with the stiffening elements restrained in the load application direction
- Cracked with the stiffening elements unrestrained in the load application direction
- Cracked with the stiffening elements restrained in the load application direction

The uncracked models were used to obtain stress estimates for weight function solutions. The crack was a through crack and the size was kept constant at 2a = 80 mm. With the exception of the crack plane region, similar model meshes were used for the cracked and uncracked geometries.

Once again a 290 MPa nominal stress was applied to the 1000 mm long model in the load controlled model and a 1.4 mm displacement (that provided a nominal stress of 290 MPa in the at uncracked case) in the displacement controlled models.

The results are presented in Tables 5.3 and 5.4. While there is a significant difference due to the load and displacement controlled boundary conditions, there is only a minor effect on K_I due to the addition of and the restraint applied to the stiffeners in this example. However, the fact that there is a difference suggests that further investigation into the effects of stiffening elements on a wider range of geometries and loading conditions would be a worthwhile exercise.

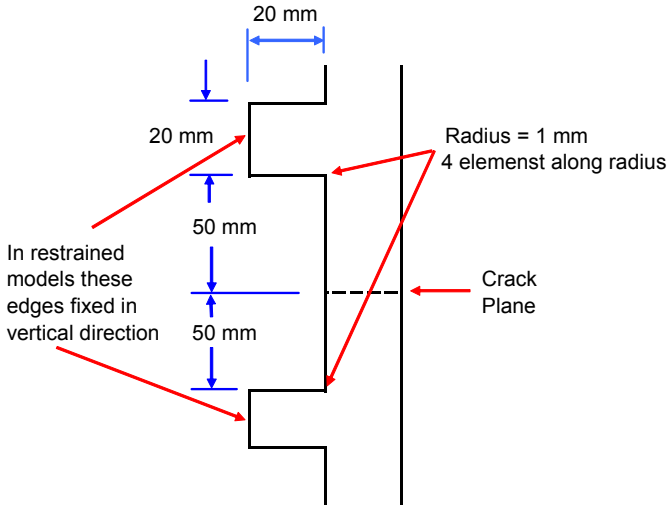

Figure 5.4: Addition of Stiffening Components to Through Crack Model

Table 5.3: Effects of Stiffeners and Stiffener Restraint on the Load Controlled Examples

Crack Half Length, a [mm]	Plate Half Width, b [mm]	ANSYS K_I Estimates [MPa(mm)$^{1/2}$]				Weight Function K_I Estimates [MPa(mm)$^{1/2}$]	
		Restrained Stiffener		Unrestrained Stiffener		Restrained Stiffener	Unrestrained Stiffener
		Plane Strain	Plane Stress	Plane Strain	Plane Stress		
40	**50**	6113	5563	6227	5666	5776	5833

Table 5.4: Effects of Stiffeners and Stiffener Restraint on the Displacement Controlled Examples

Crack Half Length, a [mm]	Plate Half Width, b [mm]	ANSYS K_I Estimates [MPa(mm)$^{1/2}$]				Weight Function K_I Estimates [MPa(mm)$^{1/2}$]	
		Restrained Stiffener		Unrestrained Stiffener		Restrained Stiffener	Unrestrained Stiffener
		Plane Strain	Plane Stress	Plane Strain	Plane Stress		
40	**50**	5229	4758	5325	4845	5800	5867

6. APPLICATION OF LOAD CONTROLLED BOUNDARY CONDITIONS TO CALIBRATION MODELS

After reviewing the results of the studies conducted in Section 5, it was decided to re-run the edge crack and through crack calibration models discussed in Section 3 approximating load controlled boundary conditions in the submodels.

This was not a simple task since ANSYS does not permit a direct interpolation of stress from global model to submodel boundaries. One method for future consideration would be to explicitly model the cracks in the global model and then interpolating the degree of freedom boundary conditions from the cracked global models. The time and costs associated with regenerating 12 global models containing cracks did not permit that option under the scope of the current project. Instead, the stresses normal to the crack plane were extracted from the global models at the locations of the submodel boundaries. Curve fitting was performed to approximate the stress distributions and then a macro was written in ANSYS to apply the stress profiles normal to the submodel boundaries. The load application and results are described in the following subsections.

6.1 Edge Crack Calibration Models Subjected to Load Controlled Boundary Conditions

The submodel geometry depicted in Figure 2.11 was used for this work. Stresses were applied to the forward and aft edges normal to the planes indicated in Figure 6.1.

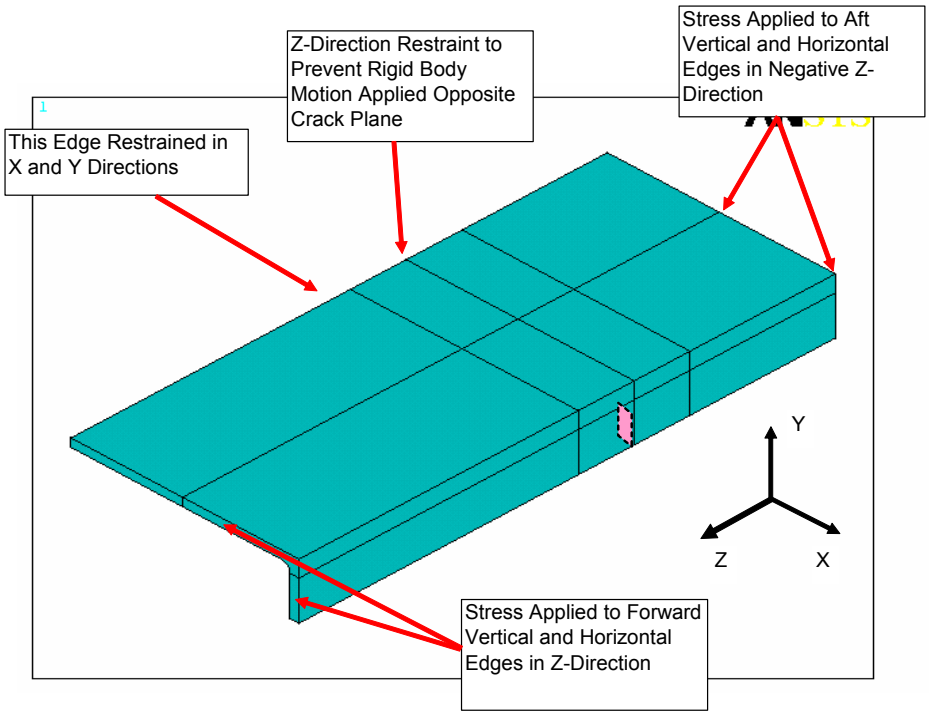

Figure 6.1: Load Controlled Edge Crack Calibration Model Boundary Conditions

The stress profiles and approximate linear curve fits applied to the submodel boundaries are illustrated in Figures 6.2 and 6.3. The edge of the submodel closest to the side-shell location was restrained to prevent rigid body motion but no stress profile was applied.

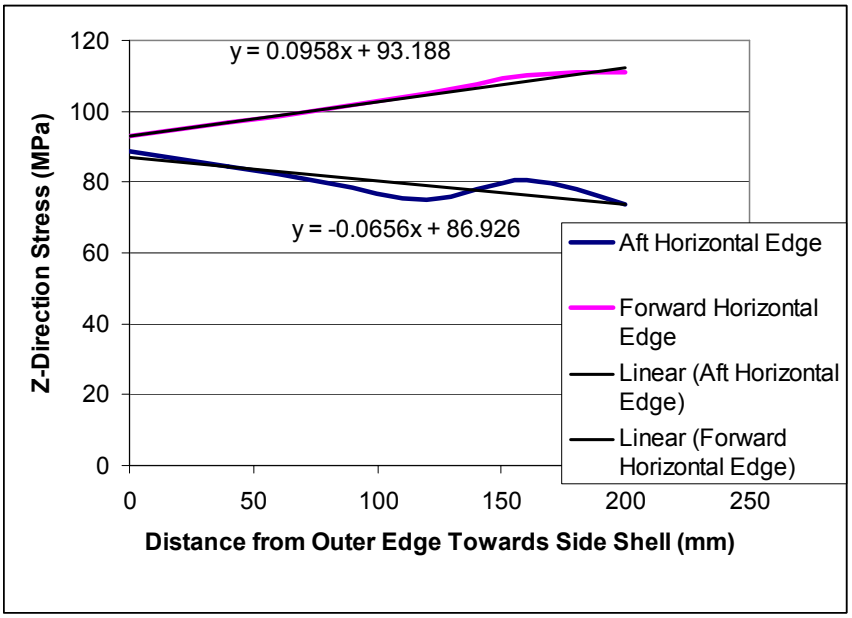

Figure 6.2: Stress Profile Approximations Applied to Horizontal Edges of Submodels

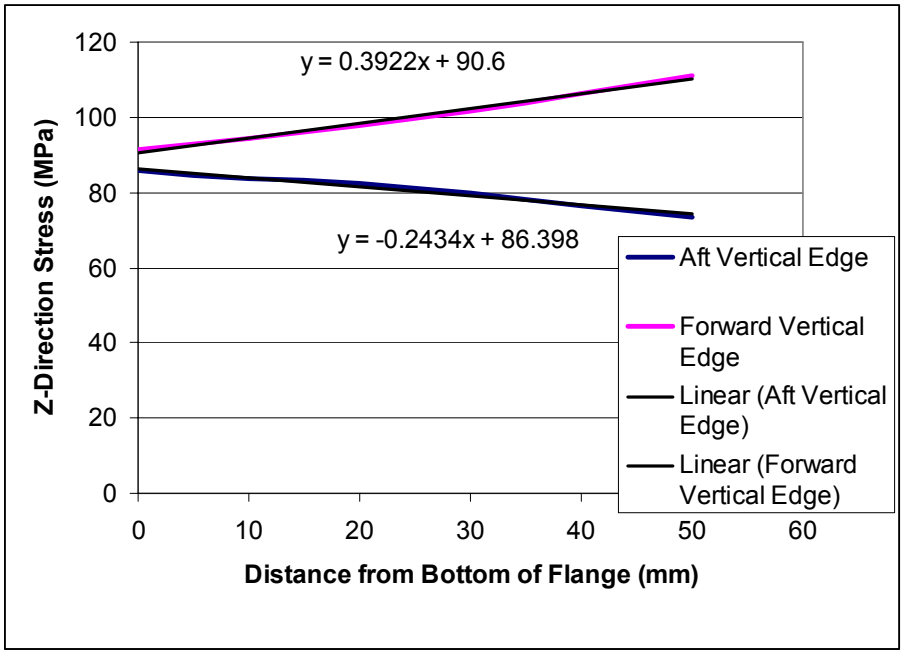

Figure 6.3: Stress Profile Approximations Applied to Vertical Edges of Submodels

The K_I estimates from the load control edge cracked calibration models are provided in Table 6.1. There is a much better agreement between the ANSYS estimates and the weight function solutions compared to the original modeling results (maximum difference of 1.3 times as opposed to 2.25 times). An improvement in the agreement may be possible with more detailed modeling and analysis to more accurately represent the submodel boundary conditions.

Table 6.1: Comparison of Calibration Edge Crack K_I Estimates for Load Control Submodels to Weight Function Solutions for a Single Edge Crack in a Plate

Crack Length, a (mm)	Plate Width, w (mm)	FE Model K_I Estimate $MPa(mm)^{1/2}$		Single Edge Crack Weight Function K_I Estimate $MPa(mm)^{1/2}$
		Plane Strain	Plane Stress	
5	46	416	378	367
10		657	595	595
15		934	850	930
20		1293	1176	1303
25		1790	1629	1897
30		2460	2238	2921

6.2 Through Crack Calibration Models Subjected to Load Controlled Boundary Conditions

Because of the large number of elements required in the models containing the crack tip elements, two stages of submodeling were performed for the through crack models as described in Section 2.3.2. The geometry of the first stage submodel was the same as that presented in Figure 2.22 with the application of the boundary conditions described in Figure 6.4. The stress profiles applied to the forward and aft vertical edges are presented in Figure 6.5. The second stage submodels were identical to those previously used.

As in the case of the re-analysis of the edge crack calibration models, the agreement between the load controlled ANSYS submodels and the weight function solutions for a through crack in a finite width plate improved significantly (1.1 times as opposed to 1.56 times) over the comparison using displacement controlled boundary conditions (Table 6.2). Further refinements in the application of the boundary conditions could provide improved results.

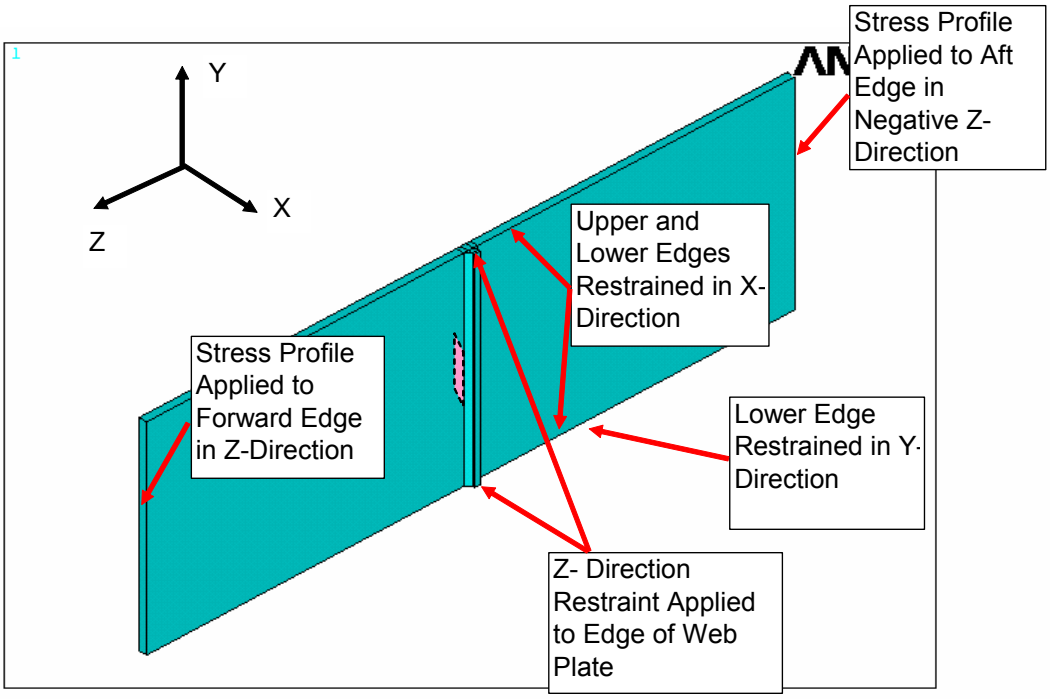

Figure 6.4: Description of Load Controlled Boundary Conditions Applied to Through Crack Calibration Models

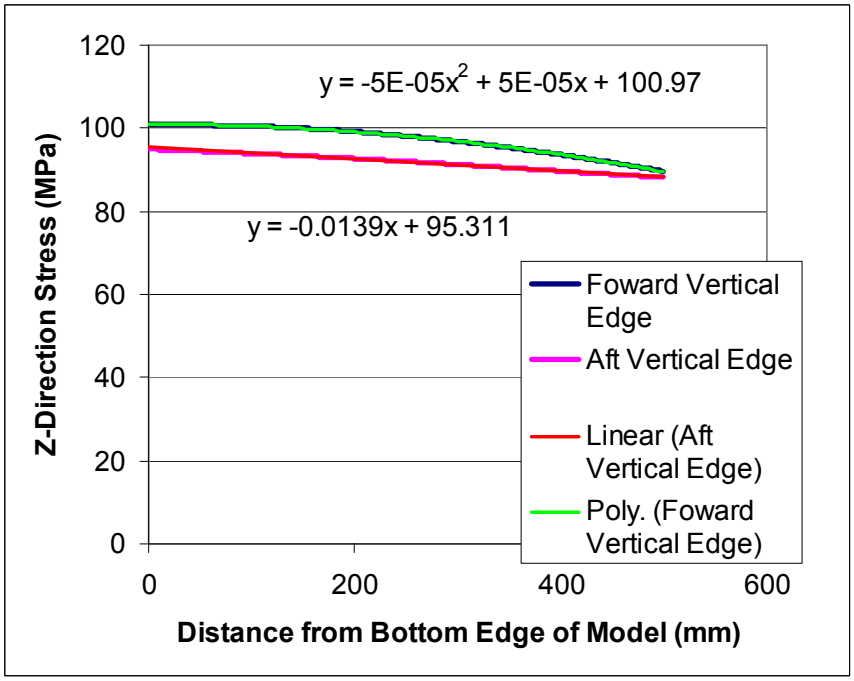

Figure 6.5: Stress Profiles Applied to Vertical Edges of Submodel

Table 6.2: Comparison of Calibration Through Crack K_I Estimates for Load Control Submodels to Weight Function Solutions for a Single Edge Crack in a Plate

	Crack Length 2a (mm)	Plate Width 2w (mm)	ANSYS KI Estimates MPa(mm)$^{1/2}$		Weight Function for a Through Crack in a Finite Width Plate MPa(mm)$^{1/2}$
			Plane Strain	Plane Stress	
Upper Crack Front	50	600	818	744	876
	100		1191	1084	1253
	150		1504	1369	1572
	200		1811	1649	1872
	250		2147	1954	2178
	300		2548	2319	2522
Lower Crack Front	50		819	744	961
	100		1193	1086	1371
	150		1508	1372	1711
	200		1815	1652	2028
	250		2148	1955	2339
	300		2545	2316	2662

7. SUMMARY AND CONCLUSIONS

With the complex structural components contained within the global model subjected to load control, the weight function solutions provided much better agreement with the ANSYS FE model predictions for K_I. However, when compared to the submodels subjected to displacement control, the weight function solutions generated very conservative estimates.

Three weight function solutions were initially targeted for investigation and a fourth was added when it appeared that restraint conditions for edge cracks suggested the addition of extra rotational resistance might be warranted. The four weight function solutions discussed in this document were:

- Edge crack in a finite width plate
- Through thickness crack in a finite width plate
- Semi-elliptical surface crack in a finite thickness plate
- Double edge cracked finite width plate (see Appendix A)

Initially, the ANSYS submodels used to generate the stress intensity factor estimates used degree of freedom boundary restraints extracted from an uncracked global model of a hypothetical ship structure. In theory, if these degrees of freedom boundary restraints are applied at a remote distance, the discrepancy between load controlled and displacement controlled stress intensity factor estimates should be minimal for small crack sizes in relation to the dimensions of the structural component. This behavior was observed for many of the smaller cracks, but as the crack sizes increased, discrepancies began to appear between the ANSYS displacement controlled solutions and the load controlled derived weight function solutions. For the edge crack and through crack examples, these discrepancies began at a/w values smaller than 0.3 and 0.15 respectively. The comparisons between the ANSYS displacement controlled model results and the load controlled weight function results for the calibration cracks are summarized in Table 7.1.

Based upon the comparisons between simpler ANSYS models and handbook solutions it is acknowledged that minor differences between the ANSYS K_I estimates and the weight function solutions could be attributed to the FE model mesh and geometry. A 5% difference between handbook and ANSYS model solutions was regularly observed. In addition, restraints resulting from attachments could contribute to the differences however, it is difficult at present to quantify the differences based upon the available information. Even if these two factors are considered they do not explain the significant differences presented in Table 7.1 (i.e. greater than 150%).

Table 7.2 presents a comparison of the edge crack and through crack ANSYS models with estimated load controlled boundary conditions extracted from the global model. There is a significant improvement in the agreement over the K_I estimates generated using displacement controlled boundary conditions. These results indicate that the majority of the differences calculated in Table 7.1 are due to difference in load and displacement controlled boundary conditions. It is anticipated that further study of the loading could improve the results.

Table 7.1: Comparison of ANSYS Displacement Controlled Calibration Model Results to Load Controlled Weight Function Estimates for K_I

Crack Type [mm]	Crack Length [mm]	Crack Depth [mm]	Plate Width [mm]	Plate Thickness [mm]	ANSYS KI Estimate [MPa(mm)$^{1/2}$]		Weight Function Estimate [MPa(mm)$^{1/2}$]	Percent Difference (%)
					Plane Strain	Plane Stress		
Edge Crack	5	-	46	-	402	366	367	0.3
	10				612	557	595	6.8
	15				818	744	930	25
	20				1030	938	1303	39
	25				1241	1130	1897	68
	30				1424	1296	2921	125
Through Crack Lower Crack Front	50	-	600	-	861	784	961	12
	100				1158	1036	1371	18
	150				1393	1267	1711	22
	200				1540	1401	2028	32
	250				1638	1490	2339	43
	300				1691	1539	2662	57
Surface Crack	50	1.6 Deepest	295	8	254	N/A	315	24
		1.6 Surface			N/A	167	123	26
	100	1.6 Deepest			272	N/A	324	19
		1.6 Surface			N/A	290	90	31
	50	3.2 Deepest			330	N/A	478	45
		3.2 Surface			N/A	206	243	18
	100	3.2 Deepest			359	N/A	549	53
		3.2 Surface			N/A	180	187	3.8
	50	4.8 Deepest			389	N/A	600	54
		4.8 Surface			N/A	305	393	29
	100	4.8 Deepest			442	N/A	817	85
		4.8 Surface			N/A	264	323	22

Notes: 1) Edge crack and surface crack surface location weight function estimates compared to ANSYS plane stress estimates.
2) Through crack and surface crack deepest location weight function estimates compared to ANSYS plane strain estimates.
3) Positive difference indicates weight function solution overestimates compared to ANSYS solution.

Table 7.2: Comparison of ANSYS Load Controlled Calibration Model Results to Load Controlled Weight Function Estimates for K_I

Crack Type [mm]	Crack Length [mm]	Crack Depth [mm]	Plate Width [mm]	Plate Thickness [mm]	ANSYS KI Estimate [MPa(mm)$^{1/2}$]		Weight Function Estimate [MPa(mm)$^{1/2}$]	Percent Difference (%)
					Plane Strain	Plane Stress		
Edge Crack	5	-	46	-	416	378	367	-2.9
	10				657	595	595	0.0
	15				934	850	930	9.4
	20				1293	1176	1303	11
	25				1790	1629	1897	17
	30				2460	2238	2921	31
Through Crack Lower Crack Front	50	-	600	-	819	744	961	17
	100				1193	1086	1371	15
	150				1508	1372	1711	14
	200				1815	1652	2028	12
	250				2148	1955	2339	8.9
	300				2545	2316	2662	4.6

Notes: 1) Edge crack weight function estimates compared to ANSYS plane stress estimates.
2) Through crack weight function estimates compared to ANSYS plane strain estimates.
3) Positive difference indicates weight function solution overestimates compared to ANSYS solution.

There are significant implications arising from the aforementioned observations. First of all, in the event that the weight function solutions presented in Section 3 are used, the K_I estimate appears to be conservative if the structure is subjected to displacement control conditions. In a ship structure, the complexity of the entire structure viewed as a whole allows for a certain amount of redundancy and a variety of load paths. Introducing a crack in a member may not always increase the stress proportionally in that member as load may be transferred to an uncracked component. This implies that the application of weight function solutions derived under the assumption of a load controlled scenario could, in some situations, be very conservative.

The corrections proposed by SaFFD (see Appendix A) to address the load versus displacement controlled load application have not provided consistent results for the models discussed in this report. Further investigation into the generation of correction factors or the generation of displacement control weight function solutions may be required. Along with this work, an investigation into the load behavior of a cracked ship structure will be required to determine when the displacement control versus load control assumptions are valid. Such an investigation may involve modeling a larger section of a ship structure, or possibly and entire structure and identifying changes in stress and displacement as cracks are introduced in various locations.

8. RECOMMENDATIONS

The following recommendations are provided based upon the outcome of this project work:

- The submodeling should be reevaluated for all of the geometries proposed to confirm that the standard weight function solutions do in fact give accurate K_I estimates for the ship structural details under load controlled applications. One way to accomplish this task would be to regenerate the global model to introduce the cracks prior to the submodeling step.
- Further analysis should be conducted to either generate weight function solutions for displacement controlled loading conditions or to improve the correction factors/procedures for the load controlled solutions to predict displacement controlled results. The most efficient means of undertaking this task would be to start with simple geometric configurations before moving to more complex ship details.
- The implications of introducing cracks into a complex global model containing redundant load paths should be investigated in detail. This information would be useful for estimating K_I using explicit finite element crack modeling of weight functions.
- Weight function solutions should be validated against additional structural detail geometries and a variety of loading conditions. The effects of stiffened components should be examined thoroughly.

9. REFERENCES

1. Tada, H., Paris, P., & G. Irwin, "The Stress Analysis of Cracks Handbook", Third Edition, ASME Press, 2000.
2. Bueckner, H. F., "A novel principle for the computation of stress intensity factors", *Zeitschrift fur Angewandte Mathematik und Mechanik*, vol. 50, pp.529-546, 1970.
3. Rice J. R., "Some remarks on elastic crack-tip stress field", *International Journal of Solids and Structures,* vol. 8, pp. 751-758, 1972.
4. Glinka, G., & G. Shen, "Universal features of weight functions for cracks in mode I", *Engineering Fracture Mechanics*, vol. 40, pp. 1135-1146, 1991.
5. Shen, G., & G. Glinka, "Determination of weight functions from reference stress intensity factors", *Theoretical and Applied Fracture Mechanics*, vol. 15, pp. 237-245, 1991.
6. Gross, B., & J.E. Srawley, "Stress Intensity Factors for a Single-Edge-Notched Tension Specimen by Boundary Collocation of a Stress Function", NASA TN D-2395, 1964.
7. Brown, W.F. Jr., & J.E. Srawley, "Plain Strain Crack Toughness Testing of High Strength Metallic Materials", ASTM STP 410, 1966.
8. Glinka, G., "Rapid Stress Intensity Factors Estimations", Progress Report 2 Submitted to BMT Fleet Technology Limited for SSC Project SR-1430.
9. Fichter, W.B., "Stresses at the Tip of Longitudinal Crack in a Plate Strip", NASA Technical Report, TR-R-265, NAA Langley, 1967.
10. Rice, J.R., "Stresses in an Infinite Strip Containing a Semi-Infinite Crack", (Discussion to W.G. Knauss, Vol. 33, p. 356, 1966), Trans. ASME, Ser. E, Journal of Applied Mechanics, Vol. 34, p.248, 1967.
11. Isida, M., "Effects of Width and Length on Stress Intensity Factors of Internally Cracked Plates under Various Boundary Conditions", International Journal of Fracture Mechanics, Vol. 7, p.301, 1971.
12. Raju, I.S., & J.C. Newman, "Stress intensity factors for a wide range of semi-elliptical surface cracks in finite width plates", *Engineer Fracture Mechanics*, 11 (4) pp. 817-829, 1979.
13. British Standards Association, "Guide on methods for assessing the acceptability of flaws in metallic structures", BS 7910 Incorporating Amendment No. 1, 1999.
14. ANSYS 7.0 Manuals, Chapter 11, "Fracture Mechanics".
15. Koiter, W.T., "Note on the Stress Intensity Factor for Sheet Strips with Cracks under Tensile Loads", university of Technology, laboratory of Engineering Mechanics, Report No. 314, Delft, Netherlands, 1965.

APPENDIX A
Investigation of Correction Factors

Throughout the course of this project, SaFFD attempted to develop a series of correction factors to:

- account for differences between the flaw and specimen geometries used to generate the simple weight function solutions and the more complex geometries of the ship structures examples,
- account for the effects of the displacement controlled boundary conditions,

in order to reduce the discrepancies observed between the weight function solutions and the K_I estimates obtained from the ANSYS models using displacement controlled boundary conditions.

To date, attempts at developing such correction factors have not been successful and SaFFD has proposed that a more fundamental approach may be required to be successful.

While good agreement has been shown between the ANSYS models using load controlled boundary conditions and the weight function solutions, further work is required to determine whether ship structural details experience predominantly load or displacement controlled service loading. This depends upon the redundancy in the load paths within the structure and the nature of the applied loading. In all likelihood, many details may experience a loading scenario which falls between those two extremes. In any case, without information to suggest that structure is experiencing a displacement controlled load condition, the use of the weight function solutions derived for load controlled applications appear to provide conservative K_I estimates.

This section of the report will summarize the attempts made by SaFFD to develop correction factors during this project.

A1 Edge Crack Correction Factors

SaFFD [8] has suggested that the differences in the K_I estimates may be attributable to features of the stiffener geometry. The single edge crack weight function was derived for the geometrical configuration illustrated in Figure 3.5. However, the actual stiffener geometry is different because of the web effect and it was proposed that the web could be treated as extra stiffening element on the upper edge of the cracked flange.

The use of the displacement boundary conditions extrapolated from the global model results in a displacement controlled loading scenario for the cracked models since the global model did not contain the edge cracks. Standard weight functions (as in the case of those presented in this document) are generally derived for load control scenarios for single path loading.

The implications of the load versus displacement controlled assumption can be illustrated with the use of a simple example. Consider first Figure A.1. If the load, P, is applied to the structure as shown (assuming that the cross member is infinitely rigid), then simple mechanics will show that the load transferred to Bar B is equal to the load transferred to Bar A. If the load is replaced and by a uniform deflection of the cross-member, δ, the load in Bar B is actually ½ of the load in Bar A. Compare this to a scenario where two identical stiffeners are located in a ship structural detail under a constant displacement loading.

If the cross-sectional area of the stiffener is reduced due to the presence of a crack, but the global displacement of that detail remains constant because of redundancies elsewhere in the structure, the load in the cracked stiffener actually reduces and more of the load is transferred to the uncracked stiffener.

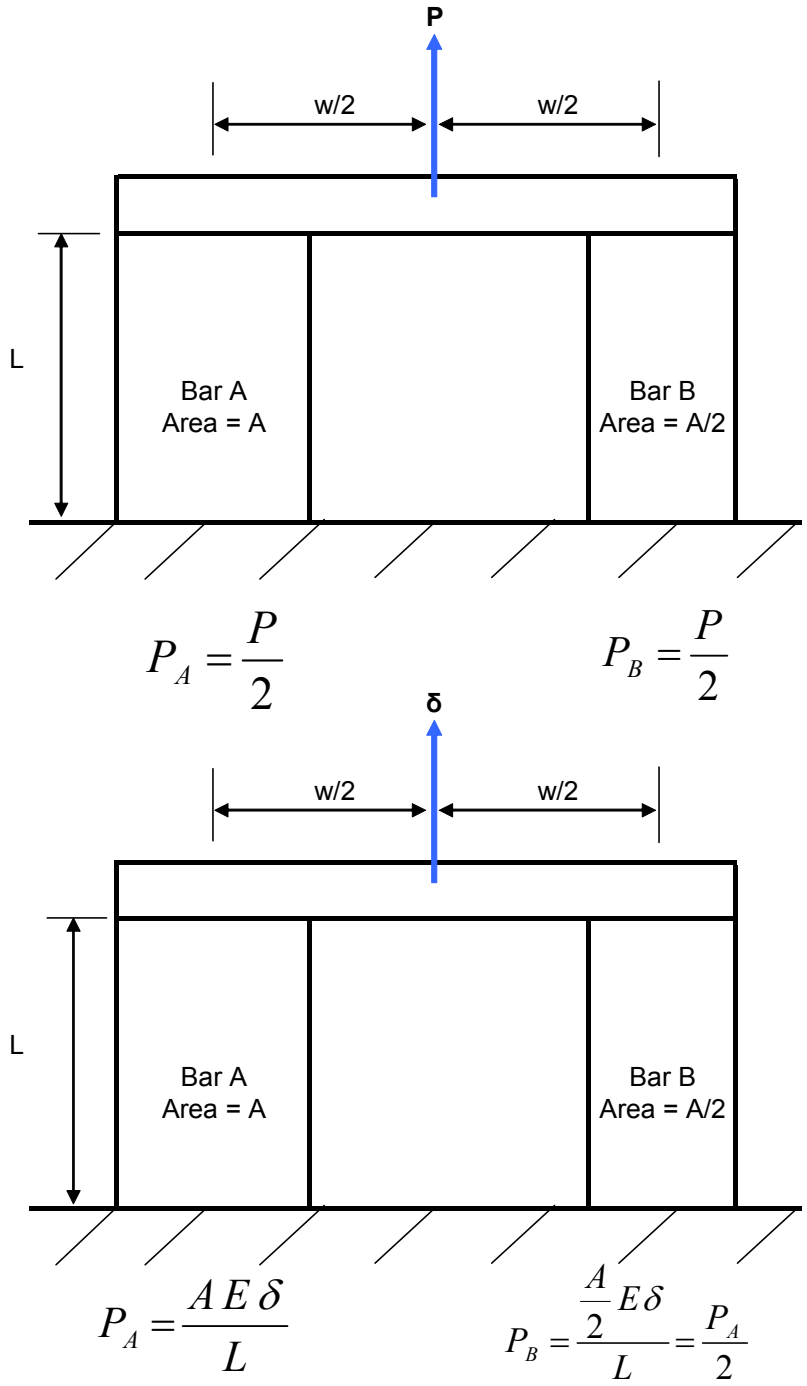

Figure A.1: Comparison of Load versus Displacement Controlled Scenarios

Weight function solutions derived for load controlled scenarios would be based on the assumption that the load remains constant in the present of the crack (i.e. the stress in the component increases proportionally to the decrease in cross-sectional area). Under displacement control in a redundant structure, the increase in stress (if any) will not be directly proportional to the change in cross-section (i.e. load shedding may occur).

A1.1 Initial Set of Proposed Correction Factors

In the case of the calibration edge crack models, there was additional stiffness due to the web of the stiffener. The web restricted rotation of the cracked flange. Restraining the upper edge as shown in Figure A.2 can subsequently simulate such a stiffening effect. The stiffening effect is in turn analogous to adding a symmetry effect, i.e. replacing the single edge crack model with a stiffened edge by a double edge cracked weight function solution as illustrated in Figure A.3. The weight function solution for a double edge crack plate has the same general form as that for the edge and through cracks with changes to the M_1, M_2 and M_3 parameters. The values for M_1, M_2 and M_3 follow and are valid for $0 < a/w < 0.9$.

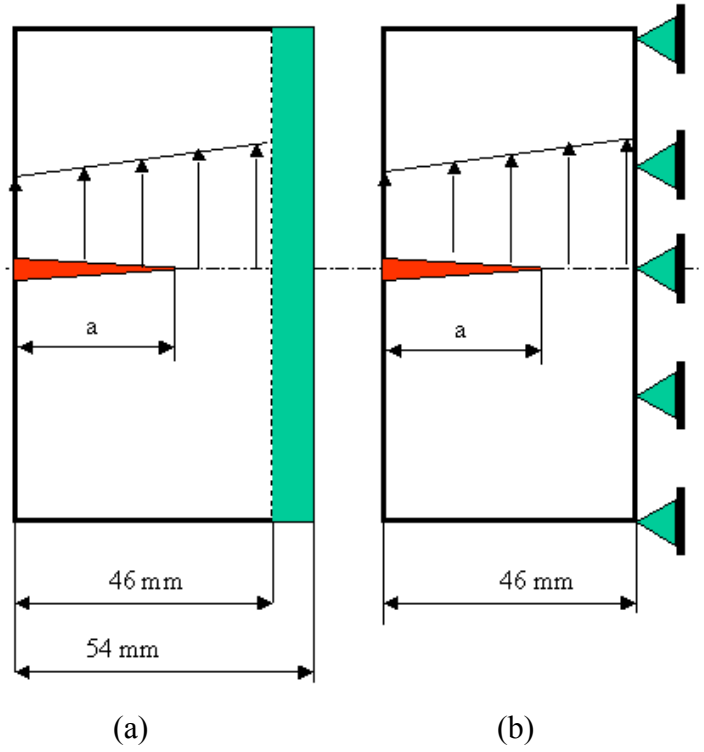

Figure A.2: (a) Geometry of the Section of the Side Shell Stiffener used in the Submodel with (b) the Effects of the Web Replaced with Rigid Restraints

$$M_1 = 0.08502 - 0.02230\left(\frac{a}{w}\right) - 1.41028\left(\frac{a}{w}\right)^2 + 4.64559\left(\frac{a}{w}\right)^3 + 19.6924\left(\frac{a}{w}\right)^4 - 148.266\left(\frac{a}{w}\right)^5 + 336.837\left(\frac{a}{w}\right)^6 - 336.591\left(\frac{a}{w}\right)^7 + 127.009\left(\frac{a}{w}\right)^8$$

$$M_2 = 0.2234 - 0.6146\left(\frac{a}{w}\right) + 11.1687\left(\frac{a}{w}\right)^2 - 56.5326\left(\frac{a}{w}\right)^3 + 151.937\left(\frac{a}{w}\right)^4 - 182.634\left(\frac{a}{w}\right)^5 + 86.4731\left(\frac{a}{w}\right)^6$$

$$M_3 = 0.4983 + 0.7512\left(\frac{a}{w}\right) - 10.5597\left(\frac{a}{w}\right)^2 + 47.9251\left(\frac{a}{w}\right)^3 - 115.933\left(\frac{a}{w}\right)^4 + 131.976\left(\frac{a}{w}\right)^5 - 59.8893\left(\frac{a}{w}\right)^6$$

The stress intensity factor generally depends on three factors [8]:

- The stress field
- The component stiffness
- The remaining net cross section area

The relative decrease of the effective cross section area caused by the crack of depth 'a' may have been different in the generic models used for the derivation of the weight functions for either the single edge cracked or doubled edge cracked plates than in the actual stiffener. Therefore, a further possible correction for the stress intensity factor calculated on the basis of the weight function derived for a double edge crack in a plate was proposed to correct for the relative loss of the effective cross section area. It was reported that this correction was used when the weight function solutions for edge cracks were applied to structural details such as I, L or C-sections [8].

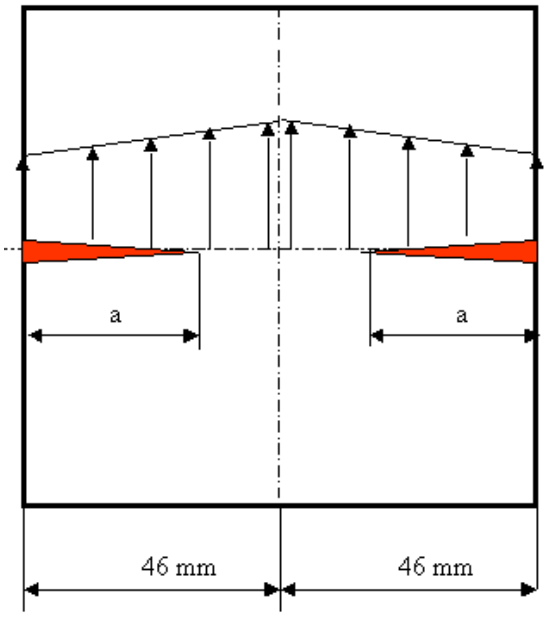

Figure A.3: Double Edge Cracked Plate Geometry

In general terms, the geometry of the stiffener is defined as shown in Figure A.4, where:

a = crack length

w = height of the flange, from the bottom edge to the bottom edge of the flange

L = length of the flange

t_f = thickness of the flange

t_w = thickness of web

The relative loss of cross-sectional area for the flange can be expressed as:

$$\alpha_{flange} = \frac{A_{flange} - A_{crack}}{A_{flange}} = \frac{wt_f - at_f}{wt_f}$$

The relative loss of cross-sectional area for the entire stiffener is:

$$\alpha_{stiff} = \frac{(A_{flange} + A_{web}) - A_{crack}}{(A_{flange} + A_{web})} = \frac{(wt_f + Lt_w) - at_f}{(wt_f + Lt_w)}$$

The correction factor required to account for the relative loss of cross-sectional area for a structural shape then becomes:

$$C_{Ar} = \sqrt{\frac{\alpha_{flange}}{\alpha_{stiff}}}$$

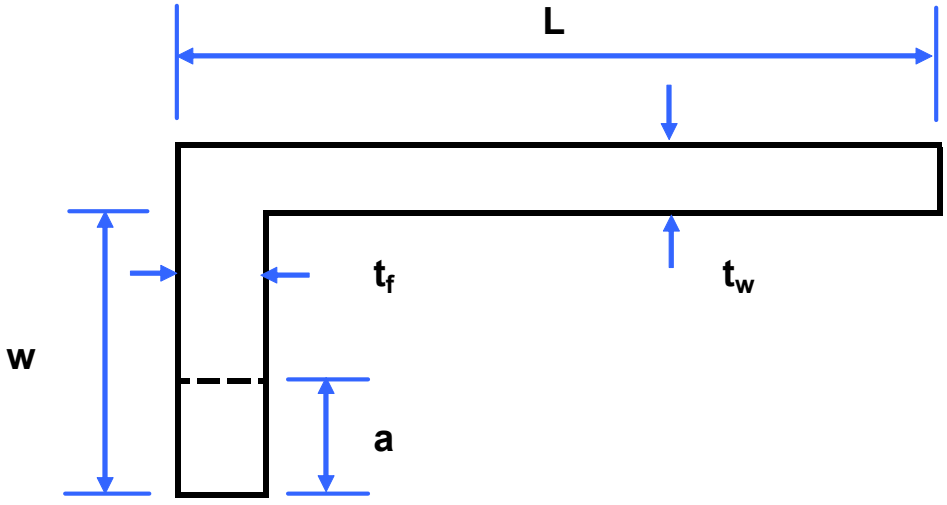

Figure A.4: Geometry of Side Shell Stiffener Defined Parametrically

The relative loss of the cross section for this specific stiffener geometry is illustrated in Figure A.5. Since the thickness is essentially constant, the loss of the cross section area in a flat plate with a single edge crack is proportional to the depth of the crack 'a' and it can be written as:

$$\alpha_{flange} = \frac{46 - a}{46}$$

The relative loss of the cross section area in the stiffener is less than in the single plate and again since the thickness is constant it can be determined as:

$$\alpha_{stiff} = \frac{344 - a}{344}$$

The proposed correction for the stress intensity factor due to the relative loss of cross-sectional area of the stiffener compared to a plate would be:

$$K_I = C_{Ar} \cdot \int_0^a \sigma(x) m(x,a) dx = \sqrt{\frac{344}{344-a} \cdot \frac{46-a}{46}} \cdot \int_0^a \sigma(x) m(x,a) dx$$

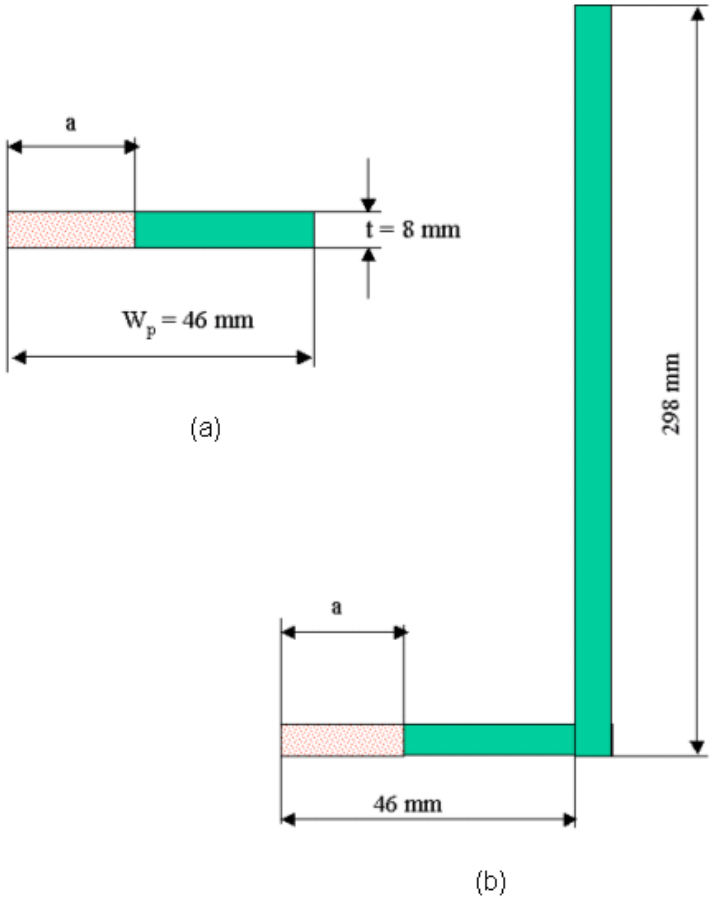

Figure A.5: Relative Loss of Cross-Sectional Area for (a) the Flange and (b) the Total Stiffener

Rather than deriving displacement controlled weight functions, SaFFD proposed a possible correction factor [8] to compensate for differences from load-controlled scenarios. The magnitude of the load acting on the cracked component depends on its stiffness, which is approximately proportional to the remaining cross section area. Theoretical analyses and observations of cracked redundant structures indicate that the loss of stiffness and subsequent decrease of the load on given component is proportional to the ratio of the actual effective cross-section area to the cross-section area of the uncracked component. This is supported by the example presented in Figure A.1 where the change in load in Bars A and B going from load to displacement control is proportional to the change in the cross-sectional area. In the case of the stiffener cross section shown in Figure A.5, the loss of stiffness can be approximately described as the ratio of the remaining area to the area of the uncracked member:

$$C_{stif} = \frac{A_r}{A} = \frac{(W_{stif} - a)\cdot t}{W_{stif}\cdot t} = \frac{344 - a}{344}$$

Thus, the final expression for the stress intensity factor accounting for the relative loss of the cross section area and for the change of stiffness can be written in the form of:

$$K = C_{Ar}\cdot C_{stif}\int_0^a \sigma(x)m(x,a)dx$$

In the case of the component shown in Figure A.5, the correction factors are:

$$C_{Ar} = \sqrt{\frac{46-a}{46}\cdot\frac{344}{344-a}} \qquad C_{stif} = \frac{344-a}{344}$$

The finite element results and those obtained from the weight function with and without correction for the loss of the effective cross section are shown in Table A.1 and Figure A.6. The application of the proposed correction factors result in a significant underestimation of K_I with respect to the ANSYS results.

Table A.1: Comparison of Stress Intensity Factor Estimates Using the Modified Edge Crack Weight Function Solution

Crack Length, a (mm)	Plate Width, w (mm)	FE Model K_I Estimate MPa(mm)$^{1/2}$ Plane Stress	Weight Function K_I Estimate for Edge Crack without Correction Factors MPa(mm)$^{1/2}$	Modified Weight Function K_I Estimate, Double-Edge Crack with Correction Factors MPa(mm)$^{1/2}$
5	**46**	366	367	347
10		557	595	462
15		744	930	533
20		938	1303	579
25		1130	1897	609
30		1296	2921	626

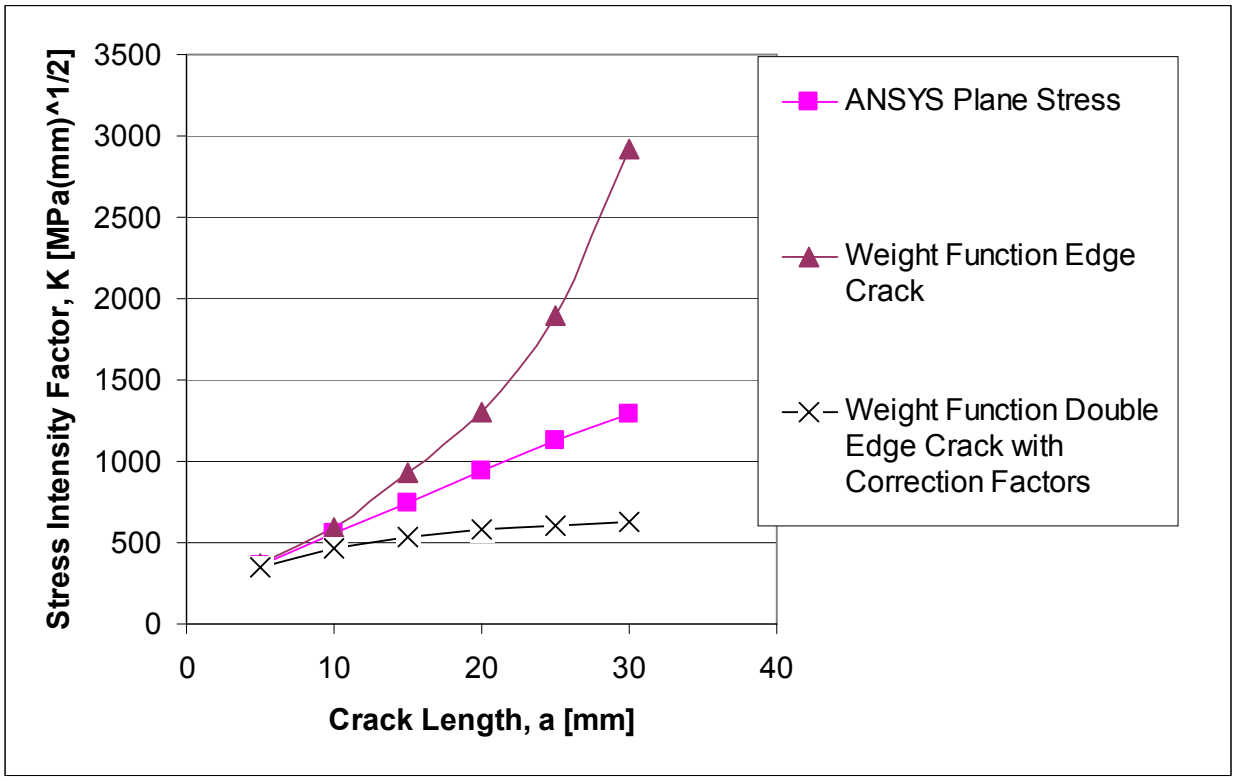

Figure A.6: Comparison of the FE Model and the Original and Modified Weight Function Solutions for the Edge Crack Calibration Examples

A1.2 Second Attempt to Develop Correction Factors

Since the simplified approach in Section A1 was not successful an alternate method was proposed.

In order to address displacement versus load control boundary control issues, the correction factor F_1 [1] shown in Figure A.7 was used. SaFFD suggested that F_1 could be multiplied to the shape function, Y, for the flaw size and specimen geometry to account for the influence of h/a under displacement control. Note that for the example shown in Figure A.7, a through crack in an infinite plate, Y = 1, therefore $K = F_1 \sigma (\pi a)^{1/2}$.

To account for addition effects of h/w (w being the ½ width of the plate) not incorporated into F_1, SaFFD proposed an additional correction:

$$\alpha_{plate} = \sqrt{1 - \frac{h}{3W}}$$

For the case of the edge cracked stiffener used for the calibration models W is the height of the flange, w, plus the length of the web, L, and α_{plate} becomes:

$$\alpha_{plate} = \sqrt{1 - \frac{h}{3(w+L)}}$$

The use of the double edge crack weight function solution to increase rotational stiffness resulting from the web results in the assumption that the member is very stiff resulting in a lower bound estimate of K_I. At the other extreme, the assumption resulting in the least stiffness would be that the cracked member geometry is a single edge crack configuration with the plate width equal to the flange height, w. This would generate an upper bound estimate of K_I. In reality, the additional stiffness generated by the web is likely somewhere in between these two extremes and it was proposed that an effective plate width, w_{eff}, could be used:

$$w_{eff} = \beta\left(w + t_w\right)$$

In the above equation, t_w, is the thickness of the web. The parameter β is calculated using the formula below. It approaches and limiting value of 2 as h becomes much larger than the width of the plate.

$$\beta = 2 + \frac{3}{2}\left(\frac{w + t_w}{h}\right)$$

For the edge crack calibration examples w_{eff} was calculated to be 113.9 mm.

A final correction was proposed to account for the relative loss of cross-sectional area due to the crack:

$$\alpha = \sqrt{\frac{\left(A_{flange} + A_{web}\right) - A_{crack}}{A_{flange} + A_{web}}} = \sqrt{1 - \frac{a\,t_f}{w t_f + L t_w}} = \sqrt{1 - \frac{a}{w + L}}$$

Therefore, using w_{eff} in the weight function calculation, the proposed correction factor was:

$$F = F_1\sqrt{\left(1 - \frac{a}{w + l}\right)\left(1 - \frac{h}{3\left(w + L\right)}\right)} \qquad \text{for } \frac{h}{w + L} \le 3$$

$$F = F_1 \qquad \text{for } \frac{h}{w + L} > 3$$

The limiting value of 3 was chosen based upon data available and may change depending upon the results of future investigations.

Table A.2 provides the results of applying these corrections to the edge crack calibration examples. There is good agreement between the ANSYS FE model results and the corrected weight function K_I estimates. Note however that the use of w_{eff} alone appeared to provide good agreement with the ANSYS estimates.

$$s = \frac{a}{a+h} = \frac{a/h}{1+a/h} = \frac{1}{1+h/a}$$

$$K_I = \sigma\sqrt{\pi a}\cdot F_1(s)$$

$$= \sigma\sqrt{h}\cdot F_2(s)$$

$$s \to 0 (a/h \to 0) : F_1 = 1, F_2 \to \sqrt{\frac{\pi a}{h}}$$

$$s \to 1 \left(\frac{a}{h} \to \infty\right) : \quad F_2 = \sqrt{1-\nu^2}$$

$$F_1 \to \sqrt{1-\nu^2}\sqrt{\frac{h}{\pi a}}$$

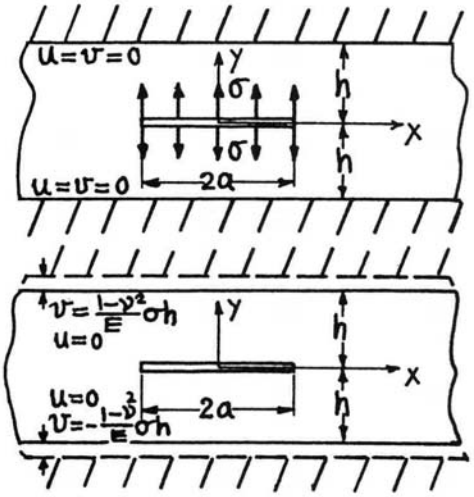

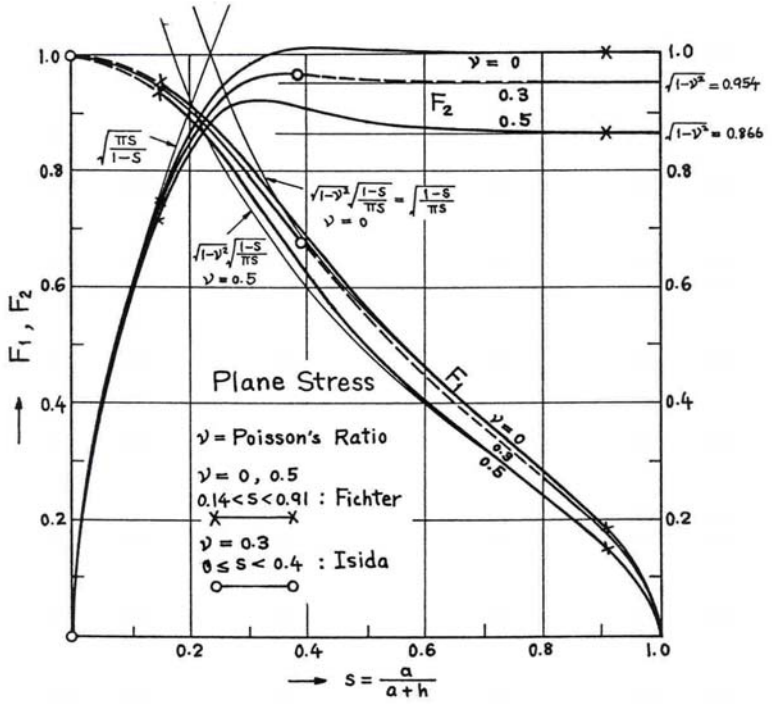

Methods: Expansions of Complex Stress Potentials (Isida), Fourier Transform (Fichter), $s \to 0$: Solution for Infinite Plate, $s \to 1$: Energy Balance (Rice)
Accuracy: Order of 1%
References: **Fichter 1967; Rice 1967; Isida 1971a**

NOTE: For plane strain $F_2(s \to 1) = \sqrt{1-2\nu}/(1-\nu)$, etc.

Figure A.7: Proposed Correction factor F_1 to Account for Displacement Controlled Boundary Conditions

Table A.2: Corrected Weight Functions Solutions for the Edge Crack Calibration Models using the Second Iteration Correction Factors

Crack Length a (mm)	ANSYS KI Estimates		Weight Function KI Estimates			
	Plane Strain MPa.mm^1/2	Plane Stress MPa.mm^1/2	EdgeCrack Weff=113.6 MPa.mm^1/2	F1	F	WF Corrected MPa.mm^1/2
5	402	366	381	0.999	0.993	378
10	612	557	566	0.997	0.984	557
15	818	744	736	0.996	0.976	718
20	1030	938	910	0.990	0.964	877
25	1241	1130	1101	0.988	0.955	1052
30	1424	1296	1319	0.986	0.947	1249

When the above correction factors were applied to the edge crack validation examples, however, the agreement was not as promising as shown in Tables A.3 and A.4. It would appear that the proposed second iteration correction factors are not universally applicable. While the agreement for the Calibration cracks and Validation Crack 3 are within 10% of the ANSYS results, the corrected value for Validation Crack 2 is still about 35% higher than the ANSYS estimate. There appears to be some promise in this approach, however further investigation is required.

Table A.3: Validation Crack 2 Edge Crack Example with Proposed Second Iteration Correction Factors

Crack Length, a (mm)	Plate Width, w (mm)	FE Model K_I Estimate MPa(mm)$^{1/2}$		Weight Function K_I Estimate MPa(mm)$^{1/2}$	
				Single Edge Crack Uncorrected	Single Edge Crack Corrected
		Plane Strain	Plane Stress	ANSYS Stress Estimate	ANSYS Stress Estimate w_{eff} = 886 mm
125	**295**	1198	1091	3226	1475

Table A.4: Validation Crack 3 Edge Crack Example with Proposed Second Iteration Correction Factors

Crack Length, a (mm)	Plate Width, w (mm)	FE Model K_I Estimate MPa(mm)$^{1/2}$		Single Edge Crack Weight Function K_I Estimate Uncorrected MPa(mm)$^{1/2}$	Single Edge Crack Weight Function K_I Estimate Corrected MPa(mm)$^{1/2}$ w_{eff} = 950 mm
		Plane Strain	Plane Stress		
60	**295**	904	823	1403	886

A2 Through Crack Correction Factors

A similar approach to that reported in Section A1 was examined to identify possible correction factors for the through crack examples. The first two iterations considered the F1 parameter and the correction for loss of stiffness, C_{stif}, based upon the area reduction independently for the calibration examples. As shown in Table A.5 and Figure A.8, neither option appeared to be appropriate.

$$C_{stif} = \frac{A_{plate} - A_{crack}}{A_{plate}} = \frac{w - a}{w}$$

Table A.5: Upper Crack Front Mid-Thickness Weight Function Solution Comparison for Through Crack Calibration Example

Crack Length a (mm)	ANSYS Solutions MPa(mm)$^{1/2}$ Plane Strain	Weight Function Solution MPa(mm)$^{1/2}$	F_1	Weight Function Solution Modified by F_1 MPa(mm)$^{1/2}$	C_{Stif}	Weight Function Solution Modified by C_{stif} MPa(mm)$^{1/2}$
50	853	876	0.99	867	0.91	797
100	1138	1253	0.98	1228	0.83	1044
150	1359	1572	0.98	1541	0.75	1155
200	1493	1872	0.97	1816	0.67	1254
250	1576	2178	0.94	2047	0.58	1263
300	1617	2522	0.93	2345	0.5	1261

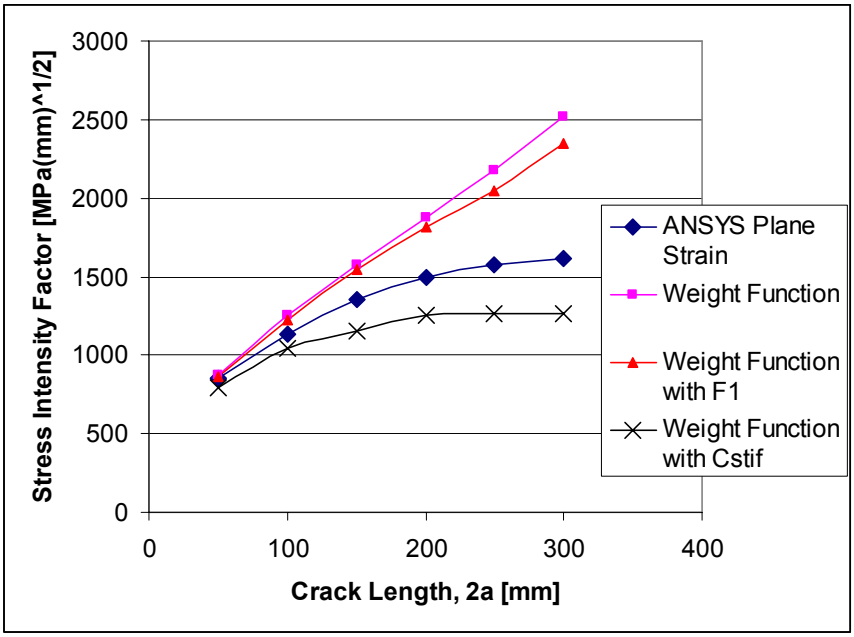

Figure A.8: Comparison of ANSYS and Weight Function Estimates of Stress Intensity Factors for the Through Thickness Crack Calibration Example along the Upper Crack Front

As a next attempt, the correction factor F, described in Section A1.2, was applied to the simple through crack displacement controlled results discussed in Section 5.2. In this case w_{eff} was not applicable. As seen in Table A.6, the proposed correction factors still resulted in up to a 20% overestimate of K_I. Similar differences were observed when F was applied to the through crack calibration models.

Table A.6: Application of Correction Factor F to Simple Through Crack Model (all KI values in MPa(mm)$^{1/2}$

a (mm)	w (mm)	a/w	ANSYS KI Estimates, MPa.sqrt(mm) (Displacement Controlled B.C.)		SaFFD Weight Function	F1	F	SaFFD WF Cor	% Difference with ANSYS Plane Stress
			Plane Strain	Plane Stress					
5	50	0.1	1232	1121	1155	1.000	1.000	1143	2.0
10	50	0.2	1734	1578	1670	0.999	0.999	1667	5.6
20	50	0.4	2614	2379	2565	0.998	0.998	2555	7.4
25	50	0.5	3074	2797	3064	0.997	0.997	3046	8.9
30	50	0.6	3607	3282	3684	0.995	0.995	3647	11.1
35	50	0.7	4294	3908	4512	0.995	0.995	4467	14.3
40	50	0.8	5304	4827	5825	0.990	0.990	5709	18.3

APPENDIX B
Documentation and Help File for Weight Function Calculator Software

Weight Function Stress Intensity Calculator Software
Instructions and Help Document
BMT Fleet Technology Limited
September 2003
Rev. 0

SR-1430
BMT FTL Project No. 5359C

Introduction

This document contains a description of the Stress Intensity Factor Calculator software provided to the US Ship Structures Committee as a deliverable for Project SR-1430, "Rapid Stress Intensity Factor Solution Estimation for Ship Structures Application" (BMT FTL Project No. 5359). The software incorporates Shen-Glinka [1] weight function solutions for:

- Edge cracks in finite width plates
- Double-edge cracks in finite width plates
- Through-thickness cracks in finite width plates
- Semi-elliptical surface cracks in finite width plates

A description of the software operation and input requirements is provided. Discussions related to the weight function solutions are provided in the BMT FTL Report 5359C-FR.

Software Modules

The software is comprised of two primary modules:

- The calculation module, wfmain.exe
- The user interface, StressIntensityFactorCalc.exe

An ASCII text document is generated by the calculation modules containing the name of the input stress file, the input parameters, the shape function, Y, and the stress intensity factor, K. This text file is called WFMAIN.OUT and will be over-written with every execution of the calculation module. If it is desirable to keep the information in the text file, it is recommended that the file be renamed prior to executing a new calculation.

Note the general equation for K is:

$$K = Y \sigma \sqrt{\pi a}$$

Where: K = stress intensity factor

Y = shape function based upon flaw and plate geometry

a = the crack length of depth

wfmain.exe

The source code for the wfmain.exe module was created by SaFFD Inc. in FORTRAN. BMT FTL converted the source code to ANSI C and generated the executable used with StressIntensityFactorCalc.exe. In addition to the executable, the source code has been provided and it is compatible with any ANSI C compiler.

StressIntensityFactorCalc.exe

This module was created by BMT FTL as a Windows-based user interface with the calculation module. It is used to supply the input data and view the output results for the weight function calculations.

The main screen is shown in Figure 1. From this screen the user has the option of selecting one of the four crack types. A separate pop-up window appears for each crack type. The windows contain cells for data entry and a figure illustrating the geometry of the crack being analyzed.

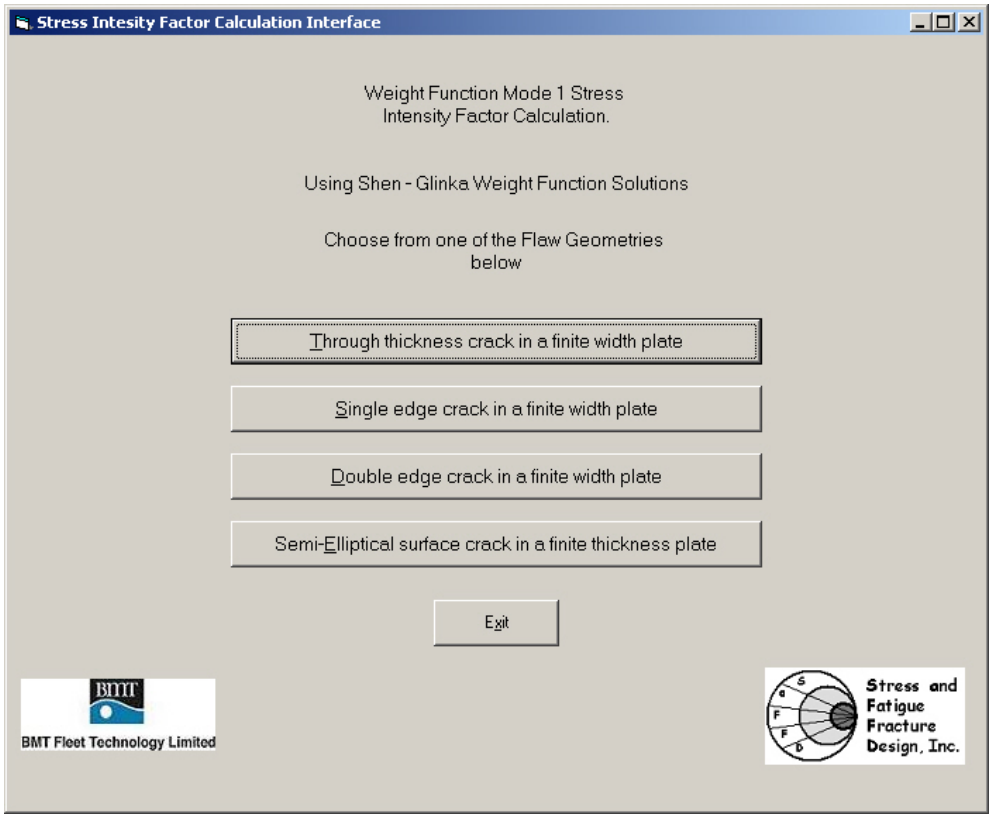

Figure 1: Main Screen for StressIntensityFactorCalc.exe

Stress Data

All calculations require a stress file of the format shown below. The filename must have the extension .dat so it can be executed by wfmain.exe. The number in the first row (not followed by a comma) gives the number of rows containing data in the file (maximum of 100 allowed).

Each row that follows contains the distance and the stress value separated by a comma. For the example below, the stress file would contain 100 entries of distance stress pairs.

A sample stress data file, sample.dat, is provided with the software.

Example Stress file format.

```
100
0, 290
0.5,300
1.0,310
.
.
.
49,260
```

The stress profiles required for typical calculations for edge, through and surface cracks are illustrated in Figure 2. In general, the stress is extracted perpendicular to the crack plane at the mid-point along the crack front, even when calculating K for the surface point of a semi-elliptical surface crack. It is assumed that the stress acting over the crack front is uniform. If the stress varies, K values can be estimated at specific locations along the crack front by using the stress profile perpendicular to the crack plane at that location.

In the case of edge, double-edge and surface cracks, the location X = 0 (the first data point in the stress file) is located at the mouth of the crack. X= a is at the crack front. For the double-edge crack geometry the stress profile is required along the length of one crack only, similar to an edge crack.

For a through thickness crack, X = 0 is the mid-point along the crack length and the stress profile is only required over half of the crack length assuming the cracked specimen is uniformly loaded. If the crack is not uniformly loaded, then K values can be calculated for each crack front separately.

To calculate K using the software for scenarios where the stress does not vary along the crack face, a stress file can be generated with all rows having the same stress value. This can be easily created in a spreadsheet.

NOTE: The stress data file has to be in the same directory as the StressIntensityFactorCalc.exe and wfmain.exe modules

Units

The weight function calculations are not restricted to a specific set of units, but units must be consistent. For example:

- To obtain K in MPa$(mm)^{1/2}$ the stress is in MPa, distance in mm and crack and specimen geometry in mm.
- To obtain K in MPa$(m)^{1/2}$ the stress is in MPa, distance in m and crack and specimen geometry in m.
- To obtain K in ksi$(in)^{1/2}$ the stress is in ksi, distance in inches and crack and specimen geometry in inches.

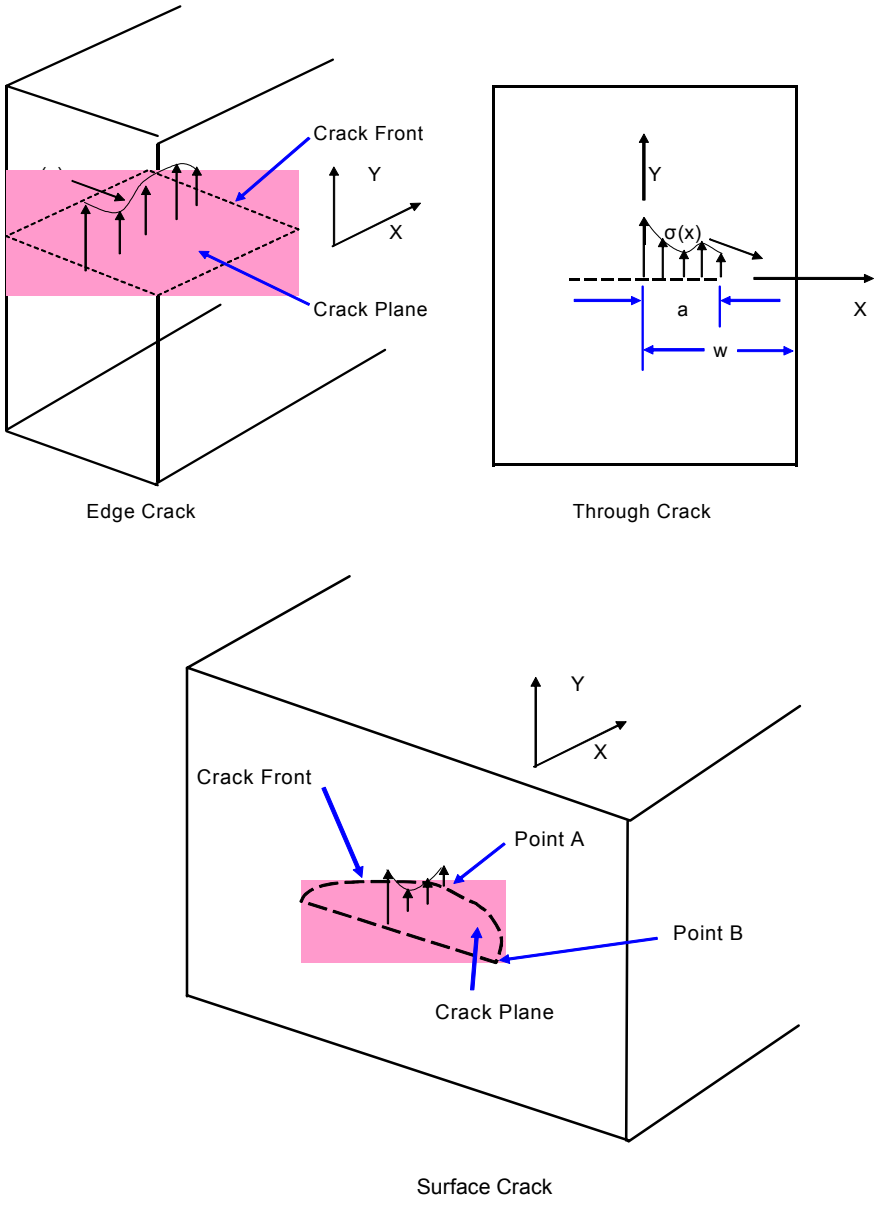

Figure 2: Locations for Required Stress Data

Through Thickness Crack Module

The through thickness crack module interface is shown in Figure 3. The required input data is:

- The stress data file
- The half crack length, a
- The half plate width, w

The output values are the shape function, Y, and stress intensity factor, K. The limit of applicability is $0 < a/w \leq 0.8$.

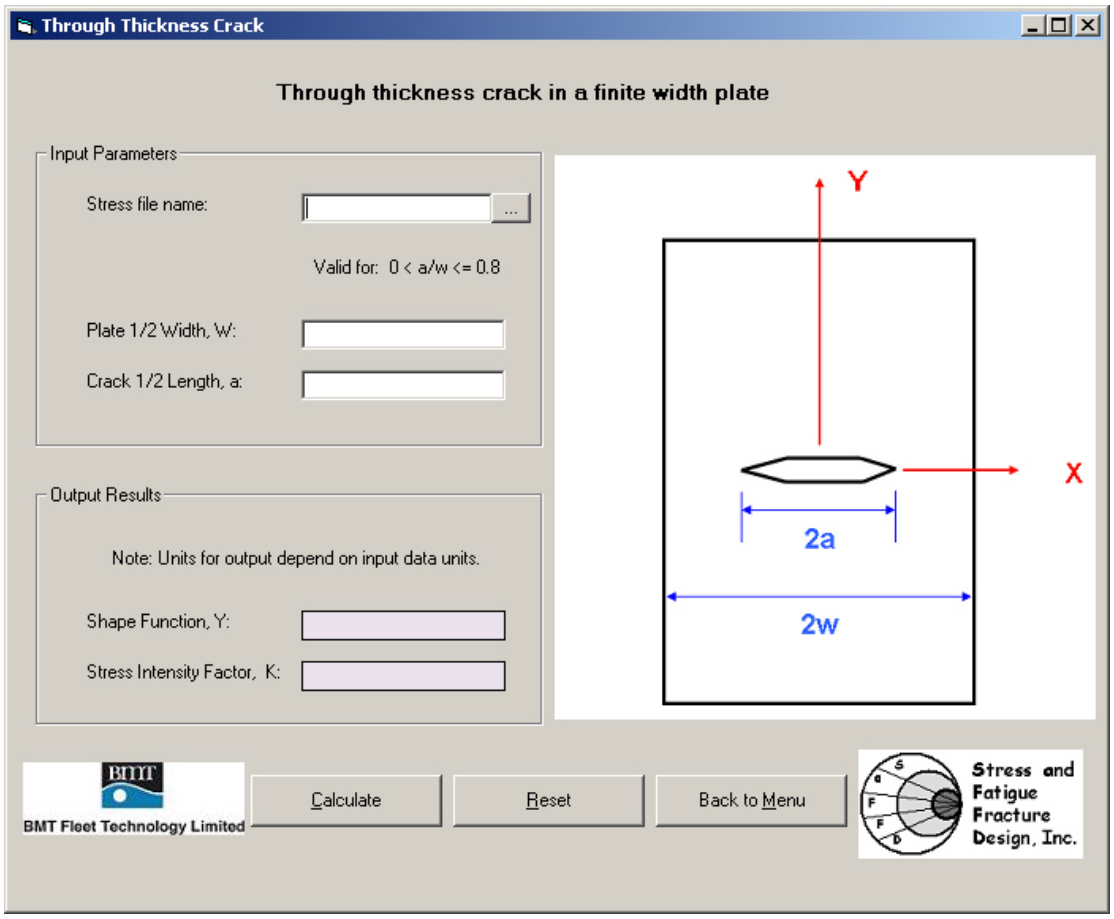

Figure 3: Through Thickness Crack Module

Single Edge Crack Module

The single edge crack module interface is shown in Figure 4. The required input data is:

- The stress data file
- The crack length, a
- The plate width, w

The output values are the shape function, Y, and stress intensity factor, K. The limit of applicability is $0 < a/w \leq 0.8$.

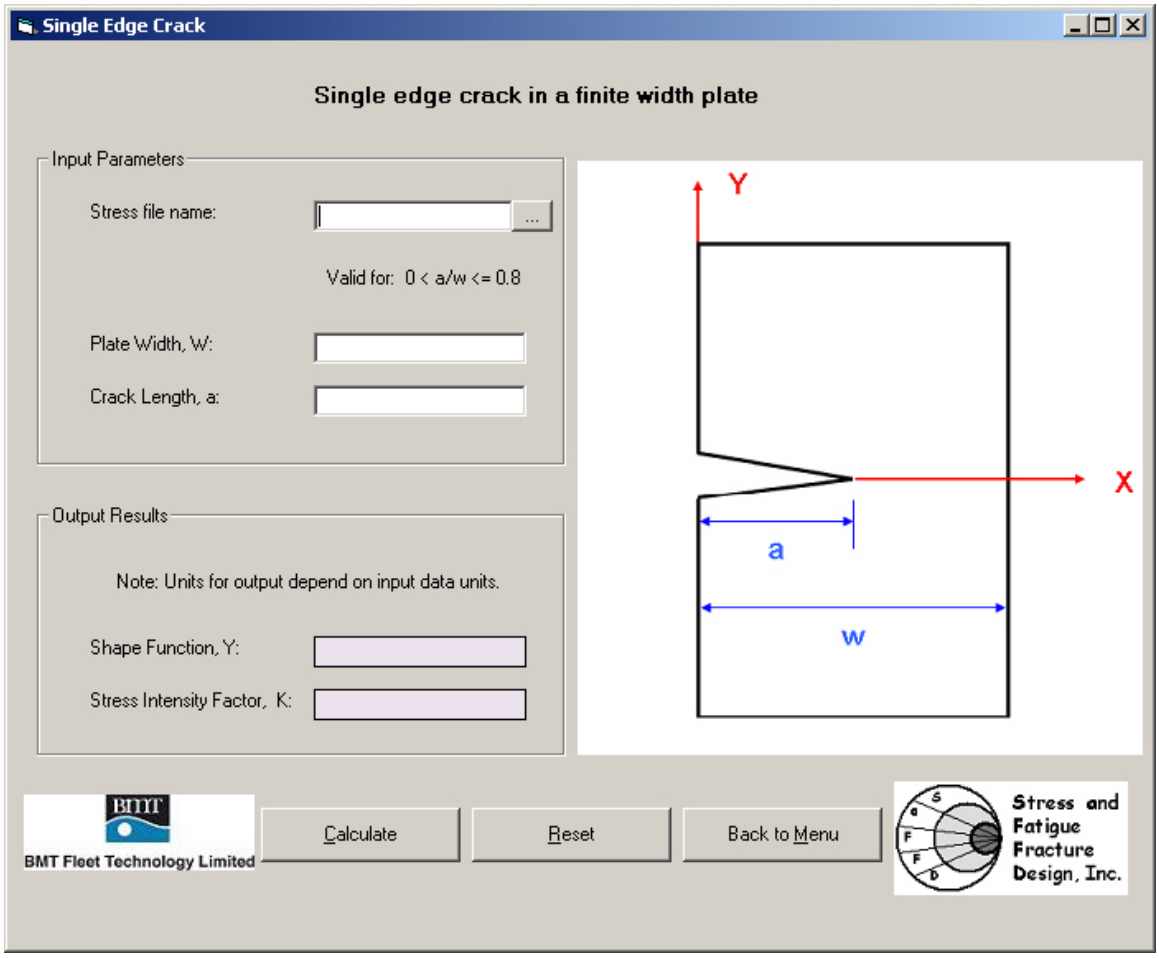

Figure 4: Single Edge Crack Module

Double Edge Crack Module

The double-edge crack module interface is shown in Figure 5. The required input data is:

- The stress data file
- The crack length, a
- The plate half width, w

The output values are the shape function, Y, and stress intensity factor, K. The limit of applicability is $0 < a/w \leq 0.8$.

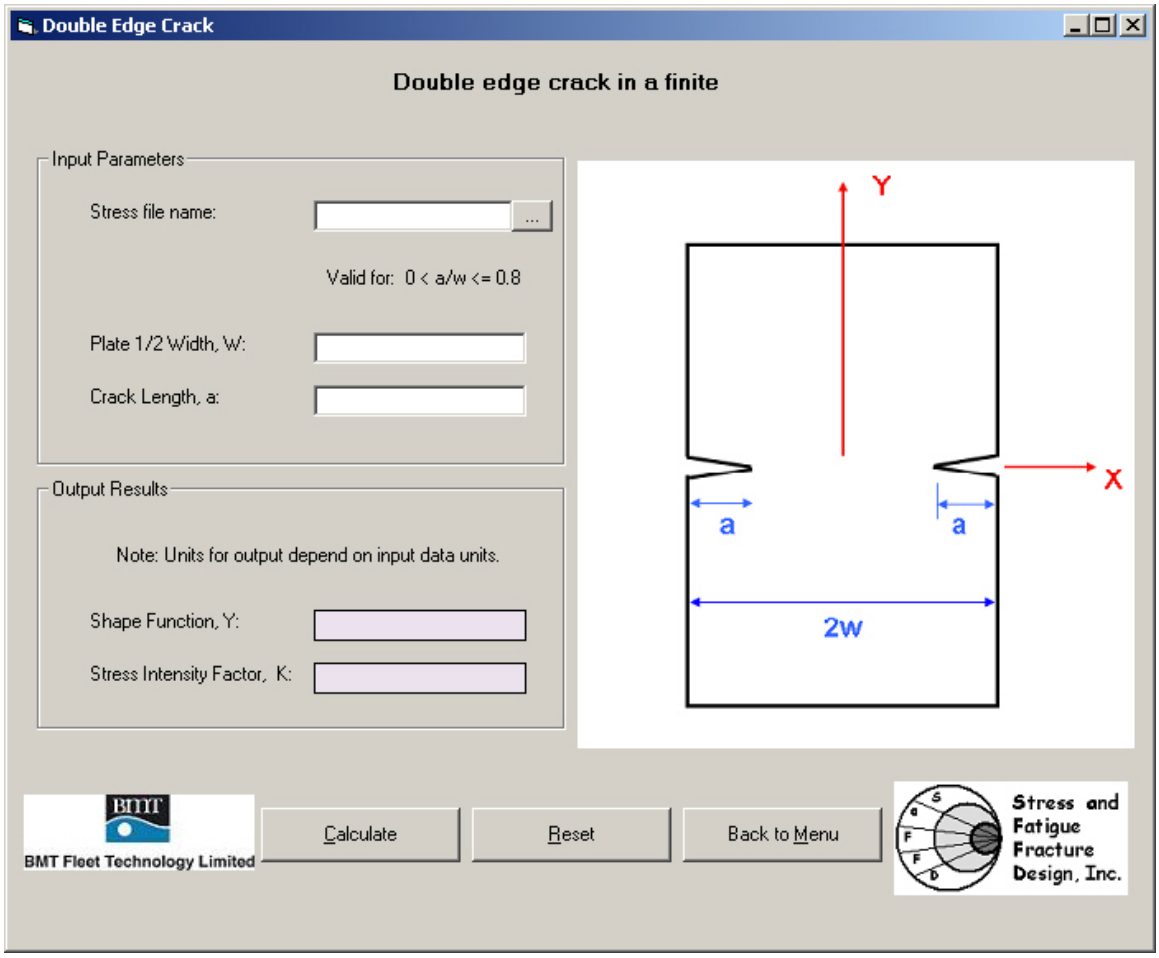

Figure 5: Double Edge Crack Module

Semi-Elliptical Surface Crack Module

The semi-elliptical surface crack module interface is shown in Figure 6. The required input data is:

- The stress data file
- The crack depth, a
- The plate thickness, t
- The crack aspect ratio, a/c

The output values are the shape function, Y, and stress intensity factor, K, for both the deepest point on the crack front, Point A, and the surface point, Point B. The limit of applicability is $0 < a/t \leq 0.8$ and $0.2 \leq a/c \leq 2$.

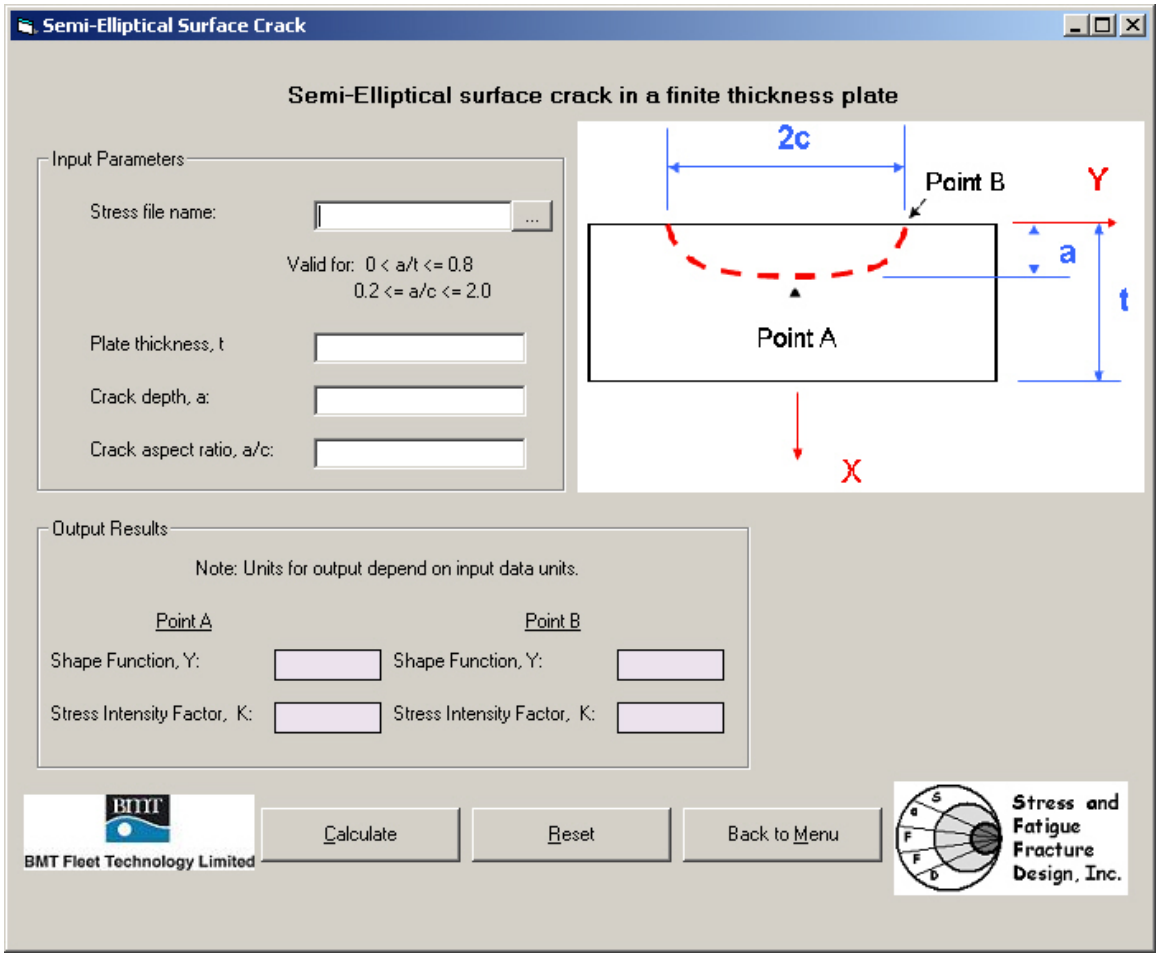

Figure 6: Semi-Elliptical Surface Crack Module

SHIP STRUCTURE COMMITTEE PARTNERS AND LIAISON MEMBERS

PARTNERS

The Society of Naval Architects and Marine Engineers

Mr. Joe Cuneo
President,
Society of Naval Architects and Marine Engineers

Dr. John Daidola
Chairman,
SNAME Technical & Research Steering Committee

The Gulf Coast Region Maritime Technology Center

Dr. John Crisp
Executive Director,
Gulf Coast Maritime Technology Center

Dr. Bill Vorus
Site Director,
Gulf Coast Maritime Technology Center

LIAISON MEMBERS

American Iron and Steel Institute
American Society for Testing & Materials
American Society of Naval Engineers
American Welding Society
Bethlehem Steel Corporation
Canada Center for Minerals & Energy Technology
Colorado School of Mines
Edison Welding Institute
International Maritime Organization
International Ship and Offshore Structure Congress
INTERTANKO
Massachusetts Institute of Technology
Memorial University of Newfoundland
National Cargo Bureau
Office of Naval Research
Oil Companies International Maritime Forum
Tanker Structure Cooperative Forum
Technical University of Nova Scotia
United States Coast Guard Academy
United States Merchant Marine Academy
United States Naval Academy
University of British Columbia
University of California Berkeley
University of Houston - Composites Eng & Appl.
University of Maryland
University of Michigan
University of Waterloo
Virginia Polytechnic and State Institute
Webb Institute
Welding Research Council
Worchester Polytechnic Institute
World Maritime Consulting, INC

Mr. Alexander Wilson
Captain Charles Piersall (Ret.)
Captain Dennis K. Kruse (USN Ret.)
Mr. Richard Frank
Dr. Harold Reemsnyder
Dr. William R. Tyson
Dr. Stephen Liu
Mr. Dave Edmonds
Mr. Tom Allen
Dr. Alaa Mansour
Mr. Dragos Rauta
Mr. Dave Burke / Captain Chip McCord
Dr. M. R. Haddara
Captain Jim McNamara
Dr. Yapa Rajapaksie
Mr. Phillip Murphy
Mr. Rong Huang
Dr. C. Hsiung
Commander Kurt Colella
Dr. C. B. Kim
Dr. Ramswar Bhattacharyya
Dr. S. Calisal
Dr. Robert Bea
Dr. Jerry Williams
Dr. Bilal Ayyub
Dr. Michael Bernitsas
Dr. J. Roorda
Dr. Alan Brown
Dr. Kirsi Tikka
Dr. Martin Prager
Dr. Nick Dembsey
VADM Gene Henn, USCG Ret.

RECENT SHIP STRUCTURE COMMITTEE PUBLICATIONS

Ship Structure Committee Publications on the Web - All reports from SSC 392 and forward are available to be downloaded from the Ship Structure Committee Web Site at URL:
http://www.shipstructure.org
SSC 391 and below are available on the SSC CD-ROM Library. Visit the National Technical Information Service (NTIS) Web Site for ordering information at URL:
http://www.ntis.gov/fcpc/cpn7833.htm

SSC Report Number	Report Bibliography
SSC 428	**In-Service Non-Destructive Evaluation of Fatigue and Fracture Properties for Ship Structure** S. Tiku 2003
SSC 427	**Life Expectancy Assessment of Ship Structures** A. Dinovitzer 2003
SSC 426	**Post Yield Stability of Framing** J. DesRochers, C. Pothier, E. Crocker 2003
SSC 425	**Fatigue Strength and Adequacy of Weld Repairs** R.J. Dexter, R.J. Fitzpatrick, D.L. St. Peters 2003
SSC 424	**Evaluation of Accidental Oil Spills from Bunker Tanks (Phase I)** T. McAllister, C. Rekart, K. Michel 2003
SSC 423	**Green Water Loading on Ship Deck Structures** M. Meinhold, D. Liut, K. Weems, T. Treakle, Woe-Min Lin 2003
SSC 422	**Modeling Structural Damage in Ship Collisions** Dr. A.J. Brown 2003
SSC 421	**Risk Informed Inspection of MarineVessels** Dr. B.M. Ayyub, U.O. Akpan, P.A. Rushton, T.S. Koko, J. Ross, J. Lua 2003
SSC 420	**Failure Definition for Structural Reliability Assessment** Dr. B.M. Ayyub, P.E. Hess III, D.E. Knight 2002
SSC 419	**Supplemental Commercial Design Guidance for Fatigue** R.A. Sielski, J.R. Wilkins, J.A. Hults 2001
SSC 418	**Compensation for Openings in Primary Ship Structure** J.J. Hopkinson, M. Gupta, P. Sefcsik 2002
SSC 417	**Prediction of Structural Response in Grounding Application to Structural Design** K.K. Tikka 2001
SSC 416	**Risk Based Life Cycle Management of Ship Structure** Dr. B.M. Ayyub, U.O. Akpan, G.F. DeSouza, T.S. Koko, X. Luo 2001